

Daniel TREICHL, BSc

Construction and experimental analysis of a heat pump system with speed controlled compressor, vapour injection and desuperheater

MASTER'S THESIS

to achieve the university degree of

Diplom-Ingenieur

Master's degree programme: Mechanical Engineering

submitted to

Graz University of Technology

Supervisor

Dipl.-Ing. Dr.techn. Andreas Heinz
Dipl.-Ing. BSc Franz Hengel
Institute of Thermal Engineering

Assessor

Ao. Univ.-Prof. Dipl.-Ing. Dr.techn. René Rieberer
Institute of Thermal Engineering

Graz, November 2015

AFFIDAVIT

I declare that I have authored this thesis independently, that I have not used other than the declared sources/resources, and that I have explicitly indicated all material which has been quoted either literally or by content from the sources used. The text document uploaded to TUGRAZonline is identical to the present master's thesis.

Graz,
Date

.....
Signature

ABSTRACT

Title: Construction and experimental analysis of a heat pump system with speed controlled compressor, vapour injection and desuperheater

Author: Daniel Treichl

1st keyword: scroll compressor

2nd keyword: economiser

3rd keyword: heat pump control

This master thesis is part of a project funded by the European Union, which investigates combined solar and heat pump systems. Within this thesis a brine-to-water R410A heat pump system with speed controlled compressor, vapour injection and desuperheater was constructed. Afterwards measurements were performed for the evaluation of the system.

For the construction the main requirements were minimised pipe lengths to and from the thermal energy storage and a compact size of the heat pump system. Therefore the heat exchangers were arranged vertically and all other components were positioned as close as possible to the thermal energy storage.

With steady state measurements the performance of the compressor itself and the heat pump system were evaluated. All operating points varied within a range from -15 to 15 °C at the brine inlet and from 20 to 50 °C at the condenser inlet. The compressor showed an overall isentropic efficiency from 0.51 to 0.64 and the heat pump's coefficient of performance was within a range of 2.13 to 6.99. These values strongly depend on the compressor's pressure ratio of the operating point.

The control software of the heat pump system was adjusted for an automatic operation within the overall heating system used in the project. Thereby different stabilisation and safety programmes were embedded as the control of the system is sensitive to oscillations. With dynamic measurements real conditions were simulated for an optimisation of the heat pump's software parameters. To obtain a high efficiency at all operating conditions, it was tried to achieve a minimum amount of refrigerant superheating at the evaporator outlet.

KURZFASSUNG

Titel: Aufbau und messtechnische Analyse einer drehzahlgeregelten Kompressionswärmepumpe mit Economiser-Schaltung und Enthitzer

Autor: Daniel Treichl

1. Stichwort: Scrollverdichter
2. Stichwort: Dampfeinspritzung
3. Stichwort: Wärmepumpenregelung

Die vorliegende Arbeit ist Teil eines europäischen Projektes im 7. Rahmenprogramm, welches sich mit der Untersuchung eines kombinierten Solar-Wärmepumpen Heizungssystems befasst. Im Rahmen dieser Masterarbeit wurde ein Sole/Wasser-R410A Wärmepumpensystem mit drehzahlgeregeltem Kompressor, Economiser-Schaltung und Enthitzer aufgebaut und anschließend vermessen.

Die wichtigsten Vorgaben für den Aufbau der Wärmepumpe waren die Minimierung der Leitungslängen zum thermischen Energiespeicher und die Minimierung des Bauvolumens der Wärmepumpe. Um dies zu ermöglichen wurden die Wärmetauscher vertikal angeordnet und die restlichen Komponenten wurden so nahe wie möglich am Speicher positioniert.

Es wurden stationäre Messungen im gesamten Betriebsbereich der Wärmepumpe durchgeführt. Die Betriebspunkte variierten von -15 bis $+15$ °C bei der Soleeintrittstemperatur und von 20 bis 50 °C beim wasserseitigen Kondensatoreintritt. Für den Gesamt-Isentropen Wirkungsgrad des Kompressors wurden Werte zwischen 0.51 und 0.64 gemessen und die Leistungszahl des Wärmepumpensystems variierte zwischen 2.13 und 6.99 . Die Effizienz ist stark vom Kompressor-Druckverhältnis des jeweiligen Betriebspunktes abhängig.

Für den automatischen Betrieb der Wärmepumpe innerhalb des gesamten Heizungssystems musste die Regelungs-Software angepasst werden. Es wurden unterschiedliche Programme implementiert, welche die Stabilität der Wärmepumpe verbesserten, da die Regelkreise anfällig für Schwingungen sind. Um die Programme zu optimieren, wurden dynamische Messungen durchgeführt, in denen reale Verhältnisse simuliert wurden. Durch die Regelung wurde für alle Betriebspunkte eine minimale Überhitzung des angesaugten Kältemittels angestrebt, um eine Erhöhung der Effizienz zu erreichen.

ACKNOWLEDGEMENTS

This master thesis was written in the year 2014/15 at the Institute of Thermal Engineering at Graz University of Technology. It is part of a project of the Seventh Framework Programme funded by the European Union. The project MacSheep (New **M**aterials and **C**ontrol for a next generation of compact combined **S**olar and **h**eat pump systems with boosted **e**nergetic and **e**xergetic **p**erformance) investigates combined solar thermal and heat pump heating systems.

I would like to begin by thanking several persons from the Institute of Thermal Engineering for their contributions to my thesis. I want to thank Ao. Univ.-Prof. Dipl.-Ing. Dr.techn. René Rieberer, who gave me the opportunity to write this master thesis within the project MacSheep and for supporting me the entire process. I would like to express special thanks to my supervisors Dipl.-Ing. Dr.techn. Andreas Heinz and Dipl.-Ing. BSc Franz Hengel for their patience and always having an open door. Their advices and support within this project were of great value to me. I could always count on the many helping hands at the institute during all parts of this work. From the workshop to all colleagues at my workplace, I want to thank them for helping me whenever help was needed. I want to thank Dipl.-Ing. Gerhard Baur for sharing his experiences from the test rig with me. I really enjoyed working with him on the project. Special thanks go out to Dipl.-Ing. Johannes Riedler, who was an enrichment for my thesis, especially during the most intense working phase in summer 2014.

My family supported me during all the years of study. I am very grateful to my mother Marianna, for always believing in me and always helping me to see things from a different perspective. I would like to thank my brother Florian and his wife Nadine for supporting me in any way possible. Very special thanks go out to my niece Sophia, who was born into the world a year ago and enlightens my days with her beautiful smile.

Finally I would like to thank all my friends for keeping me company during my years of study and for helping me through all the ups and downs. The last couple of years would not have been as amazing if I had not had them by my side.

Graz, 01.11.2015

Daniel Treichl

CONTENTS

1.	INTRODUCTION.....	1
2.	BASICS.....	4
2.1.	Heat pump cycle	5
2.1.1.	Refrigerant	7
2.1.2.	Compressor	9
2.1.3.	Heat exchanger	14
2.1.4.	Expansion valve	16
2.1.5.	Further cycle components	17
2.1.6.	Working fluids	18
2.2.	Measuring principles	18
2.2.1.	Temperature	18
2.2.2.	Flow	20
2.2.3.	Pressure.....	21
2.3.	Uncertainty propagation	22
2.4.	PID controller	24
2.5.	Heating curve	26
3.	DESCRIPTION OF THE TEST RIG.....	28
3.1.	Overview.....	28
3.2.	Heat pump cycle	30
3.2.1.	Compressor	30
3.2.2.	Inverter drive.....	34
3.2.3.	Heat exchanger	35
3.2.4.	Expansion valves	36
3.2.5.	Liquid receiver	37
3.2.6.	Filter dryer	38
3.2.7.	Pipes	39
3.3.	Periphery	39
3.3.1.	Heat source.....	39
3.3.2.	Heat sink	40
3.4.	Design of test rig	42
3.5.	Measuring equipment.....	44
3.5.1.	Temperature sensors	47
3.5.2.	Flow measuring systems	48
3.5.3.	Pressure sensors.....	49
3.5.4.	Electrical power.....	51
3.6.	Control.....	52
3.6.1.	Hardware.....	52
3.6.2.	Software.....	53
3.6.3.	Automation of heat pump control.....	56
3.6.4.	Optimization for system test	57

4.	EVALUATION OF MEASUREMENTS.....	59
4.1.	Evaluation of heat pump cycle	59
4.2.	Compressor evaluation	63
4.2.1.	Overall isentropic efficiency	63
4.2.2.	Volumetric efficiency	65
4.3.	Uncertainty propagation	67
5.	RESULTS AND DISCUSSION.....	68
5.1.	Compressor	68
5.1.1.	Overall isentropic efficiency	69
5.1.2.	Volumetric efficiency	71
5.2.	Heat pump system	73
5.3.	24-hour measurements	77
5.4.	Results of uncertainty propagation	85
6.	CONCLUSION	86
	REFERENCES.....	88
	LIST OF ILLUSTRATIONS.....	91
	APPENDIX.....	A-1
A-1	Software heat pump system	A-1
A-2	Measurement matrix	A-10

Nomenclature

Greek symbols

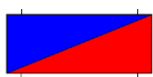
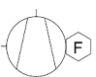





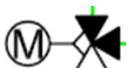

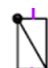


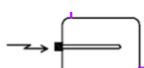


$\eta_{is1/2}$	isentropic efficiency first/second stage	[–]
$\eta_{is,overall}$	overall isentropic efficiency	[–]
$\eta_{vol1/2}$	volumetric efficiency first/second stage	[–]
$\eta_{vol,overall}$	(overall) volumetric efficiency	[–]
π	pressure ratio	[–]
ρ	density	$\frac{kg}{m^3}$

Roman symbols

a	lower systematic error limit	
b	upper systematic error limit	
c_p	specific isobaric heating capacity	$\frac{J}{kg \cdot K}$
COP	Coefficient of Performance	[–]
ΔE_{comp}	electrical energy consumption compressor	[J]
e_s	systematic deviation	
$e_{s,b}$	known systematic deviation	
$e_{s,u}$	unknown systematic deviation	
$f_{comp,loss}$	ratio of heat losses	[–]
h	specific enthalpy	$\frac{J}{kg}$
H	enthalpy	[J]
Δh_{is}	isentropic enthalpy difference	$\frac{J}{kg}$
ΔH	difference in height	[m]
K_D	derivative factor	[s]
K_I	integral factor	$\frac{1}{s}$
K_P	proportionality factor	[–]
$\dot{m}_{b/w}$	mass flow rate brine/water side	$\frac{kg}{s}$
\dot{m}_r	mass flow rate refrigerant circuit	$\frac{kg}{s}$
N	number of measurements	
n_{comp}	compressor speed	[rpm]
n_{nom}	nominal compressor speed	[rpm]
$p_1, p_o, p_{r01}, p_{evap}$	evaporation pressure	[bar]
$p_2, p_c, p_{r02}, p_{cond}$	condensation pressure	[bar]
P_{el}	electrical power consumption compressor	[W]
p_i	outlet pressure of inner compression	[bar]
p_m, p_{r07i}	medium pressure	[bar]
PF	performance factor	[–]
$\dot{Q}_{b/w}$	heating capacity brine/water side	[W]
\dot{Q}_{cond}	heating capacity condenser	[W]
$\dot{Q}_{eco,HP}$	heating capacity economiser high pressure side	[W]
$\dot{Q}_{loss,comp}$	heat losses compressor	[W]
\dot{Q}_r	heating capacity refrigerant circuit	[W]
ΔQ_{cond}	heating energy of condenser	[J]
s	specific entropy	$\frac{J}{kg \cdot K}$
t_{cond}	condensation temperature	[°C]
t_{evap}	evaporation temperature	[°C]
$T_{b/w}$	temperature brine/water side	[°C]
T_n	reset time	[s]

T_r	temperature refrigerant circuit	$[^{\circ}C]$
T_v	derivative time	$[s]$
Δt	time step	$[s]$
ΔT_{pp}	temperature difference at pinch point of heat exchanger	$[K]$
U	overall heat transfer coefficient	$\left[\frac{W}{m^2 \cdot K}\right]$
u_e	uncertainty of deviation	
u_x	overall uncertainty of measured value	
u_y	Gaussian propagation of uncertainty	
V_1	swept volume compressor	$[m^3]$
$\dot{V}_{b/w}$	volume flow rate brine/water side	$\left[\frac{m^3}{s}\right]$
V_i	clearance volume compressor	$[m^3]$
\dot{V}_{real}	real volume flow rate	$\left[\frac{m^3}{s}\right]$
V_{swept}	swept volume compressor	$[m^3]$
V_{swept2}	swept volume second stage compressor	$[m^3]$
$\dot{V}_{theoretic}$	theoretical volume flow rate	$\left[\frac{m^3}{s}\right]$
w	reference variable	
x	process variable, measured value, quality of refrigerant	
\bar{x}	mean value of measurements	
x_d	control deviation	
x_E	corrected value	
x_w	true value	
Δx_{var}	small variation of finite difference method	
y	control variable	
z	disturbance variable	

Symbols

	Heat exchanger		Speed controlled compressor with vapour injection
	Electronic expansion valve		Liquid receiver
	Filter dryer		Sight glass
	Ball valve		Motor controlled 3-way-valve
	Control valve		Non-return valve
	Speed controlled pump		Inverter cooling
	Reservoir with electrical heating rod		Expansion tank
	PID Controller		

1. INTRODUCTION

Motivation

Renewable Energy Sources (RES) are a main key for the future electrical power and heat supply. Only by using RES, emissions to the environment can be reduced to a lower level. One key technology to use the renewable thermal energy of the environment is the heat pump. By using air, water or ground as RES, the heat pump is able to supply thermal energy at a higher temperature level than the source offers. This energy can be used to cover the heating demand of buildings by putting only a fractional amount of electrical energy into the system.

Though heat pump systems are a well-known technology and have been on the market for a few decades already, there is still a lot of potential in reducing the electrical energy consumption of the compressor and also in improving the heat pump cycle itself. Single technologies are already implemented in common heat pump systems, but the combination of different new components and their dynamic interaction has not been investigated yet.

This master thesis is part of a project funded by the *European Union's Seventh Framework Programme*, called 'MacSheep' (New **M**aterials and **C**ontrol for a next generation of compact combined **S**olar and **h**eat pump systems with boosted **e**nergetic and **e**xergetic performance). The project aims to reach a reduction of the overall electrical energy consumption of 25 % at competitive costs, compared to a state of the art system. The whole system consists of a solar and a heat pump system, which are coupled via a thermal energy storage (TES). This stratified storage supplies space heating as well as domestic hot water (DHW). (Heinz et al., 2013)

The Institute of Thermal Engineering (IWT – Institut für Wärmetechnik) is responsible for the development of the heat pump system which is supposed to achieve a significant part of the energy reduction. In Figure 1 a scheme of one version of the overall system and the system boundary for the heat pump is shown. Although all physical and digital interfaces between the heat pump system and the TES are defined, the heat pump cannot be examined without considering the whole system. All improvements of the heat pump cycle are evaluated considering the effect onto the whole system performance.

Prior to this thesis, the most promising possibilities for improvements of the heat pump system were evaluated. The benefits of each optimization will be explained in the following chapters. The most promising components are:

- 1 Desuperheater
- 2 Vapour injection (Economiser)
- 3 Variable speed compressor
- 4 Optimised hydraulic integration of the heat pump

The improvements 1 to 3 were already investigated in the master thesis of Baur (2014). Measurements of the compressor and the heat pump cycle were performed to analyse and optimise the system. All investigated components were proved to be necessary to reach the goal of reduced electrical energy consumption. Also know-how of the operating behaviour of the heat pump system was gained.

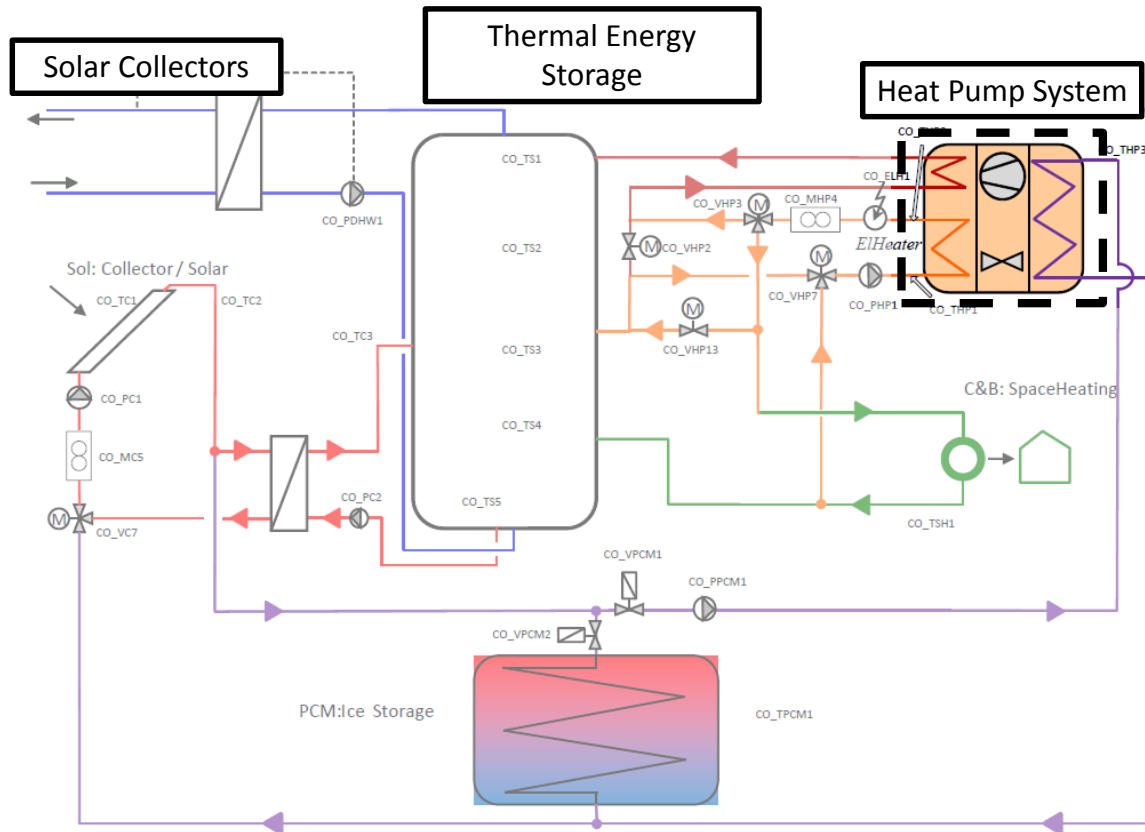


Figure 1: MacSheep heating system (version with ice storage) (Heinz et al., 2014)

The optimised hydraulic integration of the heat pump into the thermal energy storage system required defined interfaces of the two systems. To achieve this, all components of the heat pump had to be rearranged and rebuilt compared to the test rig of Baur (2014). Afterwards measurements at different operating points were accomplished to verify the performance of the heat pump system.

Additionally the software and the control of the heat pump were adjusted to test the dynamic behaviour of the system. Therefore different ambient conditions were simulated over a whole day.

After the measurements were finished the heat pump system was redesigned and almost all the measuring equipment had to be disassembled, as for the system tests at the project partner's laboratory only a minimum of sensor equipment was required to monitor and control the heat pump. The influence of the measurement equipment had to be kept at a minimum for the system tests. Conclusions of the measurements performed at the IWT were used for an optimum control of the system.

Finally the control of the heat pump system was adjusted for the systems tests at the project partner's laboratory. An intuitive use of the programme was preconditioned. The communication between the controls of TES and heat pump system was continuously improved to simplify the handling of the heat pump for the project partner as well as being able to maintain the software easily in the future.

Structure

The thesis is structured in the following way:

In Chapter 2 the basics of the heat pump system are described. Here, an emphasis is put on the functionality and the necessity of each component. Also the reasons for the optimisations will be explained in detail. As measurements were carried out the measuring principles of the used equipment are explained in this chapter as well.

The construction of the test rig is described in Chapter 3. As the heat pump had to be coupled to the TES, certain requirements had to be fulfilled. This led to a compact design of the heat pump system. The types and specifications of each installed component are described thoroughly in this chapter. Also the influence of the measuring equipment on the construction of the test rig is explained. The set-up of the heat pump control is shown at the end of Chapter 3, where the automation control and adjustments for the system tests are described thoroughly.

Measurements at different operating points were performed to verify the performance of the compressor and the heat pump system. The evaluation of the measurements is documented in Chapter 4.

The results of the measurements are discussed in Chapter 5. Additionally 24 hour-simulations were done to optimise the dynamic behaviour of the heat pump control. An analysis of these measurements can be found in this chapter as well. Finally the conclusion is given in Chapter 6.

2. BASICS

Generally a heat pump cycle is built up the same way as a refrigerant cycle for cooling purpose. The simplest cycle consists of compressor, condenser, expansion valve and evaporator, in which a working fluid circulates. As the working fluid is a refrigerant, the cycle is called refrigerant circuit. A scheme of such a circuit is shown in Figure 2 on the left.

Gaseous refrigerant at the evaporation pressure is sucked into the compressor (1), where electrical power is transferred into motion and compression of the fluid, putting it to a higher energy level. At the discharge line the gaseous refrigerant is at a higher pressure and temperature level (2). In the condenser heat is rejected at a constant pressure level (assuming no pressure drop), leading to condensation of the working fluid (3). Afterwards the liquid refrigerant is expanded to the evaporation pressure level into the vapour-liquid two-phase region by the expansion valve (4). In the evaporator the refrigerant is evaporated and superheated. The superheat ensures that only gaseous fluid is sucked by the compressor.

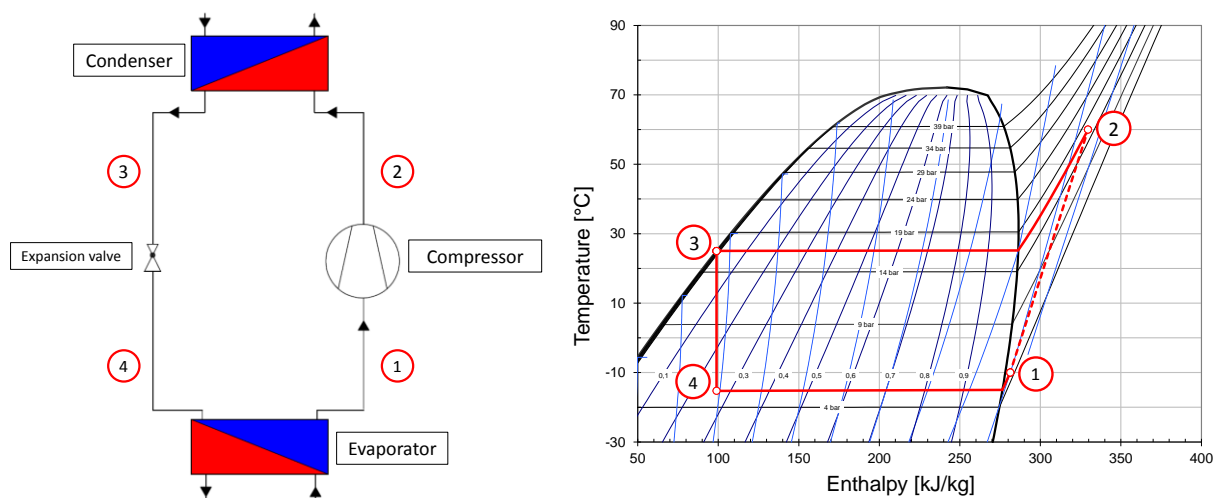


Figure 2: Refrigerant circuit, left: scheme; right: t/h-diagram R410A

Depending on the needs of the system this cycle is either used for heating or cooling. When using it for cooling the supplied heat in the evaporator is useful, whereas the rejected heat in the condenser is waste heat. The heat pump, to the contrary, uses the condenser heat for heating purposes and the heat source for the evaporator can be provided by RES at a low-temperature level. In Figure 2 on the right, a temperature-enthalpy-diagram of the refrigerant R410A shows the states of the working fluid in the cycle according to the scheme shown on the left side. For the one-stage compression the enthalpy differences can be directly compared with each other as the mass flow is the same for all components. This cannot be done for a two-stage compression, which is explained in the following paragraphs, as the mass flows of the two stages differ from each other. In Figure 2 the enthalpy differences between the points (1) to (4) and (2) to (3) directly show the exchanged heats in the evaporator and condenser, respectively.

Key aspects for the optimisation of the heat pump cycle are to increase the heating capacity of the condenser \dot{Q}_{cond} and to reduce the electrical power consumption of the compressor P_{el} . The ratio of these values is the 'Coefficient of Performance' (COP), a main efficiency indicator for heat pump systems, shown in Equation 1. It can be increased by adding different components to the cycle. Their benefits will be explained in the following chapters.

$$COP = \frac{\dot{Q}_{cond}}{P_{el}} \quad \text{Equation 1}$$

2.1. Heat pump cycle

A heat pump system has its best performance at low pressure ratios π . It is defined as the ratio of the condensation pressure p_{cond} to the evaporation pressure p_{evap} (Equation 2).

$$\pi = \frac{p_{cond}}{p_{evap}} \quad \text{Equation 2}$$

However, operating conditions vary in a wide range especially when ambient air is used as heat source. At low ambient air temperatures the demand for space heating rises which leads to high pressure ratios. With increasing ratio the single-stage compression cycle as shown in Figure 2 faces certain limits. In Pohlmann (2010) these limits are listed as follows:

The working fluid is a mixture of the refrigerant itself and a suitable lubricant (oil). This oil/refrigerant-mixture circulates in the refrigerant cycle. At the discharge line of the compressor the temperature of the working fluid is at its highest level. For all mixtures temperature limits are given, which are not allowed to be exceeded as decomposition of the oil would follow.

With rising pressure ratio the volumetric efficiency of the compressor (η_{vol}) decreases. This leads to a lower refrigerant mass flow rate and as a result to a reduced heating capacity. Based on the suction condition (Point 1 in Figure 2), the volumetric efficiency compares the geometrically possible volume flow rate $\dot{V}_{theoretic}$ to the real volume flow rate \dot{V}_{real} of the compressor, see Equation 3. It will be explained in detail in Chapter 4.2.2. The overall isentropic efficiency $\eta_{is,overall}$ describes the relation of the ideal isentropic compression ($\Delta h_{is} \cdot \dot{m}_r$) to the electrical power input of the compressor P_{el} , as shown in Equation 4. Also the overall isentropic efficiency, which is thoroughly described in Chapter 4.2.1, decreases with a rising pressure ratio. This means that the electrical energy input for a certain mass flow rate increases.

$$\eta_{vol} = \frac{\dot{V}_{real}}{\dot{V}_{theoretic}} \quad \text{Equation 3}$$

$$\eta_{is,overall} = \frac{\Delta h_{is} \cdot \dot{m}_r}{P_{el}} \quad \text{Equation 4}$$

All in all these aspects lead to a *COP* decrease with increasing pressure ratio. As for heating purposes this is a conflict, the heat pump cycle should be modified in order to achieve high efficiencies at high pressure ratios.

Vapour injection

A two-stage cycle makes the pressure ratio for each stage lower, but it only leads to a reduction of electrical energy input and a lower discharge temperature if the refrigerant is cooled between the two stages. Although Pohlmann (2010) shows variations of accomplished cooling concepts between the stages only one variant is described in the following paragraphs.

In this master thesis the concept of an economiser, shown in Figure 3, is realised. The refrigerant mass flow is split after the condenser. At first the main mass flow (m) remains at condensation pressure p_c , while the injection mass flow (i) is expanded (TEV) to medium pressure p_m . By expanding the refrigerant it also cools to a lower temperature. The log p/h-diagram on the right of Figure 3 shows that the injection mass flow (i) is in the two-phase

region after the expansion. Afterwards an additional heat exchanger (HX), the so called economiser, transfers heat between these mass flows (m and i) at different pressure levels. While the main mass flow (m) is subcooled, the injection mass flow is evaporated and superheated. The subcooled main mass flow (m) is expanded (TEV) to the low pressure p_o before it is superheated in the evaporator.

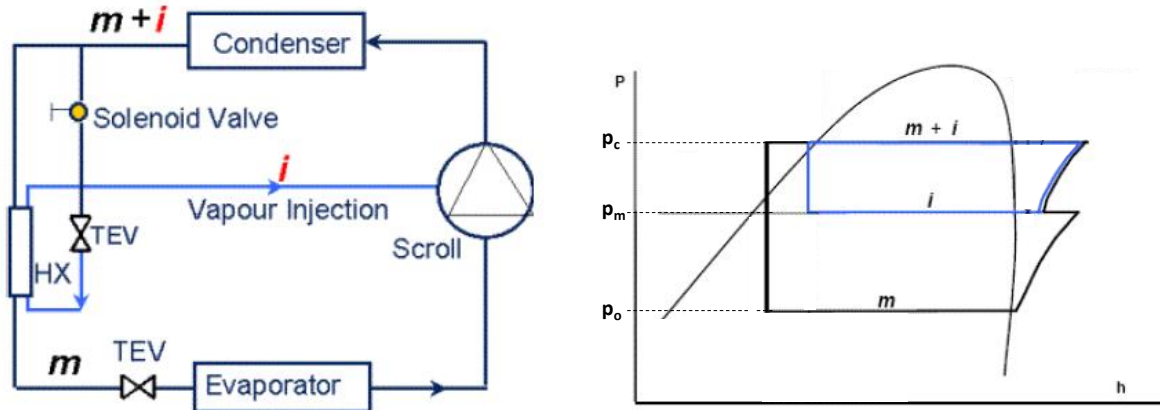


Figure 3: Economiser circuit, left: scheme; right: log p/h-diagram (Copeland, 2011a)

Usually two-stage concepts are accomplished with two piston compressors in two separate casings. In this set-up a scroll compressor, which is a continuous displacement machine is used. The two stages are within one casing and the injection takes place at predefined positions leading to the medium pressure. These positions are designed to get two identical pressure ratios for each stage (at design condition). The medium pressure (p_m) defined in Equation 5 leads to equal pressure ratios for the two stages (Pohlmann, 2010).

$$p_m = \sqrt{p_o \cdot p_c}$$

Equation 5

The injection at medium pressure results in cooling of the superheated refrigerant of the first stage. Due to this, the discharge temperature is decreased. Additionally the injection mass flow increases the mass flow over the condenser ($m+i$) and thereby the heating capacity of the cycle.

Desuperheater

The second modification of the heat pump cycle is motivated by the requirement of domestic hot water (DHW) preparation, where a temperature level of at least 45 °C (Recknagel and Sprenger, 2007) should be provided to the consumer. With a heat pump this is achieved by either having a high condensation pressure, which leads to a high pressure ratio and low COP, or by using a desuperheater, which continuously produces hot water with a reduced capacity at a low pressure level as a side-product of space heating operation. In Figure 4 on the left a scheme of a heat pump cycle with desuperheater and economiser is shown. It is installed at the discharge line right after the compressor and prior to the condenser. The desuperheater uses the sensible heat of the superheated refrigerant, whereas the condenser (mainly) uses its latent heat. On the right side of Figure 4 the cycle is illustrated in a t/h-diagram. Between the points (2) and (3) the sensible heat is rejected from the refrigerant. In comparison to the enthalpy difference of (3) and (4), which represents the heat rejected by the condenser, the heating capacity of the desuperheater is much smaller. On the other hand the temperature level is much higher. The design of the heat pump cycle considers a preparation of DHW simultaneously to space heating.

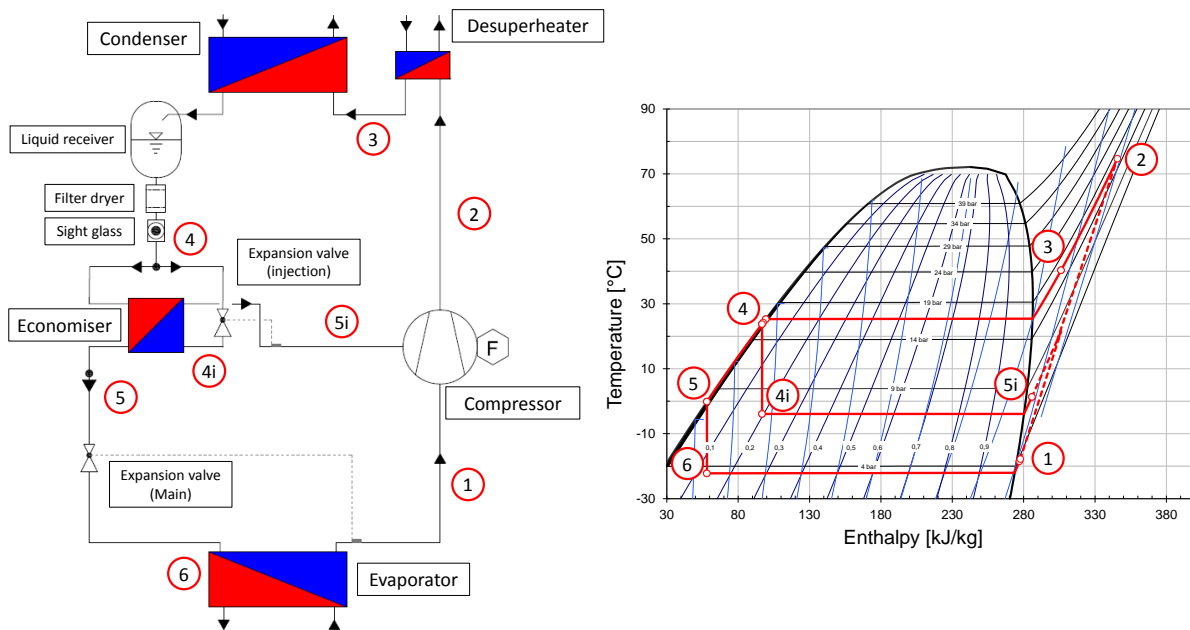


Figure 4: Heat pump cycle with economiser and desuperheater, left: scheme; right: t/h-diagram (Copeland, 2011a)

2.1.1. Refrigerant

In this chapter a short summary of the extensive information about refrigerants in Rieberer et al. (2013b) and Bitzer (2015) is given. The working fluid in a refrigerant circuit has a big impact on the performance of the system. It has to be carefully adjusted to the requirements of the cycle, as the range of application is predefined with a certain refrigerant. For the heat pump system itself the most important parameters are refrigeration capacity, temperature glide, boiling and critical temperature as well as safety issues. Over the last few decades also environmental and political aspects affect the choice of the appropriate refrigerant. Considering these limitations several refrigerants were developed and proposed for different kinds of applications.

In 1930 the first challenge of developing working fluids for refrigerant circuits was safety in terms of flammability and toxicity. Therefore chlorofluorocarbons (CFC) were evolved, which unfortunately showed a negative impact on the environment, as they are greenhouse gases and are boosting stratospheric ozone depletion. Even though hydrochlorofluorocarbons (HCFC) with lower ozone depletion potential were developed, an international withdrawal from all CFCs and HCFCs was ratified due to environmental concerns.

Those prohibited refrigerants were replaced by hydrofluorocarbons (HFC) and their mixtures. However, the range of appropriate fluids is shortened, as R134a is the only non-flammable pure substance and HFC-mixtures are showing a temperature glide, which can lead to problems within the cycle. Temperature glide means that the isobaric phase transition in the evaporator and condenser is not isothermal. The phase transition is always within a temperature range. Additionally the global warming potential (GWP) of HFCs is high, which leads to political discussions. Natural refrigerants as ammonia (R717), carbon dioxide (R744) and isobutane (R600a) have no impact on the environment. However, they are causing problems as toxicity, low critical temperature and flammability.

To be able to compare refrigerants according to their environmental impact, different indicators have been introduced: (Rieberer et al., 2013b)

Ozone Depletion Potential (ODP) is defined with the refrigerant R11 (ODP=1). HFCs have an ODP of 0 as no chlorine is in the fluid.

Global Warming Potential (GWP) [$\text{kg}_{\text{CO}_2\text{-eq}}/\text{kg}$] is defined with carbon dioxide as reference and is used as a coefficient for the greenhouse effect. Additionally a reference time of usually 100 years is given as the residence time of the gases is varying. For HFCs and their mixtures the GWP is rather high.

Total Equivalent Warming Impact (TEWI) [$\text{kg}_{\text{CO}_2\text{-eq}}/\text{kg}$] combines the impact on the environment of direct refrigerant losses due to leakage and recovery losses and indirect CO_2 -emissions that emerge for providing electrical driving power for the cycle.

Table 1 shows an excerpt of different types of refrigerants whereas a detailed list is given in Bitzer (2015). In the heat pump system of this master thesis the HFC-mixture R410A is used. It is a high pressure refrigerant meaning that the standard 30 bar technology for R134a cannot be used. All components have to be designed for 45 bar maximum pressure. With the higher pressure level a higher volumetric refrigeration capacity comes along. This means that compressors can be built smaller compared to e.g. R134a.

Although R410A is a zeotropic mixture the temperature glide is small and it can be treated as an azeotropic mixture. The high GWP of about $2088 \text{ kg}_{\text{CO}_2\text{-eq}}/\text{kg}$ will possibly lead to a substitution of this refrigerant by refrigerants with lower GWP in the future.

Table 1: Refrigerant data (Bitzer, 2015)

Refrigerant	Type	Composition	ODP [R11=1.0]	GWP (100a) [$\text{CO}_2=1.0$]	Boiling Temp. [°C]	Temp. Glide (at 1 bar abs) [K]	Critical Temp. [°C]	Condensation Temp. (at 26 bar abs) [°C]
R22	HCFC	CHClF_2	0.055	1810	-41	0	96	63
R134a	HFC	$\text{CF}_3\text{CH}_2\text{F}$	0	1430	-26	0	101	80
R407C	HFC- mixture	R32/125/134 a	0	1774	-44	7.4	87	58
R410A	HFC- mixture	R32/125	0	2088	-51	<0.2	72	43
R717	natural	NH_3	0	0	-33	0	133	60
R744	natural	CO_2	0	1	-57	0	31	-11

Within the refrigerant circuit the only moving part that is supposed to be lubricated is the compressor. A certain amount of lubricant is transported through the cycle being in permanent contact and interaction with the working fluid. The oil decreases the heat transfer coefficient of the refrigerant and the pressure drop increases due to a higher viscosity. Oil and refrigerant have to be adjusted to each other.

Polyolester lubricant (POE) is recommended by Copeland (2011b) for the compressor used in the heat pump cycle developed within this work. It shows a better solubility than mineral oils. A disadvantage of POE compared to mineral oils is its hygroscopic behaviour. This means that the oil absorbs humidity from the air, which leads to decomposition and loss of lubrication property. Also acids could be formed, which can lead to damage of the components. In Figure 5 the hygroscopic behaviour of POE compared to mineral oil is illustrated. Already after a few hours the recommended maximum amount of moisture in the oil of 50 ppm is exceeded. Therefore the oil is not allowed to be exposed to ambient air for

long periods and a liquid dryer has to be installed in the cycle to keep the moisture at an acceptable level. The level of moisture can be monitored with a sight glass with an implemented humidity indicator.

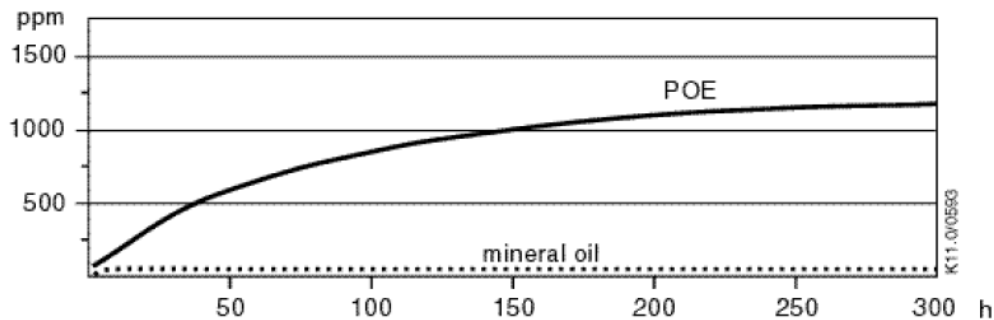


Figure 5: Absorption of moisture in POE oil and mineral oil in ppm by weight at 25°C and 50% relative humidity (h=hours) (Copeland, 2011b)

2.1.2. Compressor

For heating applications several compressor types are available, each having its advantages and disadvantages. A detailed description of reciprocating piston compressors, screw compressors and rotating piston compressors is given in Rieberer et al. (2013b). As in this master thesis a scroll compressor is used, only the functionality of this concept will be explained in detail.

Chen et al. (2002) have analysed the geometry of the scrolls and also have taken a short look on the history of this compressor type. The working principle of a scroll compressor was already invented in 1905. However, first scrolls were manufactured not before the 1970's as high accuracy is required for a matching pair of scrolls. It belongs to the family of rotating compressors and its advantages are a low level of noise and vibration, high efficiency, few moving parts and high reliability. The main components of a scroll compressor are two spirals, the so called scrolls. One scroll is fixed, while the other is orbiting. They are positioned in a way that they touch each other at several points. By this some crescent-shaped pockets are formed as shown in Figure 6. At the beginning of the motion of the orbiting scroll, suction gas streams into the suction chambers. As soon as one revolution is finished the compression of the gas begins as the gas is trapped and no suction gas can enter the pocket. The chambers get continuously smaller and transport the fluid to the centre of the scrolls, where the discharge port is positioned. At the end of the discharge process the two symmetric chambers are combined and lead to the discharge port where the compressed gas is released.

Due to its rotating motion the compressor has a smooth running and as several compressions are accomplished at the same time, it can be compared with a multi-piston compressor, though having a much smaller clearance volume. It has a fixed volume ratio due to the scroll geometry. The high reliability was mentioned as a main advantage of the scroll compressor. This is, besides of having fewer moving parts, because the compressor is not that sensitive to liquid drops in the suction gas as for example piston compressors are, as described in Rieberer et al. (2013b). The field of application is mainly for a motor capacity of 0.8 to 4.8 kW and they are generally accomplished as hermetic compressors. As the motion of the compressor is rotating it is perfectly suited for speed control.

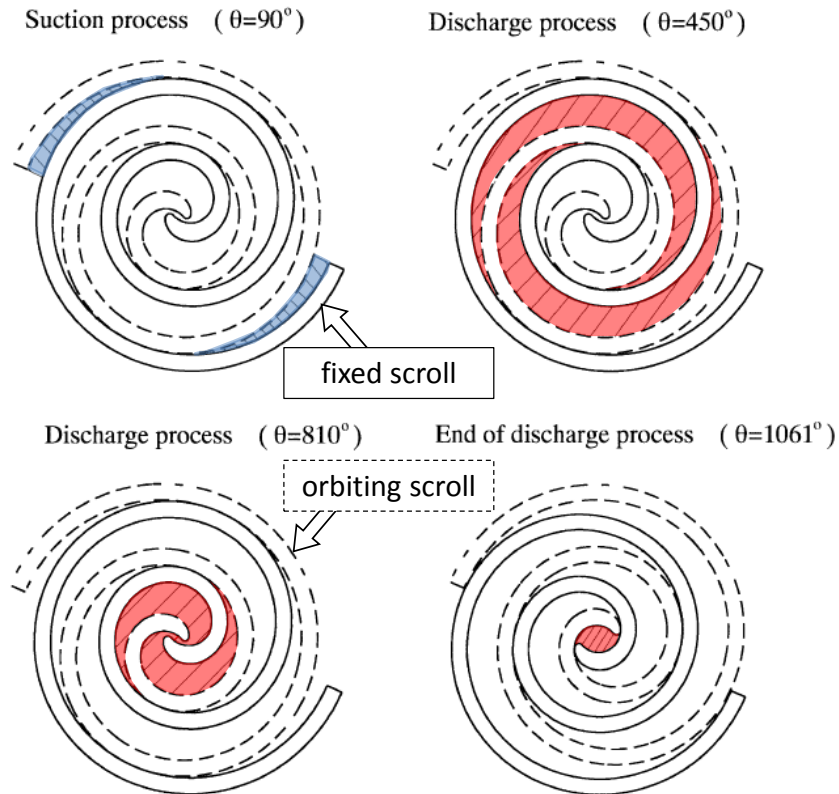


Figure 6: Working principle of a scroll compressor (Chen et al., 2002)

To be able to compare different compressor types with each other, two coefficients are used to describe the compressor behaviour within this master thesis. The overall isentropic efficiency $\eta_{is,overall}$ is defined as shown in Equation 4. It includes inner heat losses due to compression and overall heat losses of the compressor and its components to the ambient. On the other hand the volumetric efficiency η_{vol} takes the ratio of the real amount of compressed gas to theoretically possible amount of gas in consideration (see Equation 3). The reason for the real amount of compressed gas being smaller than the theoretical amount is the leakage within the scrolls and the losses due to the re-expansion of the gas from the clearance volume.

In Figure 7 three states of an idealised pressure/volume-diagram of a screw compressor are illustrated. Although Jungnickel et al. (1990) describe this figure with a compression of a screw compressor, the general statements of the compression can be applied to the scroll compressor. The geometrical swept volume V_1 as well as the clearance volume V_i , which is not usable for the compression, are marked. The fixed volume ratio of a scroll compressor also leads to a fixed outlet pressure at the end of compression for a given suction condition. This means that if the outlet pressure of the inner compression, which is given by the fixed volume ratio, is higher than the discharge pressure ($p_i > p_2$), the gas re-expands to the lower pressure of the system. This over-compression, which is illustrated in Figure 7 on the right, decreases the overall isentropic efficiency of the compressor. An under-compression occurs if a smaller outlet pressure p_i than the discharge pressure p_2 is provided by the scrolls ($p_i < p_2$). The gas is then put to the higher pressure level by a compression shock which also results in a decrease of efficiency. An optimal compression is reached when the system's pressure ratio is equal to the fixed pressure ratio of the scrolls ($p_i = p_2$).

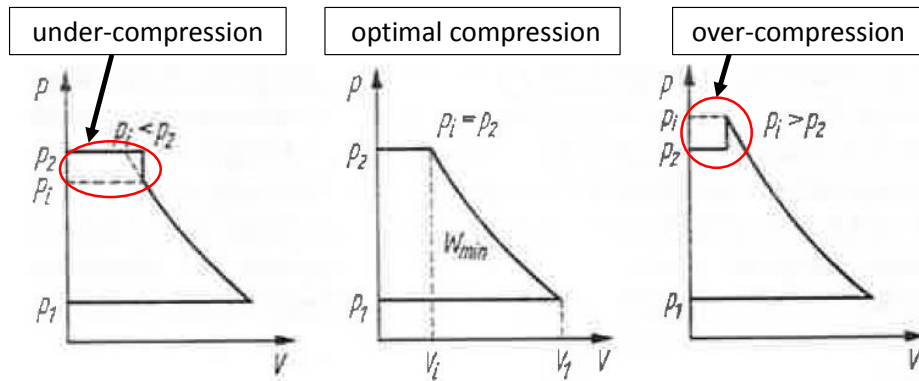


Figure 7: Idealised pressure/volume-diagram of compression (Jungnickel et al., 1990)

The leakage from the high pressure side to the low pressure side is possible due to gaps between the scrolls. Although the manufacturing accuracy is already very high some leakage cannot be avoided. Two different types of leakage are described by Chen et al. (2002) and are illustrated in Figure 8. On the left side, flank leakage is depicted where gas streams along the flanks of the scrolls. Radial leakage (Figure 8, right) occurs between the bottom or the top plate and the scrolls. The leakage of gas within the scrolls does not only lead to a decrease of the volumetric efficiency, but it is also responsible for a higher energy consumption of the compressor as the leaked gas has to be re-compressed.

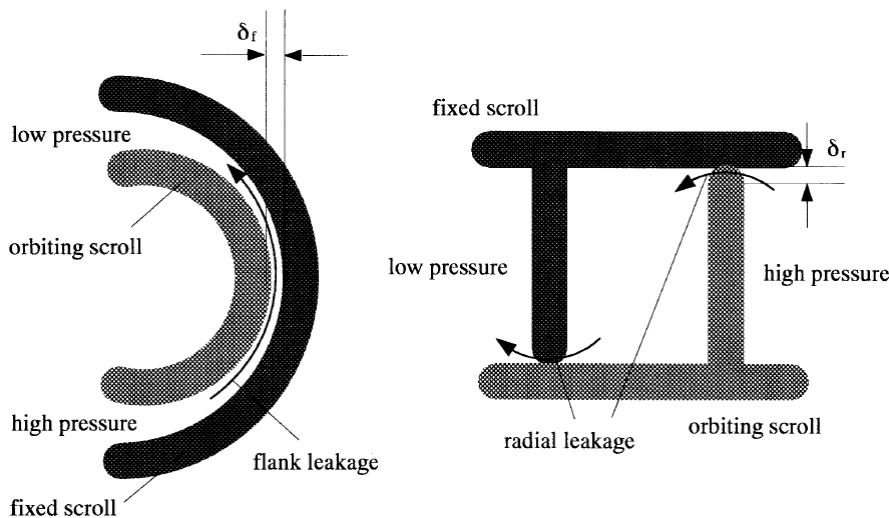


Figure 8: Types of leakage (Chen et al., 2002)

The present master thesis discusses a two-stage heat pump cycle with vapour injection and speed control. For realising a two-stage compression usually two compressors in two separate casings are necessary. When using a scroll compressor the vapour injection is accomplished within the same pair of scrolls. Thereby injection holes are drilled in the fixed scroll.

Wang et al. (2009) have investigated an optimum design of the injection port, as it causes the biggest pressure drop of the injection line. Inner leakage can be avoided when the inner diameter of the injection port is kept smaller than the thickness of the scrolls. To assure a sufficient injection mass flow at least two holes are located next to each other. The radial position of the injection ports depends on an optimum of diverging parameters. When the ports are placed at the beginning of the compression there is a lower chamber pressure at the injection. Thereby a higher pressure difference (injection line to injection chamber) is caused, which leads to a higher mass flow rate at the injection line and therefore an

increasing heating capacity. On the other hand, the compressor's effort rises as the additional injection mass flow has to be compressed over a longer way within the scrolls. This has a negative effect on the performance of the heat pump cycle. In Figure 9 on the left, possible positions of injection ports are highlighted in yellow (injection port A to B). Injecting into the first compression pocket, which is the suction chamber, would lead to a decrease of the performance. On the right of Figure 9 the disassembled compressor is shown. The position of the injection ports is identical to the recommendations (port A and port B) discussed before.

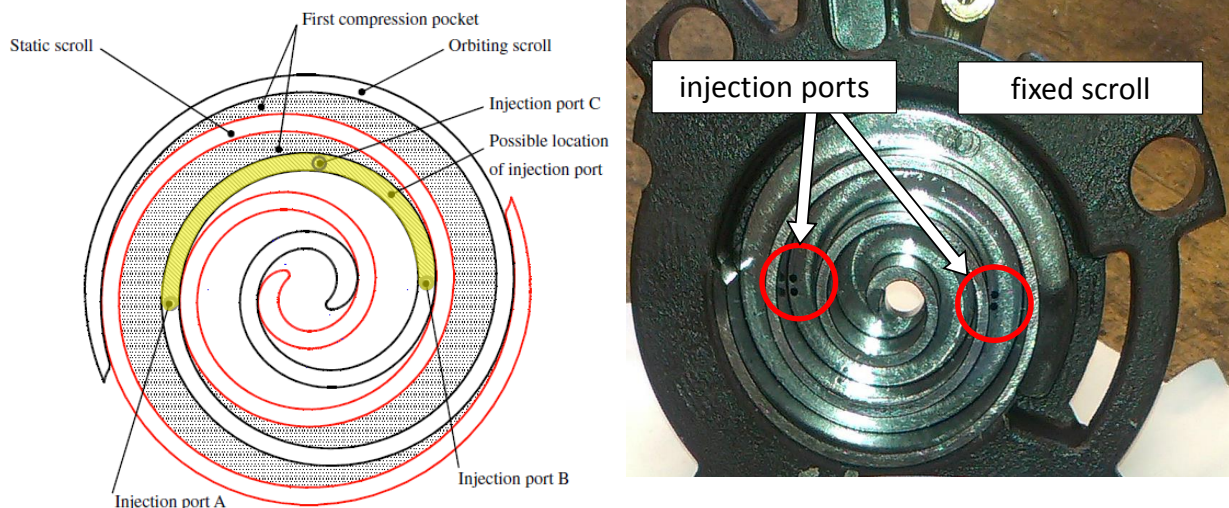


Figure 9: Injection port location, left: optimisation (Wang et al., 2009); right: disassembled compressor

Besides the vapour injection, the heat pump system is also improved by a variable speed compressor. To figure out the benefits of variable speed, the disadvantages of a compressor with constant speed are explained. When the ambient temperature decreases also the evaporation temperature of the refrigerant circuit does in case of an air-source heat pump. Thereby also the density of the suction gas decreases, which leads to a reduced mass flow. This means that at low ambient temperatures, where the heating demand is high, the heating capacity of the compressor decreases. As the heating system, which is investigated within this thesis, is designed for the maximum heat demand at a mean ambient temperature of $-12\text{ }^{\circ}\text{C}$ also the compressor is designed for the maximum heating capacity. With a single speed compressor the heating capacity will increase with increasing ambient temperatures and is therefore oversized for ambient temperatures higher than the design point. This leads to more on/off cycles of the heat pump with the disadvantage of increased start/stop losses. The on/off-cycling losses can be reduced by using a thermal energy storage.

A variable speed compressor has the ability to vary its heating capacity and adjust it to the actual heating demand. In Figure 10 the heating capacity of a variable speed compressor as well as the building load are plotted over the ambient temperature. It can be seen that the heating capacity and the heating demand of the building coincide over a wide range. Only for very low heating capacities the compressor cannot operate below a certain minimum speed and for the maximum heating capacity an additional electrical heater could be installed, as operating hours are short at these low ambient temperatures. To summarise, it can be said that by using a variable speed compressor, on/off-cycling losses are minimised, the electrical energy consumption of the compressor is reduced and a thermal energy storage can be downsized or is not required at all. Also the temperature differences at the heat exchangers are reduced, which lead to a lower pressure ratio. Nevertheless, an inverter is needed, which reduces the overall compressor efficiency.

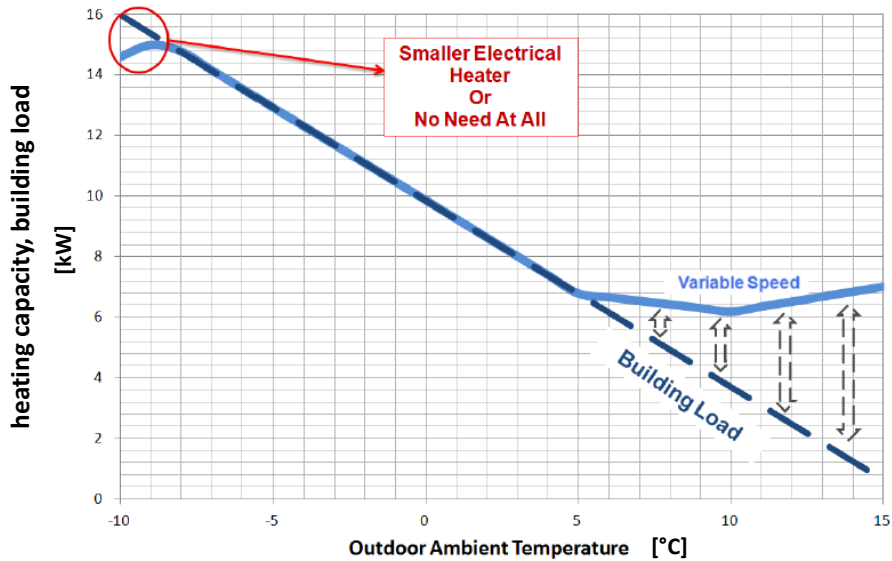


Figure 10: Heating demand and heating capacity of a heat pump with variable speed compressor (Copeland, 2011b)

Figure 11 shows simulations over a period of one heating season. A comparison of a single speed compressor (left) to a variable speed compressor (right) is illustrated. Each mark represents an hourly value of the heating capacity. The blue marks show the heating demand of the building whereas the green and red marks show the heating capacity of the heat pump for DHW preparation and space heating, respectively. For the comparison, the red marks are of interest. The heating and DHW demand stay almost constant. It can be seen that the heating capacity with the single speed compressor rises with the ambient temperature. On the right, a wide range of the heating demand matches with the heating capacity of the heat pump. The minimum compressor speed (30 % of maximum speed) shows the lower limit of the compressor's heating capacity. A reduced speed leads to a reduced energy consumption of the compressor. In case of a constant water flow rate through the condenser the water outlet temperature decreases with a speed controlled compressor, leading to a lower condensation pressure and thus a higher *COP*. Additionally starting losses are decreased as the heating capacity can be adjusted, resulting in longer operating durations.

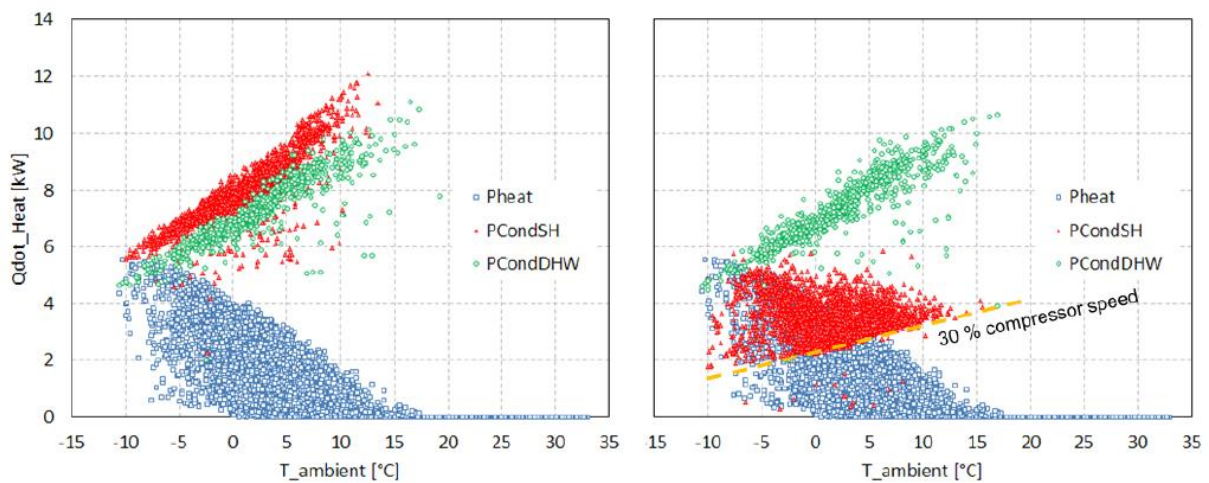


Figure 11: Hourly values of the heating capacity: radiator (Pheat), HP in SH mode (PCondSH) and DHW mode (PCondDHW); left: without speed control, right: with speed control (Heinz et al., 2013)

To be able to control the speed of the compressor an inverter is needed. It is an additional component of the compressor that is an energy consumer and that requires non-negligible space. Nevertheless, the positive effects of the speed control compensate the additional effort of this technology, if varying operating conditions and long-term operation in part load is required. The block diagram in Figure 12 shows the set-up of the inverter system. From the left, the voltage of 230 VAC (Volt Alternating Current) is supplied to the electro-magnetic interference (EMI) filter. Afterwards the voltage is converted into a direct current (DC) by the rectifier that is placed on the inverter drive. Then the DC voltage is pulse-width modulated to create an AC voltage at the desired frequency. (Copeland, 2013a)

The so-called 'Superheat and Envelope Controller' (SEC) represents the interface of the inverter drive and the user interface. It controls the speed of the compressor as well as the expansion valves to keep the superheating at a specific level and has several protection modes embedded.

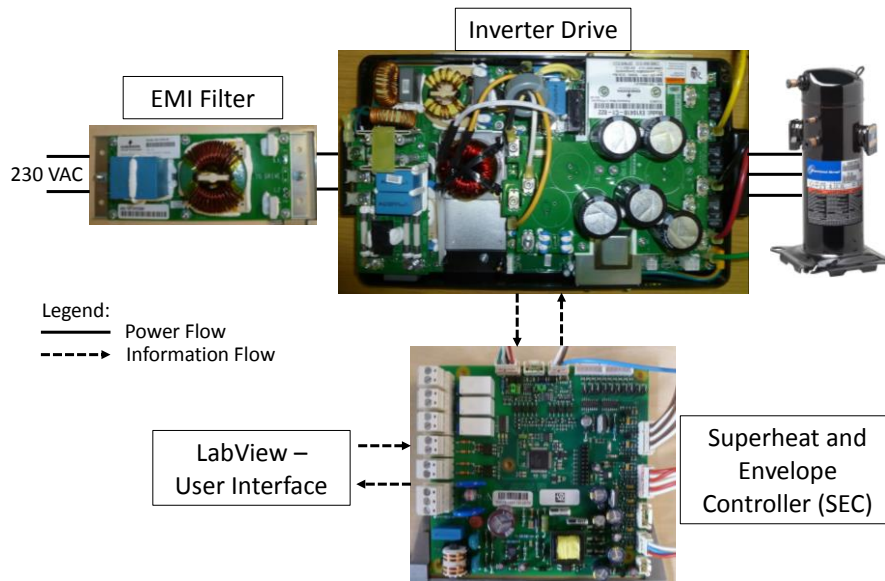


Figure 12: Block diagram of Inverter drive

2.1.3. Heat exchanger

Heat exchangers are passive components of the heat pump cycle. They have an important impact on the system efficiency. A better heat transfer of the heat exchanger results in a lower temperature difference between the two fluids. This leads to a lower condensation pressure and higher evaporation pressure. The pinch point is at the minimum temperature difference between the two heat exchanging fluids occurring in a heat exchanger. Theoretically in a heat exchanger with an infinite heat exchange surface the temperature difference in the pinch point is zero. High temperature differences would lead to an increase of the pressure ratio which is disadvantageous for the efficiency of the refrigerant circuit. In the cycle in Figure 13 four heat exchangers are installed and three pinch points are highlighted. The temperature difference of the evaporator pinch point $\Delta T_{PP, evap}$ is between the brine inlet and the superheated refrigerant outlet. With a fixed brine inlet temperature and superheating the evaporation pressure would decrease with increasing temperature difference in the pinch point. A lower density and therefore mass flow rate as well as a higher pressure ratio and lower COP would result. The minimum temperature difference of the condenser is between the temperature of the saturated refrigerant gas and the water at this point $\Delta T_{PP, cond}$. Also here a higher difference would lead to an increasing condensation pressure and compressor discharge temperature. A small temperature difference of the desuperheater pinch point $\Delta T_{PP, des}$ leads to a higher temperature level for DHW preparation.

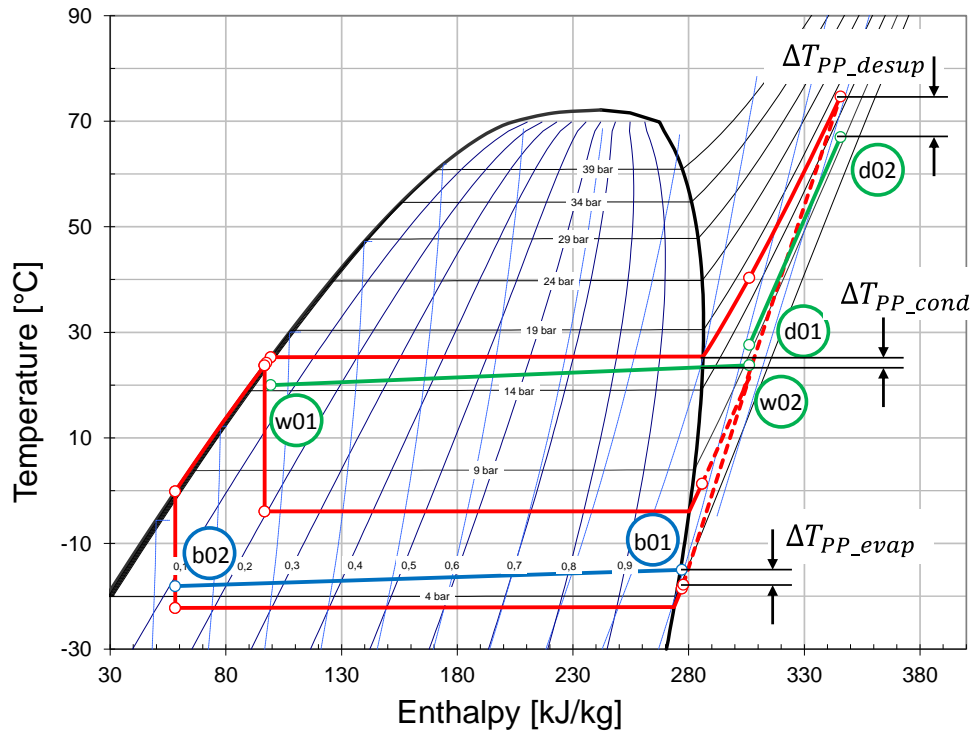


Figure 13: Pinch points of Evaporator, Condenser and Desuperheater

All heat exchangers have to be chosen according to the design point of the heat pump system. The flow direction of all heat exchangers is realised as counter current for an optimal efficiency. As the heat pump system is supposed to be built as compact as possible, all heat exchangers are designed as plate heat exchangers. This type offers a large heat exchange surface at a compact size. Several plates are brazed, welded or screwed together building a channel system where one fluid streams through every second channel (see Figure 14). All plates are undulated to enlarge turbulences and increase the heat exchange area.

An important parameter for the efficiency of a heat exchanger is the overall heat transfer coefficient (also called U-value in $[W/(m^2K)]$) indicating the heat transfer capability. With this value and the logarithmic mean temperature difference, derived from the predicted temperatures of the fluids, the number of plates can be calculated. The number of plates is also responsible for the pressure drop within the heat exchanger.

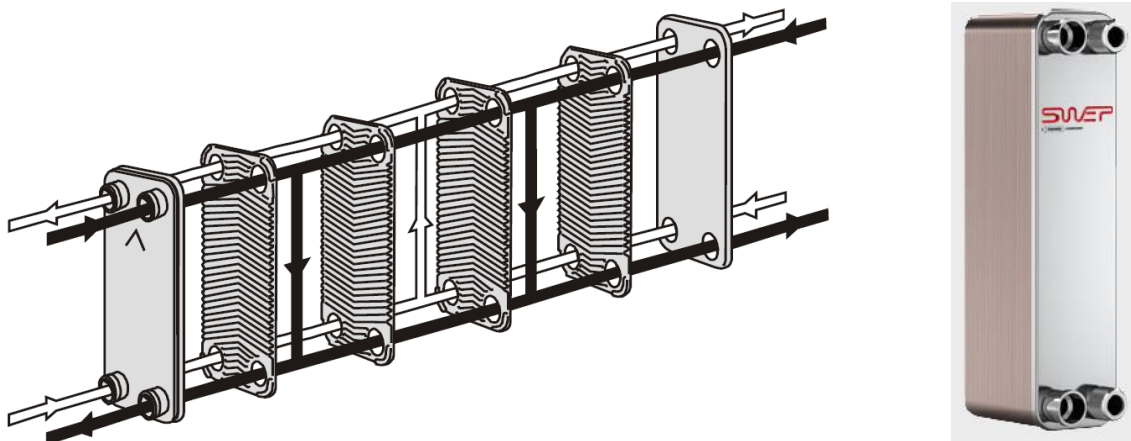


Figure 14: Plate heat exchanger SWEP (SWEP, 2014)

2.1.4. Expansion valve

Expansion valves are active components of the heat pump cycle. They do not only expand the refrigerant from the high pressure to the low pressure side, they also control the mass flow rate and therefore the superheating of the vaporised refrigerant after the evaporator and the economiser. Within this master thesis electronic expansion valves (EEV) are used.

A scheme of the EEV is depicted in Figure 15 on the left, which is described in Recknagel and Sprenger (2007). The refrigerant streams horizontally from the high pressure side (1) to the cone (3) whose sectional area is varied by the movement of the armature (6). The coil (7), which is positioned on the armature, gets a signal from the control of the heat pump system. Depending on if the mass flow rate should be enlarged or decreased, the armature is moved. When the armature is lifted the mass flow rate increases, which reduces the superheating. The present superheating is detected by the control via a temperature sensor, which is placed at the outlet of the evaporator and the evaporation pressure, which is detected with a pressure transmitter. With the evaporation pressure also the evaporation temperature is known and the superheating can be calculated as the difference of these temperatures.

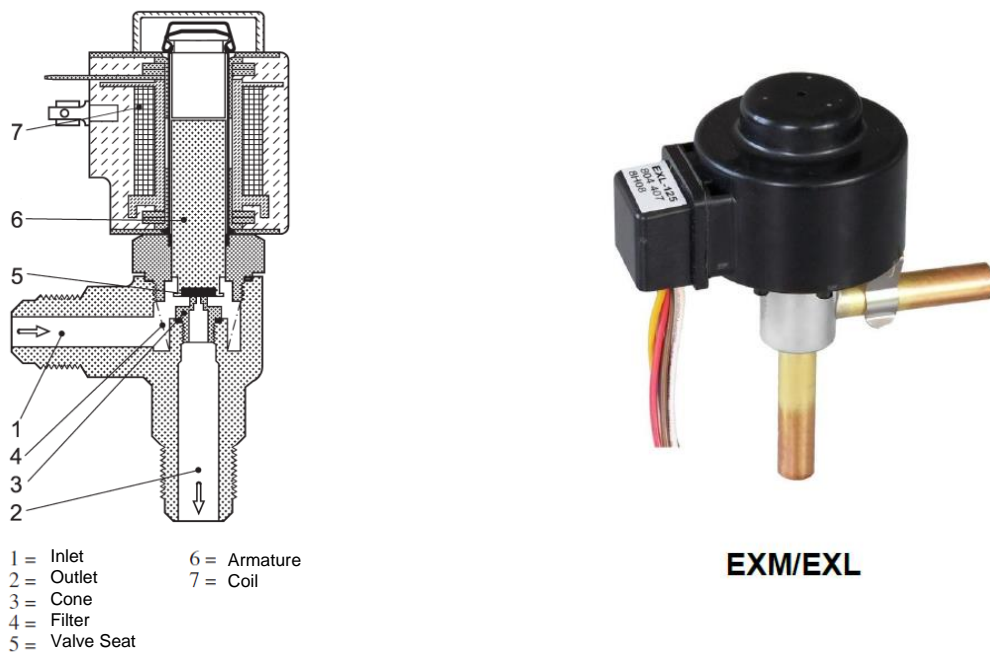


Figure 15: Electronic Expansion Valve; left: scheme (Recknagel and Sprenger, 2007), right: ALCO valve EXM/EXL series (Alco Controls, 2012)

As one key aspect of this heat pump system is to minimise the superheating in order to reach a better performance of the system, the control of the EEV was optimised. Due to the fact that the expansion valve and the temperature sensor, which detects the superheating temperature, are located at different positions on the test rig, a delay time of the control occurs. Big delay times create systems that are very sensitive for oscillations. This tendency to oscillate is further increased by the existence of a second EEV in the injection line. In the scheme of the heat pump cycle (Figure 4) the positions of the temperature sensors are depicted. On the right side of Figure 15 an EEV from the type EXM/EXL of the manufacturer Alco is shown.

2.1.5. Further cycle components

Besides the main components of the cycle explained above, there are additional passive components, which are indispensable for a stable functionality of a heat pump cycle such as the liquid receiver, filter dryer and sight glass. Those components are shown in the scheme of the heat pump cycle (Figure 4) on the liquid side after the condenser. Their function and advantages will be explained in the following paragraphs.

Liquid receiver

A liquid receiver is necessary, when different operating points occur with a large variation of pressures and therefore densities of the working fluid. Especially when a speed controlled compressor is used the operating range is very wide, which makes a liquid receiver inevitable. Besides providing enough amount of refrigerant for different conditions it is also used to ensure that there is only liquid refrigerant in the liquid line of the cycle. After the condenser there is a possibility that not the entire refrigerant has changed its phase, which leads to a two-phase system in the receiver. A standpipe guarantees that only liquid refrigerant leaves the receiver. Also the solubility of the compressor oil in the liquid refrigerant needs to be very high otherwise the oil would accumulate in the receiver. If there is too much refrigerant in the receiver the liquid refrigerant leads to an increase of the condensation pressure, as shown in Figure 16. In the opposite case there is insufficient refrigerant in the liquid receiver. The superheating increases when the expansion valve is fully opened and cannot provide a higher mass flow rate from the liquid receiver. The increased superheating leads to a decrease of the density of the suction gas and thereby a decreasing mass flow rate. Another indicator is the sight glass installed at the liquid line of the heat pump. Insufficient refrigerant leads to bubbles in the liquid line, which can be visually detected.

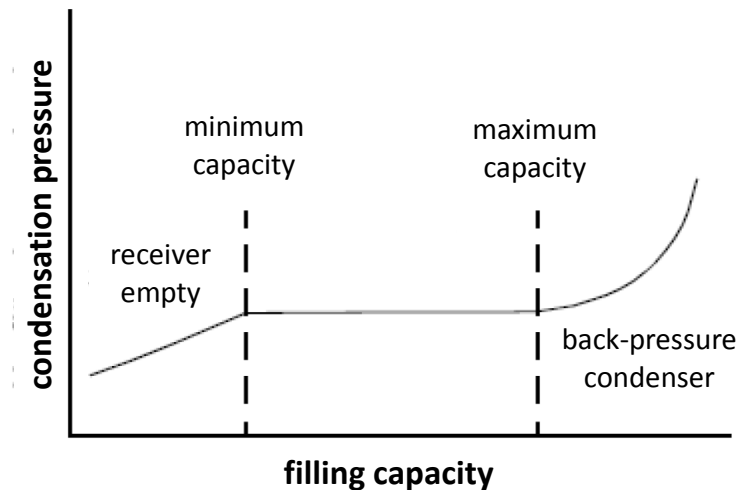


Figure 16: Liquid receiver - refrigerant charge (Rieberer et al., 2013b)

Filter dryer

A filter dryer has two functions within the heat pump cycle. The first is to filter out impurities from the refrigerant. Impurities get into the system during the construction of the cycle, such as copper splinters or oxide scale that is formed when the brazing is done without proper purging with nitrogen. Secondly, the filter dryer absorbs the humidity that is in the system. Humidity is a problem for the hygroscopic compressor oil, as already discussed in Chapter 2.1.1. This leads to acidification and possible damage to the system and the compressor.

Sight glass

Also the sight glass has two important functions within the heat pump cycle. With an indicator it can detect humidity in the refrigerant. When the indicator is green, there is no dangerous amount of humidity in the cycle. If it turns yellow, the humidity is too high, which could be concluded as a malfunction or saturation of the filter dryer.

In Chapter 3.2.4 it will be discussed that expansion valves should always face liquid refrigerant on the high pressure side, as vapour bubbles disturb their control. By having a sight glass in the liquid line of the cycle, these bubbles can be detected, if it is placed as near as possible to the expansion valves. How these bubbles are interpreted is described in Danfoss (2008). When bubbles are seen, they can either occur from a high pressure drop in the filter dryer, no subcooling or an insufficient amount of refrigerant in the cycle. All these reasons need to be determined and excluded when bubbles are detected. The sight glass should be positioned after the filter dryer and close to the expansion valves (Figure 39).

2.1.6. Working fluids

For the heat source and sink different working fluids are used. In the condenser the heat is rejected from the refrigerant and absorbed by a water cycle. The operating temperatures of water at atmospheric pressure are between 0 °C and 100 °C and no environmental impact has to be considered. On the source side the operating conditions are different. Operating temperatures are between -20 °C and 20 °C, which means that an antifreeze fluid has to be used. Therefore a glycol/water-mixture Antifrogen[®] N with a mixing ratio of 39 % vol glycol and 61 % vol water and a freezing point at -24 °C was chosen. The ratio always has to consider a maximum freezing point on the one hand and minimum pressure drop on the other. Those parameters do not coincide.

The physical properties as density and specific heat capacity as a function of temperature are generated from Engineering Equation Solver Academic Professional V9.901 (EES, 2015) for water and from the calculation tool of the manufacturer of Antifrogen[®] N (Clariant, 2015) for the used glycol/water-mixture.

2.2. Measuring principles

For the evaluation of the heat pump test rig different measurement principles are required. The measuring principles of temperature sensors, volume and mass flow meter, pressure sensors and electrical meter are explained in the following paragraphs. The exact position on the test rig and the accuracy of the sensors is described in Chapter 3.5.

2.2.1. Temperature

Temperature can be detected in several ways categorised by mechanical or electrical principle and contact-free or contact thermometer. Within this master thesis only electrical contact temperature sensors are used. All information from this chapter is summarised from Rieberer et al. (2013a).

Thermocouple

A thermocouple makes use of the Seebeck-effect, which says that if two different metals or alloys are faced with two different temperature levels, current flows in the electric circuit. By opening the electric circuit a potential difference can be detected. When the temperature of the reference junction is known, the temperature of the measuring point is a function of the

potential difference. The relation of this temperature difference and the potential is non-linear. In Figure 17 a standard circuit of a thermocouple is illustrated. At the measuring point the desired temperature is detected. The compensating line is not allowed to have an impact on the thermoelectric voltage. It has to have the same thermoelectric properties as the thermocouple. The reference junction detects the reference temperature and shall not be exposed to environmental influences.

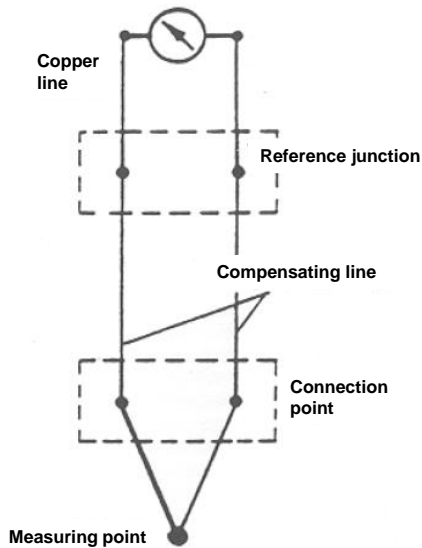


Figure 17: Thermocouple standard circuit (Rieberer et al., 2013a)

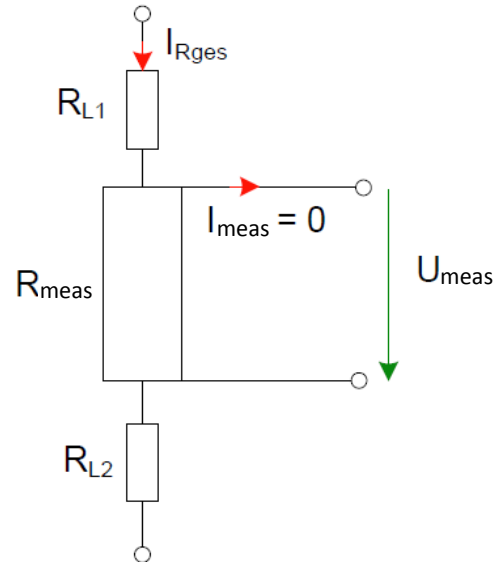


Figure 18: Resistance thermometer, four-wire configuration (Rieberer et al., 2013a)

Resistance thermometer

With a resistance thermometer the absolute temperature of an object can be detected and not only a temperature difference as with thermocouples. It uses the principle that the electric resistance of most materials is changing with their temperature level. Other than thermocouples, resistance thermometers always need supply energy. In Figure 18 a four-wire configuration of a resistance thermometer is illustrated. Two wires, which are represented by the electric resistances R_{L1} and R_{L2} , provide the supply energy I_{Rges} and the other two wires detect the voltage drop U_{meas} of the sensor resistance R_{meas} . Platinum resistance thermometers are characterised by a high accuracy over a wide temperature range and a high reliability and reproducibility. It needs to be considered that the measuring length is over several millimetres and not just a single point as it is with thermocouples.

Thermic Resistor

Thermic resistors are also resistance thermometers and change their resistance due to changes of temperature. They consist of many sintered crystals and are divided into two categories. NTC-thermistors (negative temperature coefficient) have a better electrical conductivity at hot temperatures than in cold. The resistance decreases with high temperatures. On the opposite PTC-thermistors (positive temperature coefficient) have an increasing resistance with rising temperatures and therefore a better conductivity at low temperatures. Compared to resistance thermometers as Pt-100 these sensors have a low reliability and lower accuracy.

Installation

For the installation of temperature sensors a few aspects have to be considered. For contact sensors it is very important that the measuring points of the sensors have a sufficient contact to the pipe wall. Additionally to fixing the sensor with cable connectors to the pipe also heat-conductive paste is put on the contact area. To avoid environmental influences insulation is put around the measuring head as depicted in Figure 19.

When a higher accuracy is required, temperature sensors should be installed in-stream. Figure 20 shows guidelines how the sensor should be positioned. The measuring head should always face the stream and as less area as possible should be blocked to minimise the pressure drop of the sensors. Stratification within the stream could lead to detection of a non-representative temperature.

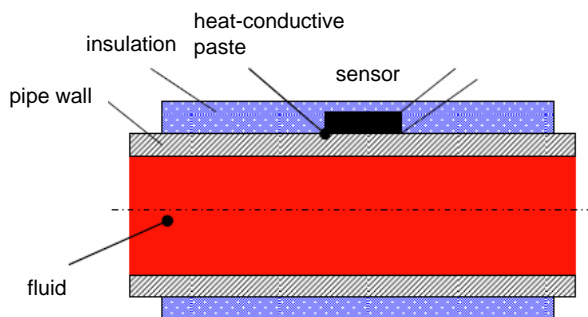


Figure 19: Contact sensor (Rieberer et al., 2013a)

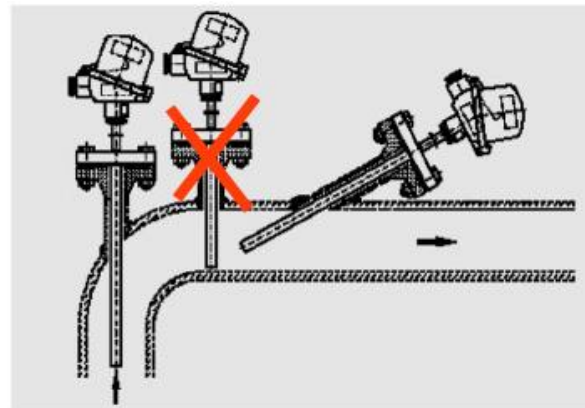


Figure 20: In-stream installation (Rieberer et al., 2013a)

2.2.2. Flow

In the refrigerant circuit a mass flow meter is installed whereas at the heat source and sink two volume flow meters are measuring the flow of the working fluids.

Volume flow meter

As described in E+H (2010) the measuring principle of the electromagnetic flow meter is based on Faraday's law of induction, which says that a voltage is induced if a conductor moves in a magnetic field. On the left of Figure 21 a scheme of the measurement set-up is depicted. A flowing medium having a flow velocity v , disturbs the magnetic field B , which is generated by the field coils and the current strength I . With electrodes an induced voltage U_e is detected. The velocity of the medium is proportional to the induced voltage.

Mass flow meter

Guggenberger (2013) explains the measuring principle of the Coriolis mass flow meter which uses the Coriolis force to detect directly the mass flow rate. This force is exerted on a body that moves relatively to a rotating system. The flowing medium streams through a U-bend which is vibrating periodically. By the stream of the medium a torsion movement is induced to the U-bend (Figure 22). This torsion is detected and its amplitude is a function of the mass flow, whereas the frequency of the motion is dependent on the density of the fluid. The accuracy of the Coriolis mass flow meter is high.

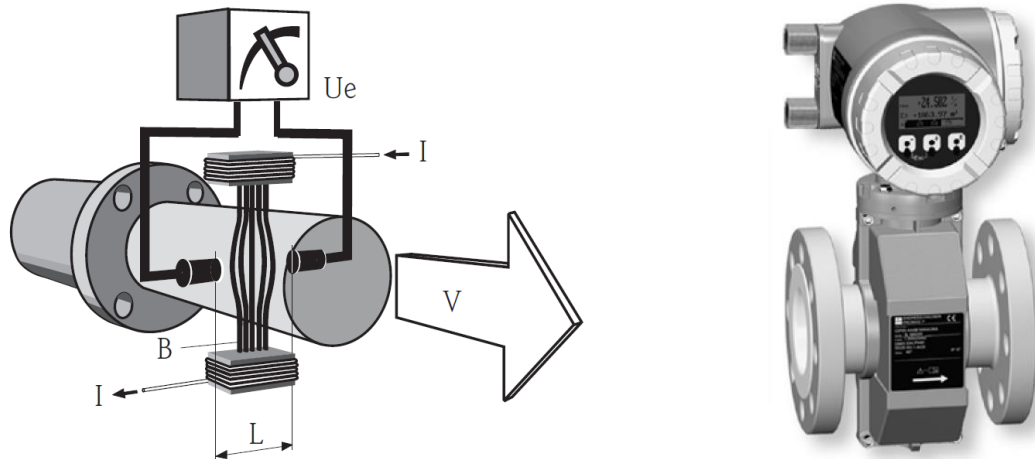


Figure 21: Electromagnetic flow meter; left: scheme; right: Proline Promag 50P (E+H, 2010)

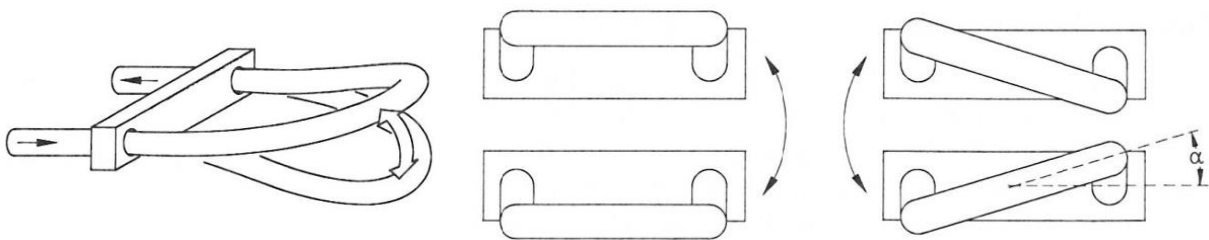


Figure 22: Measuring principle of Coriolis mass flow meter (Guggenberger, 2013)

2.2.3. Pressure

Three piezo-resistive pressure transmitters are installed in the test rig. They are differential pressure transmitters relative to the ambient pressure. The functionality of these sensors is described in Görtler (2010) as follows. The measuring principle is based on an electronic semiconductor which is changing its electrical conductivity when mechanical stress is executed on the material and is thereby deformed. This change of the conductivity is proportional to the active pressure. In Figure 23 on the left the inner set-up of the pressure transmitter is shown. The outer pressure p_1 acts on the steel diaphragm. Behind this diaphragm a chamber is filled with silicone oil, which transports the pressure without loss to the inner core. Another diaphragm that is combined with piezoelectric quartz detects the mechanical stresses. The signal is afterwards amplified and an output signal of 4 to 20 mA is generated. On the right of Figure 23 a differential pressure transmitter of ALCO is illustrated.

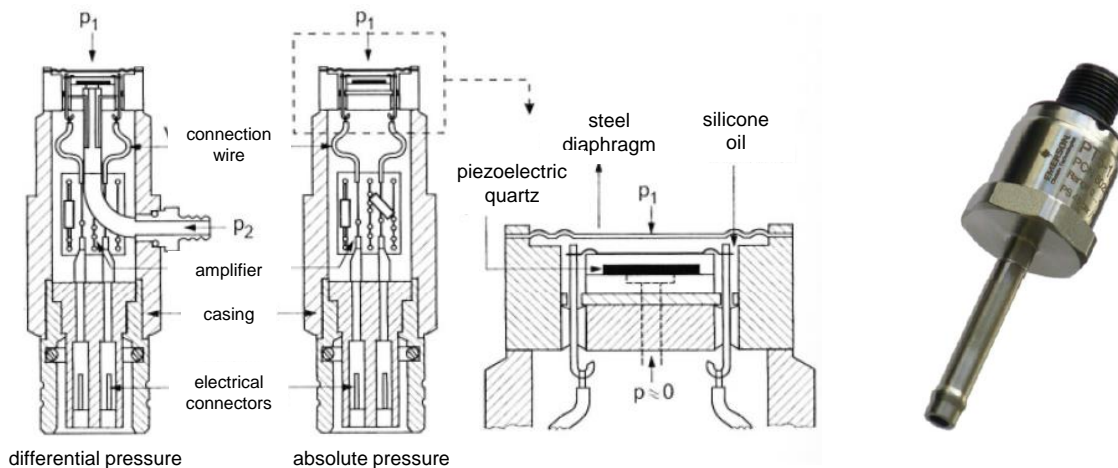


Figure 23: Piezo-resistive pressure transmitter; left: scheme (Guggenberger, 2013); right: ALCO PT5-xxT (Alco Controls, 2013)

2.3. Uncertainty propagation

When measurements are performed the measured value always differs from the true value. The measurement devices themselves as well as the method of measuring produce errors systematically and/or randomly. The uncertainty propagation quantifies these errors by categorising them considering their probability. All information of this chapter is summarised from Görtler (2010) and Rieberer et al. (2013a). Basically three types of errors are defined:

- **serious mistake**
- **systematic deviation**
- **random deviation**

A serious mistake is caused by defective measuring devices or severe mistakes of the measuring method. This error is avoided by a thorough execution of the measurements.

Systematic errors can be divided into known and unknown errors. Known systematic errors are detected via calibration of the measuring devices. They are compared to a more precise reference measuring device whose measured value is considered to be correct. The known systematic error is corrected by the use of calibration factors (offset and gradient), which are directly calculated to the measured value. After the calibration a second measurement with the applied calibration factors is accomplished to verify the repeatability. The deviation of the repeatability shows the unknown systematic error. This error is treated the same as the random error. A probability distribution is assumed for it.

Random errors originate from non-quantifiable and non-influenceable changes of the measuring device, operator and environment. They can only be detected by accomplishing an infinite amount of measurements at exactly the same conditions as the values are distributed over a mean value. This cannot be realised though and therefore a Gaussian distribution is assumed for the random error.

In Figure 24 the basic terms are visualised at the probability density function. The measured value x has a deviation e to the true value x_w . The systematic deviation e_s is summed up by the unknown systematic deviation $e_{s,u}$ and known systematic deviation $e_{s,b}$. When the measured value x is corrected by the known deviation the corrected value x_E is defined. Unknown systematic deviations can be derived from former measurements, experience, data sheets or assumed probability distribution. For measuring devices error limits (lower limit a and upper limit b) are often provided by the manufacturer or can be gained from the

repeatability test of the calibration. With these limits an uncertainty can be calculated with a rectangular distribution meaning that all values have the same probability. The uncertainty is defined as

$$u_{e_s} = \frac{b - a}{\sqrt{12}} \tag{Equation 6}$$

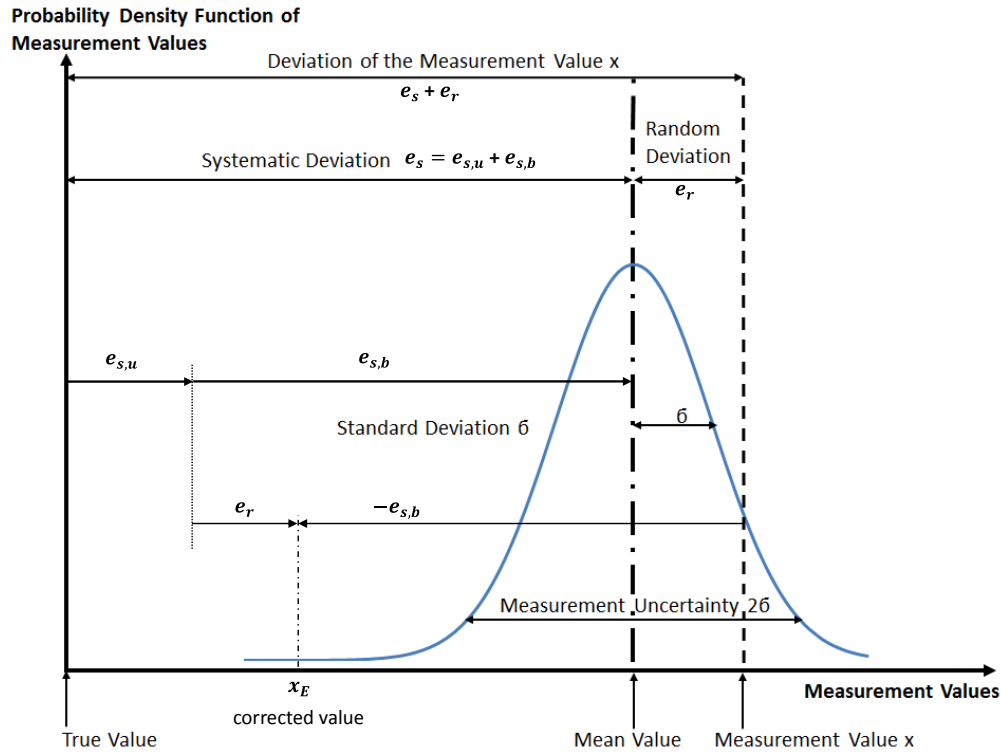


Figure 24: Probability density function (AVL, 2014)

Random deviation can only be calculated by building the mean value of many measurements. With this mean value a Gaussian distribution is assumed where a confidence interval has to be chosen. With the number of measurements N and the mean value of measurements \bar{x} , the random uncertainty u_{e_r} can be calculated as shown in Equation 7.

$$u_{e_r} = \sqrt{\frac{1}{N \cdot (N - 1)} \cdot \sum_{i=1}^N (x_i - \bar{x})^2} \tag{Equation 7}$$

This represents the random uncertainty. The overall uncertainty is a combination of both the random and the systematic uncertainty (Equation 8) and it is assumed that also the unknown systematic uncertainty is normally distributed. Often the random uncertainty is much smaller than the systematic and can therefore be neglected.

$$u_x = \sqrt{u_{e_r}^2 + u_{e_s}^2} \tag{Equation 8}$$

If the uncertainty needs to be derived from a result of measurement that is dependent on several measured values the Gaussian propagation of uncertainty u_y (Equation 9) is used. It assumes that all uncertainties are normally distributed which leads to an underestimation of the uncertainty.

$$u_y = \sqrt{\sum_{i=1}^m \left(\frac{\partial f}{\partial x_i}\right)^2 \cdot u_{x_i}^2} \tag{Equation 9}$$

2.4. PID controller

In the heat pump system several control circuits are necessary to provide specific temperatures, volume flow rates, compressor speed and superheating. Therefore controllers are embedded into the control system. The theoretical background is explained in this chapter.

A typical control circuit is depicted in Figure 25. The value of the reference variable is supposed to be achieved by the end of the control circuit. This is the set point of the control circuit. A controlled system is steadily influenced by disturbances and a controller is used to compensate that. The quality of a controller determines the speed, accuracy and vulnerability for oscillating of a system. It consists of a control algorithm and an actuator, which is directly influencing the controlled system. A measuring device detects the impact of the controller to the system via a sensor. This signal is transposed with a measuring transducer, which gives feedback to the controller. The control deviation is then again processed in the control algorithm.

The meaning of the variables is explained as follows:

- | | | | |
|-------------|----------------------|--------------------|----------------------|
| w | reference variable | $y = f(x_d)$ | control algorithm |
| x | process variable | ST | actuator |
| x_d | control deviation | MWA | sensor |
| y | control variable | MU | measuring transducer |
| z | disturbance variable | | |

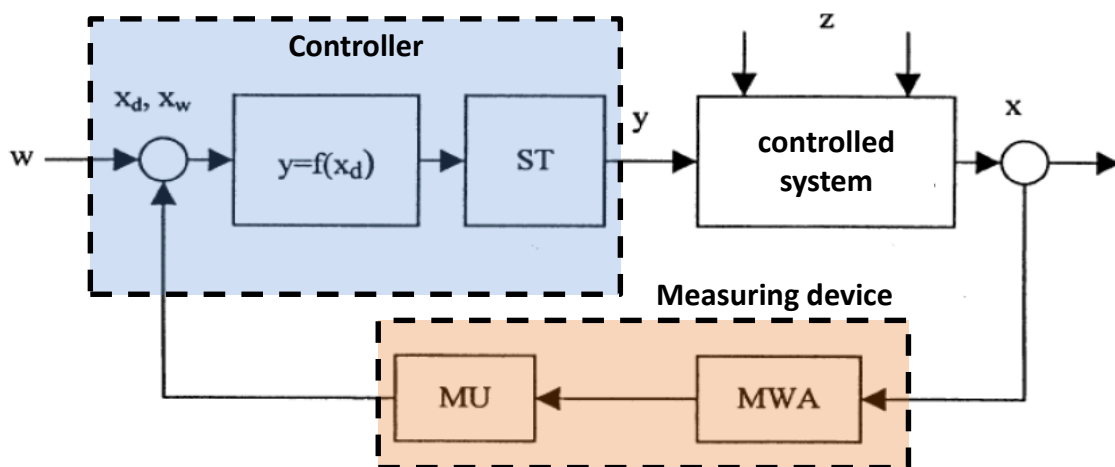


Figure 25: Control circuit (Rieberer, 2014)

The controller is responsible for compensating disturbances within the controlled system to keep the control deviation at a minimum on the one hand and to adjust the actuator to changes of the reference variable on the other hand. Therefore different control types are available that are thoroughly explained in Rieberer (2014).

Proportional-Controller (P-Controller) adjusts the control variable linearly with the proportionality factor K_p , see Equation 10. This linearity is only valid in a range around the operating point of the controller. It immediately reacts when a disturbance occurs but it is not able to compensate a disruption completely. If K_p is set high the control deviation will be smaller, the system is very likely to oscillate though.

$$y = y_0 + K_p \cdot x_d \quad \text{Equation 10}$$

Integral-Controller (I-Controller) affects the control deviation by being proportional to the speed of control (Equation 11). The impact of the I-Controller is steadily rising by a change of the process variable. It has no remaining deviation but it reacts slower than the P-Controller and is vulnerable to oscillations.

$$\frac{dy}{dt} = K_I \cdot x_d \quad y = y_0 + K_I \cdot \int x_d \cdot dt \quad \text{Equation 11}$$

By combining these controllers a **PI-Controller** is realised. It reacts fast to disturbances and has no remaining deviation. This controller is suitable for many controlled systems. With defining the reset time T_n , the equation for this controller is:

$$T_n = \frac{K_p}{K_I} \quad y = y_0 + K_p \cdot \left(x_d + \frac{1}{T_n} \cdot \int x_d \cdot dt \right) \quad \text{Equation 12}$$

If a differential element is added the **PID-Controller** is created. The differential element is defined as the rate of change of the control deviation, see Equation 13. With the definition of the derivative time T_v this leads to the controller equation (Equation 14). A PID-Controller has three parameters which dictate the behaviour of the controller. Those are the proportionality factor K_p , reset time T_n and derivative time T_v .

$$\Delta y_D = K_D \cdot \frac{dx_d}{dt} \quad \text{Equation 13}$$

$$T_v = \frac{K_D}{K_p} \quad y = y_0 + K_p \cdot \left(x_d + \frac{1}{T_n} \cdot \int x_d \cdot dt + T_v \cdot \frac{dx_d}{dt} \right) \quad \text{Equation 14}$$

In Figure 26 the step response of a PID-Controller is illustrated. The impact of the three different parts to the control variable are described in Samal and Becker (2000).

With the additional D-element the quality of the controller is increased. The control circuit is damped and the other parameters can be adjusted more aggressively. If the D-element is set too high the system tends to be unstable though. This makes it more difficult to find appropriate parameters that deliver good control behaviour altogether. For the control circuits of the heat pump cycle both PI- and PID-Controllers were used. As described above setting the parameters of the PID-Controller is very difficult. Therefore empirical methods were found to be able to get appropriate settings for the specific control circuit. The method that was used within this master thesis is the Chien Hrones Reswick scheme which is explained in Baur (2014). It is based on a step response that is done for the desired control circuit. From this step response special values are derived that can be used in a table to get the

parameters. This method is useful to find approximate values. A fine-tuning has to be done afterwards as those values are only valid for one operating point.

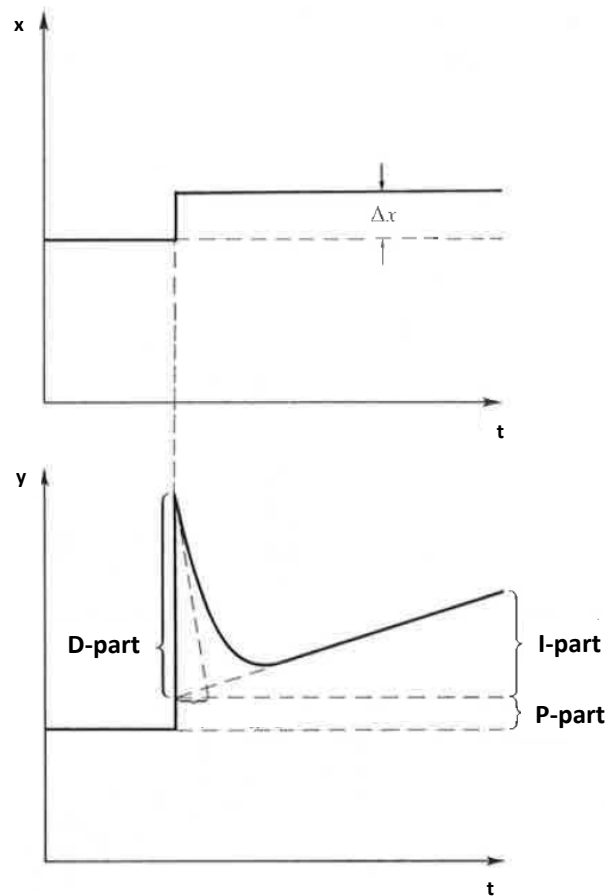


Figure 26: Step response of PID-Controller (Samal and Becker, 2000)

2.5. Heating curve

For the automation of the heat pump system the set point for the condenser outlet temperature on the water side is calculated by using a heating curve. The only information the controller gets, is the ambient temperature and if space heating is demanded. This information is obtained from a building simulation, where the heating demand of the building is calculated. The provided heating power of the heat pump system is adjusted to the actual demand of the building.

As described in Rieberer (2013) the heating curve (Figure 27) combines the ambient temperature with the inlet temperature of the heating system. At the lowest ambient temperature the maximum inlet temperature has to be reached. The progression of the curve depends on the building and the installed heating surfaces. Radiators with high inlet temperatures have steeper heating curves than a floor heating system with low inlet temperatures. In Figure 27 this is illustrated by the different values of A , shown on the right side. For example, the heating curve of $A=1.6$ demonstrates a heating system with radiators, whereas a value of $A=0.6$ represents a floor heating system.

Due to a better heat transfer to the room at higher inlet temperatures the functions are curved. The controller will steadily compare the real inlet temperature of the heating system

to the calculated and will adjust the heating capacity of the heat pump by adapting the compressor speed.

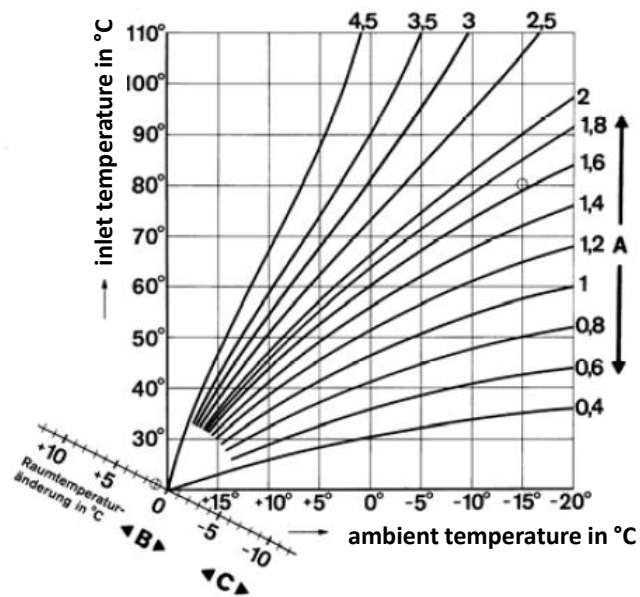


Figure 27: Heating curve (Rieberer, 2013)

3. DESCRIPTION OF THE TEST RIG

In Chapter 2 the functionality of the main parts of the heat pump cycle were described. This chapter gives an insight to the design and the components of the whole test rig as well as to the control of the heat pump.

3.1. Overview

The main parts of a heat pump cycle are the compressor, the heat exchangers and the expansion valve. Also the functionality of the liquid receiver, filter dryer and sight glass were already described theoretically. In Figure 28 the heat pump test rig with some of these components can be seen.

To simulate the heat source and sink of the heat pump two additional rigs were installed. As these test rigs are surrounding the heat pump they are called 'periphery' in the following chapters. The periphery was already available at the Institute of Thermal Engineering and had to be connected and adjusted to the heat pump test rig. A scheme of the whole test rig can be seen in Figure 29. The heat pump cycle is illustrated in the centre of the scheme, whereas the heat sink is connected to the condenser and desuperheater and therefore shown on top of the figure. At the bottom of Figure 29 the scheme of the heat source, which is directly connected to the evaporator, is depicted. The single parts of the test rig will be explained in detail later on.

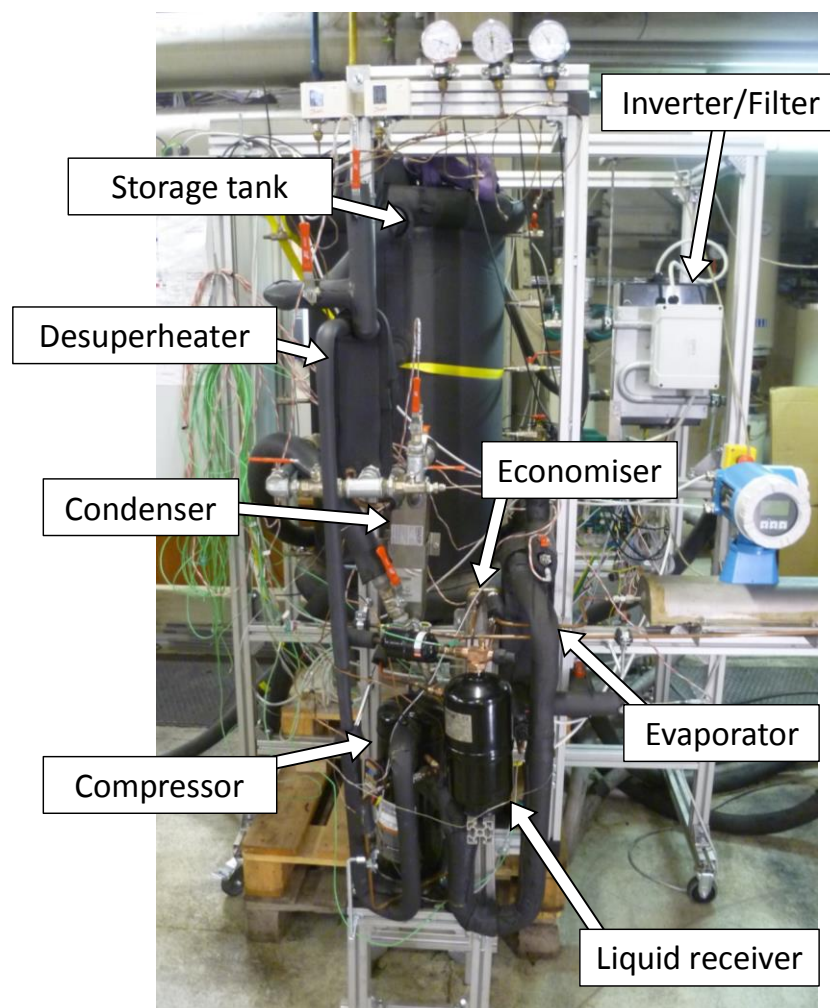


Figure 28: Test rig – Heat pump

3. DESCRIPTION OF THE TEST RIG

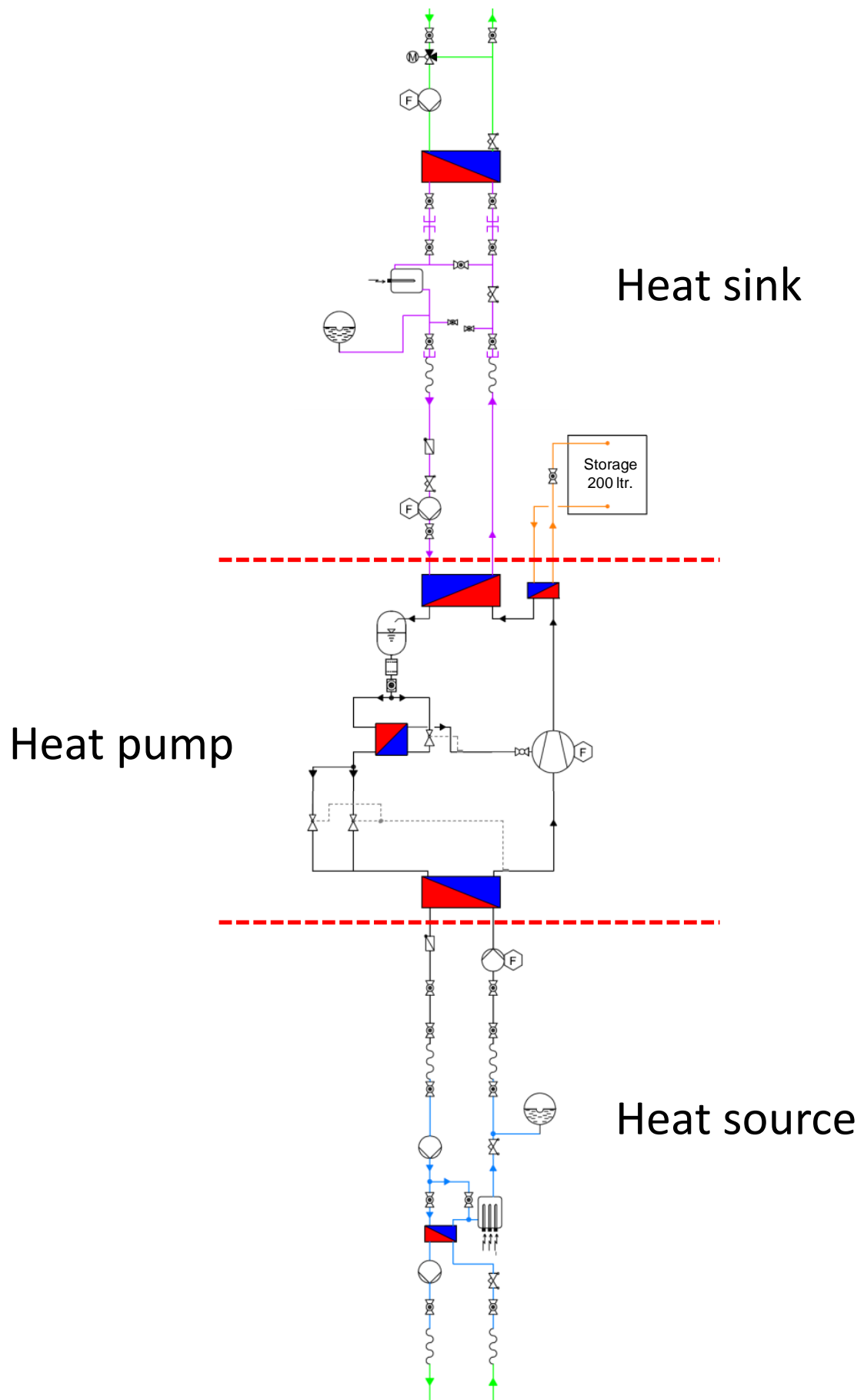


Figure 29: Scheme of whole test rig

3.2. Heat pump cycle

In this chapter, the main components of the heat pump cycle are described. Figure 30 shows the heat pump cycle as it was constructed for the experimental analysis. Besides the common components as compressor, condenser, main expansion valve and evaporator, also the components for the optimisation of the heat pump cycle as desuperheater, economiser and expansion valve for the injection mass flow are depicted. The liquid receiver, filter dryer and sight glass are positioned in the liquid line after the condenser and will be described in Chapter 3.2.5 and 3.2.6. The bubbles on the pipes show where the different measuring devices are positioned and also information about the dimensions of the copper pipes is given (DN04 to DN12).

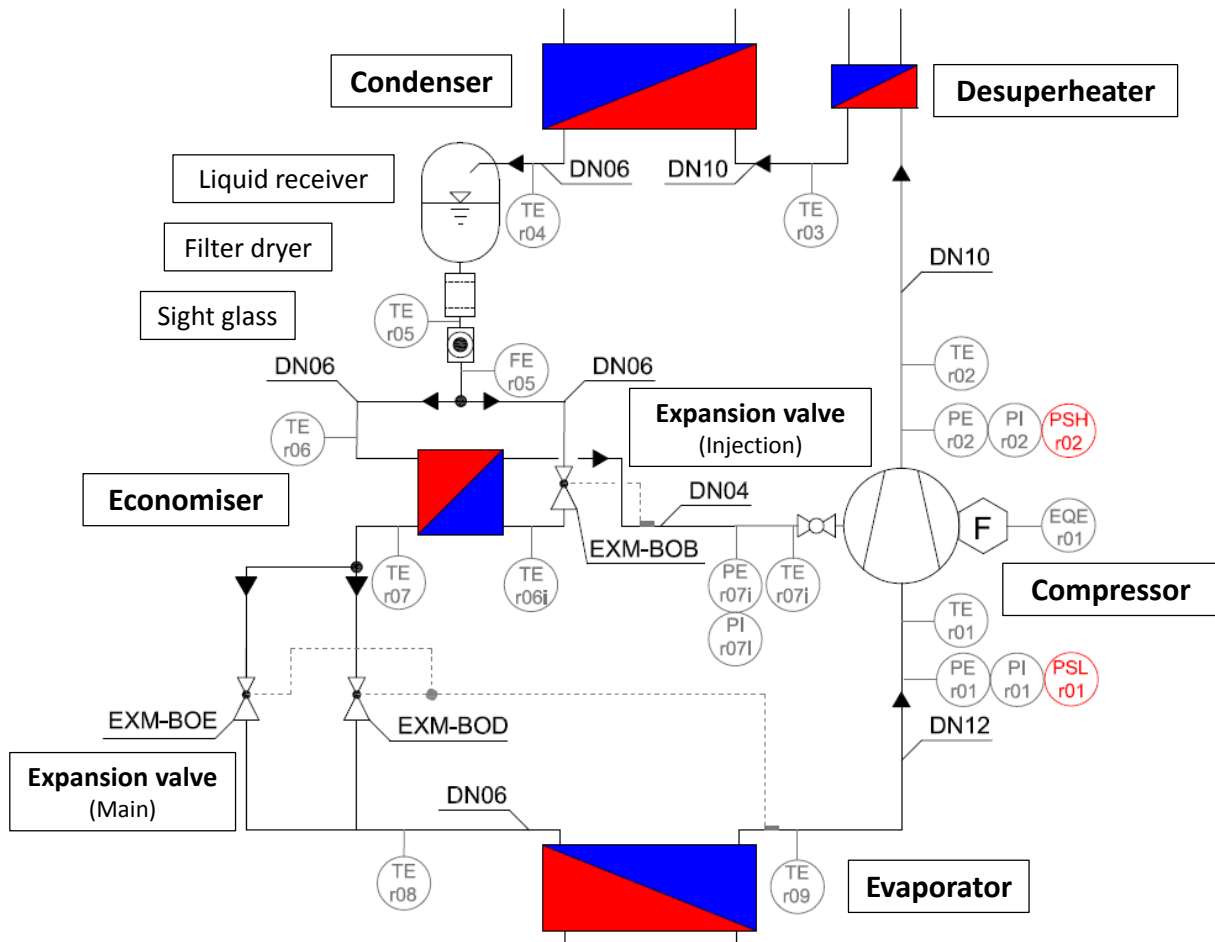


Figure 30: Heat pump cycle, scheme

3.2.1. Compressor

The scroll compressor of the test rig was provided by the company Emerson Climate Technologies. It is a speed controlled scroll compressor of Emerson's product series Copeland Scrolls. The benefits of controlling the speed of a compressor and of a vapour injection were already explained in Chapter 2.1.2.

Structural design

With a nominal heating capacity of 8 kW (at evaporation temperature $t_{evap} = -10\text{ }^{\circ}\text{C}$, condensation temperature $t_{cond} = 40\text{ }^{\circ}\text{C}$ and compressor speed $n_{comp} = 5700\text{ rpm}$) (Copeland, 2013b) this compressor is designed for a single or two-family-house. It has a

3. DESCRIPTION OF THE TEST RIG

maximum electrical input power of 4.4 kW ($t_{evap} = -5\text{ }^{\circ}\text{C}$, $t_{cond} = 60\text{ }^{\circ}\text{C}$, $n_{comp} = 7020\text{ rpm}$). The zeotropic HFC-mixture R410A is used as working fluid.

ZHW 08 K1 P – 1 E9 is the compressor type with the following denotation: (Copeland, 2011b)

- Z..... Scroll Compressor
- H Heat Pump (no Air-conditioning)
- W..... Variable speed and vapour injection
- 08 K..... Nominal heating capacity
- 1..... Model variation
- P Refrigerant R410A
- 1E9..... Motor version

In Figure 31 the shell of the compressor is illustrated on the left side. On the upper part the three copper ports for suction, vapour injection and discharge are positioned. To the left of the ports the power connector and on the right, the sensor connector are placed. In this area the scrolls of the compressor are placed. At the bottom of the compressor there is an oil sump with a centrifugal oil pump that provides the lubrication for the bearing system. In between those areas, the brushless electric motor is placed, as depicted in Figure 32. The bars to the left of Figure 31 show that the main part of the compressor is filled with suction gas during operation. This ensures cooling of the stator windings but also lubrication of the moving parts in this area, due to the refrigerant/oil-mixture.

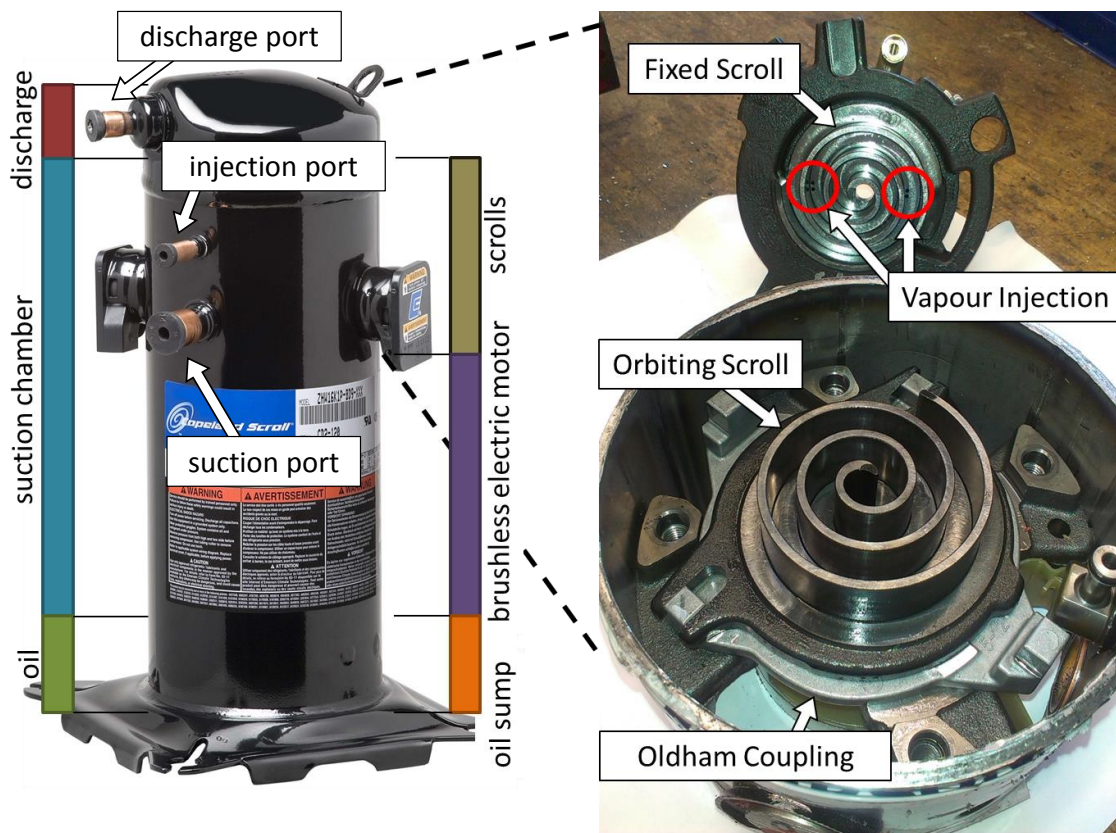


Figure 31: Scroll compressor ZHW 08 K1 P – 1 E9, left: Chassis (Copeland, 2011b), right: dismounted scrolls

The brushless permanent magnet motor rotates the shaft, which is connected to the orbiting scroll with a drive shaft and an eccentric bushing. The moving scroll makes circling motions and is kept in position by the Oldham coupling and its guiding pins. On the right picture of Figure 31, dismantled scrolls can be seen. The fixed scroll is mounted into the head of the compressor. Four boreholes are symmetrically arranged on the upper side of this scroll representing the vapour injection. The swept volume of the compressor is specified by the manufacturer with 2.8 m³/h and for the second stage with 1.99 m³/h at 50 Hz (see Chapter 5.1.2).

The discharge port is located at the centre of the fixed scroll. A floating seal separates the discharge and the suction chamber. It helps to increase pressure when the compressor is started. The check valve at the discharge port closes when the compressor is shut down to isolate the low pressure side (Copeland, 2011b).

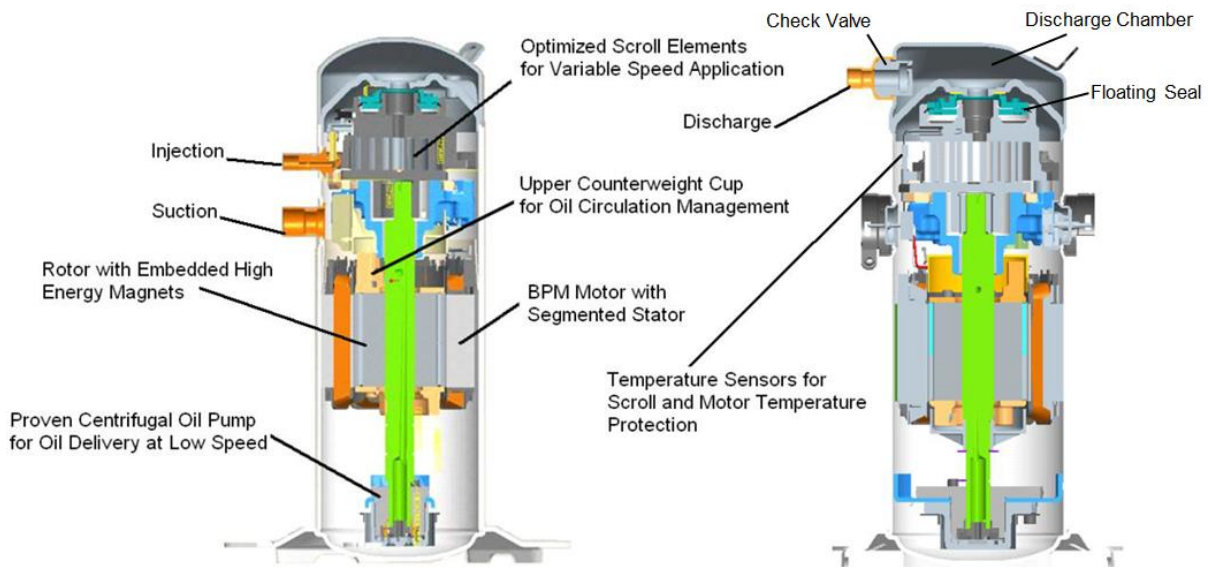


Figure 32: Cross sections of scroll compressor (Copeland, 2011b)

Two cross sections of the scroll compressor are shown in Figure 32. On the left, the section plane is at the suction and injection ports. At the bottom, a scheme of the centrifugal oil pump can be seen. It provides oil for the bearings for the whole speed range of the compressor (1800 to 7020 rpm). Above the oil pump, the brushless permanent magnet (BPM) motor is positioned. The rotor consists of permanent magnets and is placed around the shaft. The electromagnetic coils, representing the stator, are supplied via the power connector and are responsible for the rotation of the rotor.

The section plane on the right side of the figure is at the discharge port and the power and sensor connector. Behind the discharge port the check valve and the discharge chamber are placed. The floating seal separates the scroll outlet at the centre and the discharge chamber.

Envelope

Due to lubrication and the maximum electrical power input, the operating conditions of the compressor are limited. This leads to different operating ranges for different speeds that are called envelopes. The speed controlled compressor is not allowed to be operated out of these areas for a longer time than 20 minutes. Otherwise the compressor's software alarm system will shut it down.

The compressor envelopes for some compressor speeds are illustrated in Figure 33. The limits for the evaporation temperature are from $-30\text{ }^{\circ}\text{C}$ to $25\text{ }^{\circ}\text{C}$ and for the condensation temperature from $17\text{ }^{\circ}\text{C}$ to $65\text{ }^{\circ}\text{C}$. These limits vary with different compressor speeds and need to be considered during operation. In the left figure the envelopes for 1800, 3000 and 4500 rpm are depicted. With a speed of 1800 rpm, the minimum evaporation temperature is $-6\text{ }^{\circ}\text{C}$ and the maximum condensation temperature is about $55\text{ }^{\circ}\text{C}$. This area increases up to a speed of 4500 rpm. When this speed is exceeded the upper limit of the evaporation temperature decreases as can be seen on the right of Figure 33. At the maximum speed of 7020 rpm, the maximum evaporation temperature decreases to $-5\text{ }^{\circ}\text{C}$. The envelope can be extended for low evaporation temperatures (red triangle on the top left), if wet injection is accomplished. However, this was not executed within these measurements.

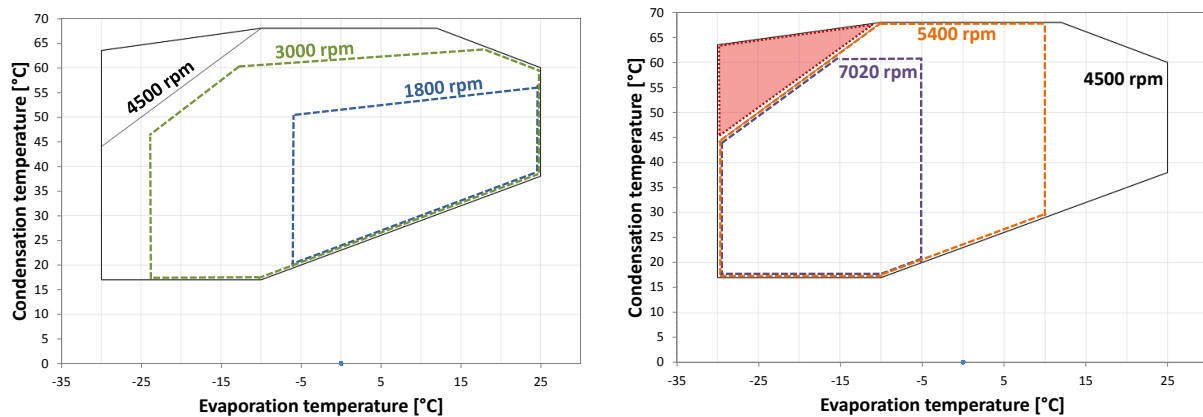


Figure 33: Envelopes, left: 1800 to 4500 rpm, right: 4500 to 7020 rpm (Copeland, 2013b)

Assembling

The used oil in combination with the refrigerant R410A is a polyolester (POE) lubricant of the type Emkarate RL 32-3MAF. The compressor oil is hygroscopic (Chapter 2.1.1) and therefore the ports are sealed with plugs until the refrigerant circuit is closed. When assembling the heat pump, the plugs are only allowed to be removed for short periods and the compressor should be brazed to the pipes at last. Thereby absorption of air humidity of the oil is prevented.

Another important aspect for the installation of the scroll compressor is that vibrations are brought into the system by the orbiting movement of the scroll. These vibrations are critical for several components of the system and can lead to damage of copper-brazed connections when the strain occurs over longer periods. The vibrations are initiated by the compressor, which means that they should be absorbed as close as possible to it. This is achieved by the following installations:

- The compressor is fixed to the test rig with four absorber grommets, which allow small movements.
- U-bends are installed into the piping straight before the inlet ports and after the outlet port. This makes the construction flexible within this area, where no other component shall be positioned. The U-bend is made from one piece of copper pipe, so that no brazed-connections are exposed to strong vibrations. In Chapter 3.4 the accomplished piping will be discussed.
- Although an improvement was achieved by these measures, there were still some pipes, especially longer sections with a rather small diameter that were suffering from vibrations

during the initial measurements. To eliminate those, the pipes were fixed to the test rig with pipe clamps, to make the construction stiffer at these particular positions.

All in all there will always be vibrations in the system that cannot be absorbed. In particular with a speed controlled compressor a broad range of frequencies is induced and different components respond to different frequencies. The compressor software provides an option, where a specific frequency band can be defined in which the compressor is not allowed to be operated because severe resonance can occur. In the used test rig no such frequency band was defined as no problems at a specific frequency were observed during the measurements.

3.2.2. Inverter drive

Using an inverter drive means having higher electrical energy consumption compared to a common compressor without speed control due to electrical conversion losses. Thereby a lot of heat is developed that needs to be removed from the drive as there is a temperature limit of maximum 65 °C for the electronics (Copeland, 2011b). If the board temperature exceeds this maximum the compressor is shut down.

One option to cool the inverter drive is to put an air-cooled aluminium finned heat exchanger on the back side of the inverter. To increase the heat convection over the fins, an electrically driven ventilator could be installed. However, this would lead to higher energy consumption of the compressor system. Another option is to mount a heat exchanger on the other side of the inverter. The cooling can either be realised with refrigerant gas from the evaporator outlet, water from the heating cycle or some other working fluid whose temperature is lower than 55 °C, to guarantee an appropriate cooling. It needs to be considered that condensation of air humidity on the heat exchanger could lead to damage of other components that are positioned below the inverter. So the temperature of the working fluid should be within a range from 15 °C to 55 °C. This cannot be reached when refrigerant is used for cooling purposes, but with water of the heating cycle.

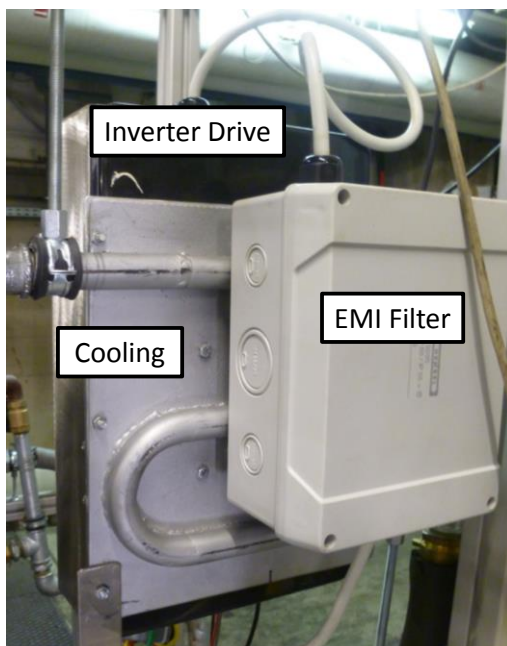


Figure 34: Inverter cooling

For this test rig the latter option was chosen, as the return of the space heating cycle has a nominal temperature of 30 °C and the additional electrical energy consumption due to the pressure drop over the heat exchanger is small compared to the overall pressure drop of the heat sink. Additionally the heat is used in the system and is not just removed from it, as the water inlet temperature to the condenser is increased.

In Figure 34 the cooling system is illustrated. At the back the inverter is installed on the heat exchanger, which is accomplished as a coiled pipe that is welded onto an iron plate. The welding seam increases the heat transfer from the plate to the water in the pipe, due to an increase of the heat exchange area. As also the electro-magnetic interference (EMI) filter generates some heat, it is positioned on the other side, directly on the coiled pipe. Both the inverter drive and the EMI filter are provided with a casing for protection reasons. In Figure 41 it is shown how the inverter cooling is embedded into the water cycle of the condenser.

3.2.3. Heat exchanger

In this heat pump cycle (Figure 30) four heat exchangers are necessary. Additionally to evaporator and condenser, a desuperheater and an economiser are installed. During the system test the desuperheater is used for domestic hot water (DHW) preparation simultaneously to the low-temperature level of the condenser. When the condenser is used for space heating at about 35 °C, the heat provided by the desuperheater can be charged into the thermal energy storage (TES). The economiser is an internal heat exchanger that evaporates and superheats the injected refrigerant vapour and on the other side subcools the liquid refrigerant. The heat exchangers were selected for the design operating point which is in this case a heating capacity of 5 kW, at the evaporator a brine inlet temperature of -10 °C and at the condenser a water outlet temperature of 35 °C (B-10W35). This design point was chosen, as unglazed solar collectors are considered as heat source of the heat pump. Thereby a brine circuit connects the collectors, which use ambient air as heat source, with the evaporator of the heat pump cycle.

In the diploma thesis of Baur (2014) the brazed plate heat exchangers were analysed and optimised. The optimisations are also used for this test rig, leading to the heat exchangers in Table 2. The condenser was optimised by increasing the number of plates. This leads to a reduced minimum temperature difference between the condensation and water temperature.

Table 2: Heat exchangers (Baur, 2014)

Heat exchanger	Type	No. Plates [-]	Area [m ²]	Power @ B-10W35 [kW]
Evaporator	SWEP B8TH	30	0.644	3.51
Condenser	SWEP B8TH	40	0.874	5.30
Desuperheater	SWEP B8TH	10	0.184	1.25
Economiser	SWEP B8TH	6	0.092	0.76

For the installation of the heat exchangers the configuration of the ports has to be considered. The heat exchangers have an arrow on the front plate. When the arrow faces upwards, the ports on the left side have one channel less than those on the right side. So the right ports have the first and the last channel of the heat exchanger. This assures that the refrigerant is always surrounded by the fluid of the heat source or heat sink, when it is connected to the left ports, which reduces the heat loss of the heat exchanger. In Figure 35 on the left, the port connections of the evaporator can be seen. After the expansion valve the expanded refrigerant flows into the lower left port and the suction gas leaves the heat exchanger on the upper left port. The brine is connected to the right ports. On the right of this illustration, the ports of the condenser are shown. Here the discharged gas enters the heat exchanger on the upper left port and heat is rejected until liquid refrigerant exits the lower port. The configuration of the desuperheater is the same as for the condenser.

An additional installation was made at the evaporator inlet. To improve the distribution of the two-phase refrigerant to the single channels of the evaporator a distribution pipe was installed. The pipe (Figure 36) was modified by Baur (2014) as the previous variant had one row with 14 boreholes (diameter of 1.6 mm) and caused a high pressure drop over the evaporator. The modified pipe has two additional rows (3 rows with 14 boreholes having a diameter of 1.6 mm each), to improve the distribution within the channels.

At first only the desuperheater and the evaporator were insulated due to heat losses and formation of condensate. Also the pipes to and from these heat exchangers were insulated. With this insulation all the measurements were carried out. During the measurements also at the economiser formation of condensate occurred at certain operating points. Therefore also this heat exchanger including the pipes was insulated (see Figure 45 right). The condenser

was not insulated as its temperatures are not far away from ambient temperature for most operating conditions and the heat losses are assumed to be small.

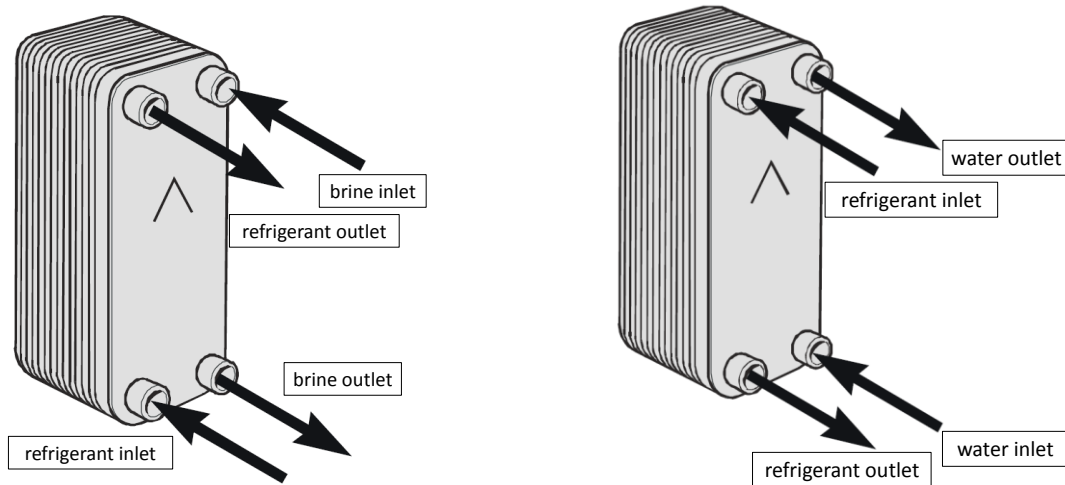


Figure 35: Port configuration, left: evaporator, right: condenser (SWEF, 2014)



Figure 36: Distribution pipe of evaporator

3.2.4. Expansion valves

The electronic expansion valves were also provided by Emerson. The control of the valves is done by the superheat and envelope controller (SEC) of the compressor. A main conclusion of the diploma thesis of Baur (2014) was that the expansion valves were oversized and were operating at a minimum opening degree, as the heat pump system was operated at lower heating capacities. Also the software of the SEC did not allow setting a superheating set point below 5 K. As controlling the superheat of the suction gas to a minimum is a key point to gain a higher Coefficient of Performance (COP), it was very important to improve this. Therefore, a new software for the SEC was provided by Emerson, allowing to set a minimum superheat set point of 3 K for both the main and vapour injection expansion valve. Nevertheless, all measurements were performed with a superheating of 5 K, as smaller values resulted in oscillations of the heat pump control.

The test rig was built to be able to test the old expansion valve EXM-BOE as well as the new EXM-BOD. They were installed in parallel and by switching the solenoid coils each of the valves could be tested individually (see Figure 30). In Figure 37 the arrangement is illustrated. The subcooled liquid refrigerant flows out of the economiser (Eco LO), is expanded in one of the valves and flows afterwards to the evaporator (Evap In). Tests showed that, at lower capacities, the EXM-BOD has a higher opening degree than the EXM-BOE. A reason for this is that the EXM-BOE was designed for a heating capacity of 13.7 kW and the EXM-BOD for a capacity of 11.6 kW. This is an improvement for the control of the expansion valve, as the control becomes worse with low opening degrees. The heat pump

mainly operates at heating capacities of 5 kW, so the EXM-BOD was used for all measurements. When the heat pump was reconstructed for the system tests, the EXM-BOE was removed from the test rig. The expansion valve for the injection (EVI) was also oversized at first, as the EXM-BOD was used. In this test rig the EXM-BOB with a capacity of 5.5 kW (Alco Controls, 2012) was installed. As can be seen in Figure 37 the liquid refrigerant is expanded in the EVI and the vapour is afterwards superheated in the economiser (Eco VI), before it is injected into the compressor.

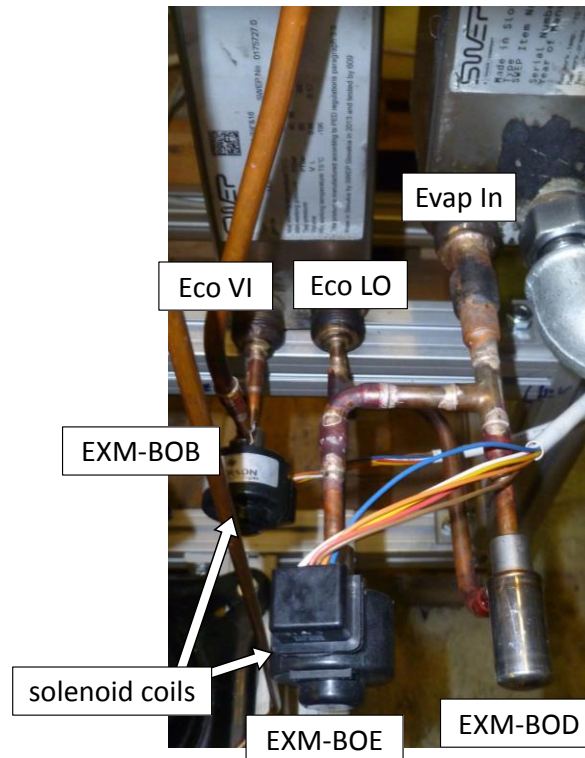


Figure 37: Expansion valves

The pipes on the liquid side of the expansion valves need to be accomplished as smooth as possible, to keep the pressure drop low. Otherwise vapour bubbles could develop, leading to problems with the control of the expansion valves. On the low pressure side of the valves, the pipes should go straight into the heat exchanger, as turbulence is still high which leads to a better distribution of the refrigerant within the channels. The maximum distance between the expansion valve and the inlet port of the plate heat exchanger should be 200 mm. To guide the pipe upwards is not allowed as an additional pressure drop would occur. For the control of the expansion valve a temperature sensor is required. To keep the response time of the control circuit at a minimum at the one hand and ensure a non-stratified flow after the heat exchanger on other hand, the distance between sensor and outlet port of the heat exchanger should be within 400 to 600 mm. These guidelines are explained in Copeland (2011a) and are depicted in Figure 38.

3.2.5. Liquid receiver

The volume of the liquid receiver, Klimal FM 2.3, is 2.3 litres and it has no sight glass installed. It is designed for a maximum pressure of 45 bar. Although this type of liquid receiver has no sight glass, it is recommended to have one, to be able to check the fluid level. Without sight glass, the right amount of refrigerant can only be checked by analysing the behaviour of the heat pump cycle, as described in Chapter 2.1.5 with Figure 16.

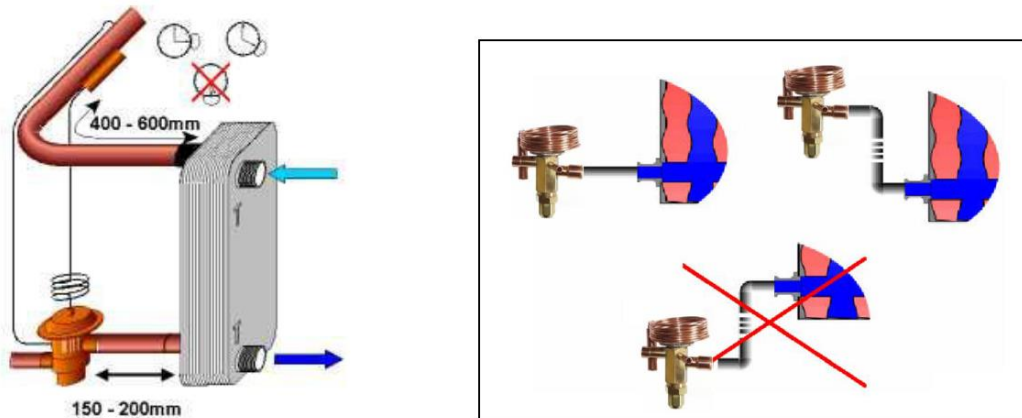


Figure 38: Positioning of expansion valve (Copeland, 2011a)

3.2.6. Filter dryer

In this test rig a DML 083s from Danfoss was installed as filter dryer (Figure 39). It consists of a molecular sieve that is able to achieve both functions described in Chapter 2.1.5. The dimension of the filter dryer can either be chosen by the amount of refrigerant and therefore the water absorption capacity of the dryer or the heating capacity of the system. It was decided to oversize the filter dryer, as it was planned to reconstruct the system after the measurements and therefore the cycle would be opened for a certain period of time. Danfoss (2008) describes that a lower velocity of the streaming refrigerant leads to a decreased pressure drop over the filter dryer. Additionally the lower speed also improves the process of absorption of the molecular sieve.

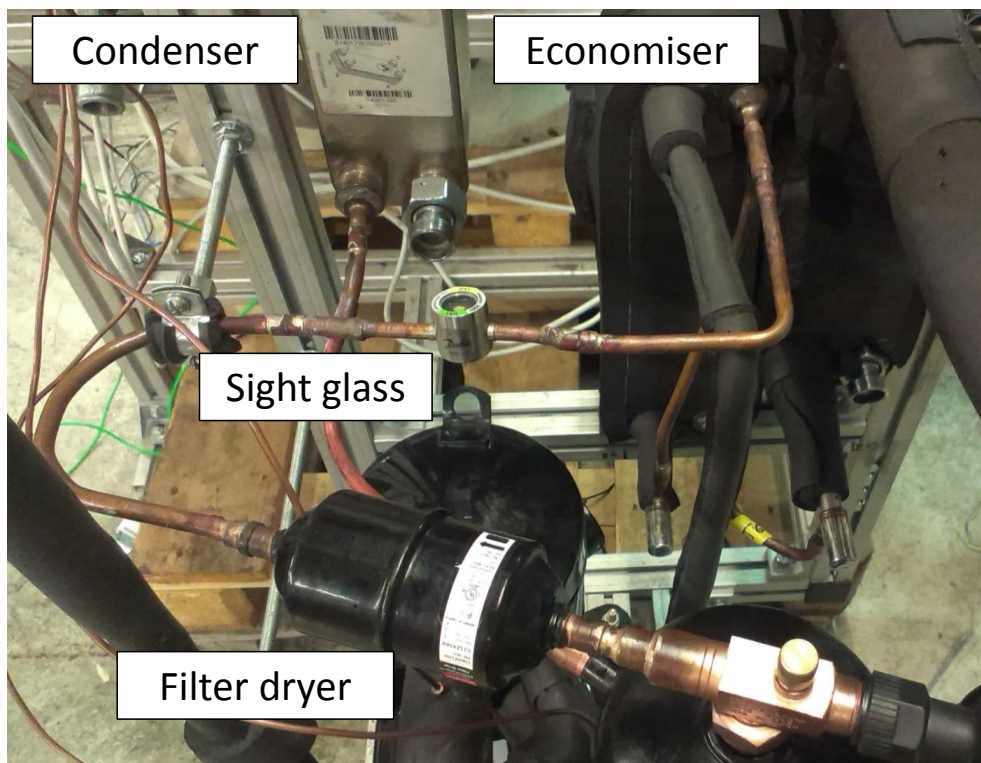


Figure 39: Filter dryer and sight glass

3.2.7. Pipes

A general description of the design of pipes is given in Chapter 3.4 where the given conditions for the test rig are explained. However, there are a few more aspects that have to be considered for the construction of a heat pump cycle.

First of all, the entire components of the high pressure side of the heat pump cycle have to sustain the maximum pressure of the system. With R410A as working fluid, the critical pressure of 49 bar is at a rather low temperature of 72 °C and the components should not be exposed to a higher pressure than 45 bar. The maximum pressure in the system depends on the used refrigerant. When dimensioning the pipes of the heat pump cycle, pressure drop and oil return need to be taken into consideration. In Pohlmann (2010) the correlation of these aspects is described. Larger diameters lead to a minimised pressure drop within the system which leads to a lower power input of the compressor. On the other hand it needs to be assured that the oil that circulates with the refrigerant is able to return to the compressor for lubrication. Especially in rising pipes at the suction and discharge line a minimum velocity of the refrigerant-oil mixture has to be guaranteed. These two conditions are diverging and therefore are optimised. In Figure 30 the inner diameters for the different pipe lines are illustrated (e.g. DN10). The suction line has an inner diameter of 12 mm as here the lowest density of the gaseous refrigerant occurs. In the discharge pipe a diameter of 10 mm was chosen and the whole liquid line is accomplished with 6 mm. As the injection pipe only transports a reduced mass flow its diameter is 4 mm.

To prevent the formation of oxide scale during brazing it is necessary to purge the pipes with dry nitrogen. Otherwise the scale could lead to damage of the compressor scrolls, clogging of an expansion valve or to a high pressure drop of the filter dryer within a short time.

3.3. Periphery

The heat pump test rig has to be able to simulate different operating points to analyse the behaviour of the heat pump cycle over the whole envelope of the compressor. This is achieved by providing a specific temperature at the inlet of the condenser and the evaporator. The condensation and evaporation temperature of the refrigerant cycle are mainly depending on these 'secondary' temperatures and the design of the heat exchangers.

3.3.1. Heat source

The 'mobile heat source' system used in the tests is shown in Figure 40. On the left side the scheme of the mobile heat source is illustrated. With a maximum heating power of 18 kW (3 electrical heating rods with 6 kW each) the ground source is simulated. The heating rods are installed into a reservoir of 35 litres. A control valve (STAD DN 25) and an expansion tank with a volume of 12 litres are placed on this rack. The speed controlled circulating pump (Wilo Stratos 25/1-8) that provides the brine mass flow rate (1078 kg/h for all steady state measurements) is installed on an additional construction on which the volume flow rate (FE b02) is measured by a magnetic inductive flow meter (Endress + Hauser, Promag 50P, DN15). Two Pt-100 temperature sensors are used to measure the inlet (TE b01) and outlet temperature (TE b02) at the evaporator.

A glycol/water mixture (Antifrogen N), as described in Chapter 2.1.6, is used as brine. The control of the heating rods and the circulation pump is embedded into the LabVIEW-Software (LabVIEW, 2012). One heating rod is continuously variable whereas the other two rods can only be operated in on/off-mode. This allows controlling a continuous heating capacity from 0 to 18 kW.

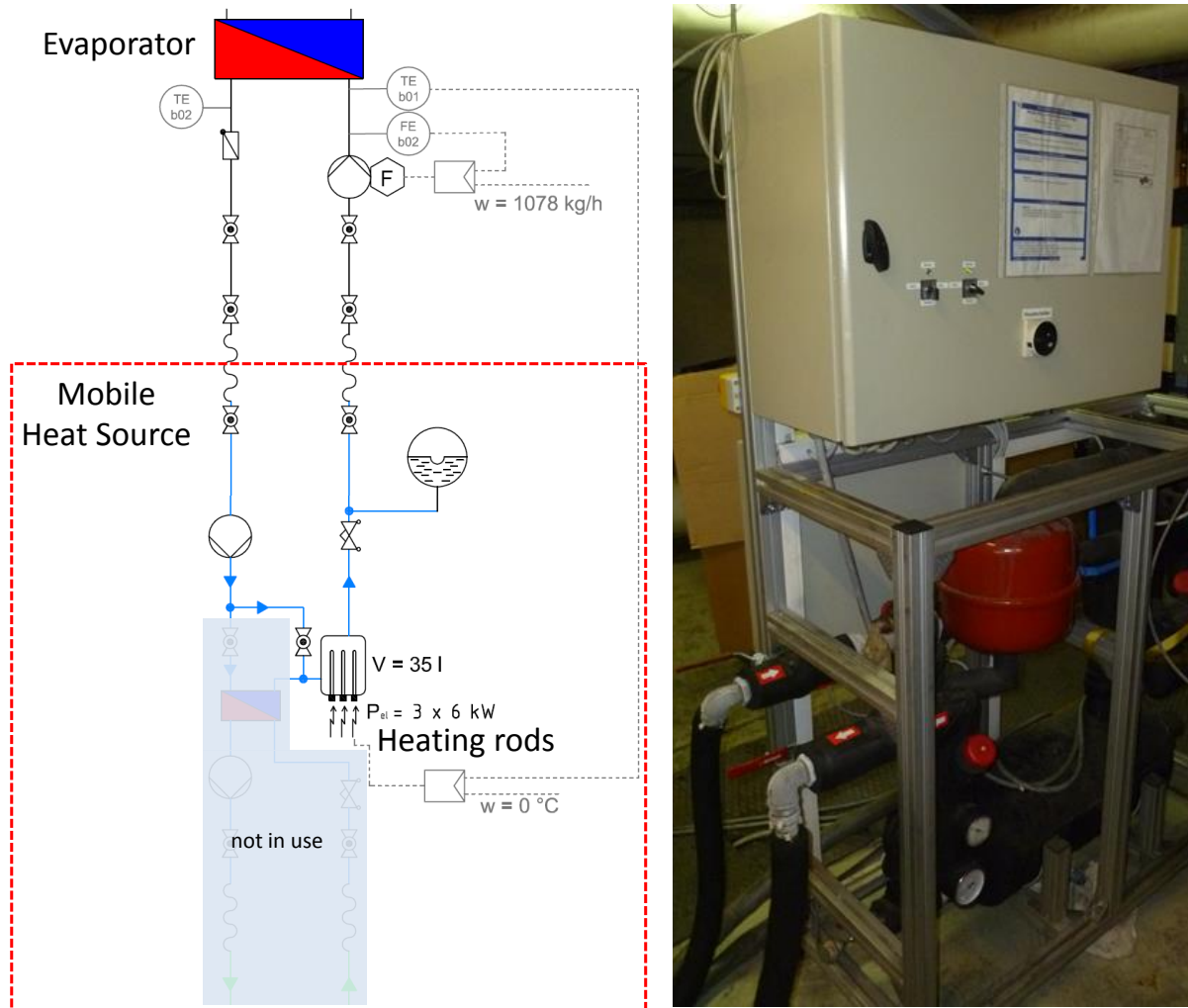


Figure 40: 'Mobile heat source', left: scheme; right: picture

3.3.2. Heat sink

To simulate the space heating and the domestic hot water preparation, a heat sink is necessary. The Institute of Thermal Engineering (IWT) provides a cooling tank which was kept at a constant temperature of 10 °C over the whole measuring period. For the connection of the tank with the heat pump test rig a 'mobile heat sink' is used. On this heat sink a heat exchanger is placed that rejects heat from the condenser cycle to the cooling tank of the system, which is filled with a glycol/water-mixture. For the control of the cooling capacity there is a speed controlled circulating pump in the system cycle. The control variable of the cooling capacity is the inlet temperature of the condenser (TE w01). To make the control circuit more dynamic another temperature sensor (TE r10) was placed directly at the outlet of the heat exchanger of the system and replaced the TE w01 as control variable. Although the circuit regulated much faster, there is a slight temperature offset to the inlet of the condenser which is compensated manually.

Additionally there is a control valve (STAD DN 25) and an expansion tank with a volume of 12 litres installed on the rack. The possibility to pre-heat the water with the installed electrical heating rod was not used for the described measurements. The scheme of the heat sink is illustrated in Figure 41, whereas a picture is shown in Figure 42 on the left.

3. DESCRIPTION OF THE TEST RIG

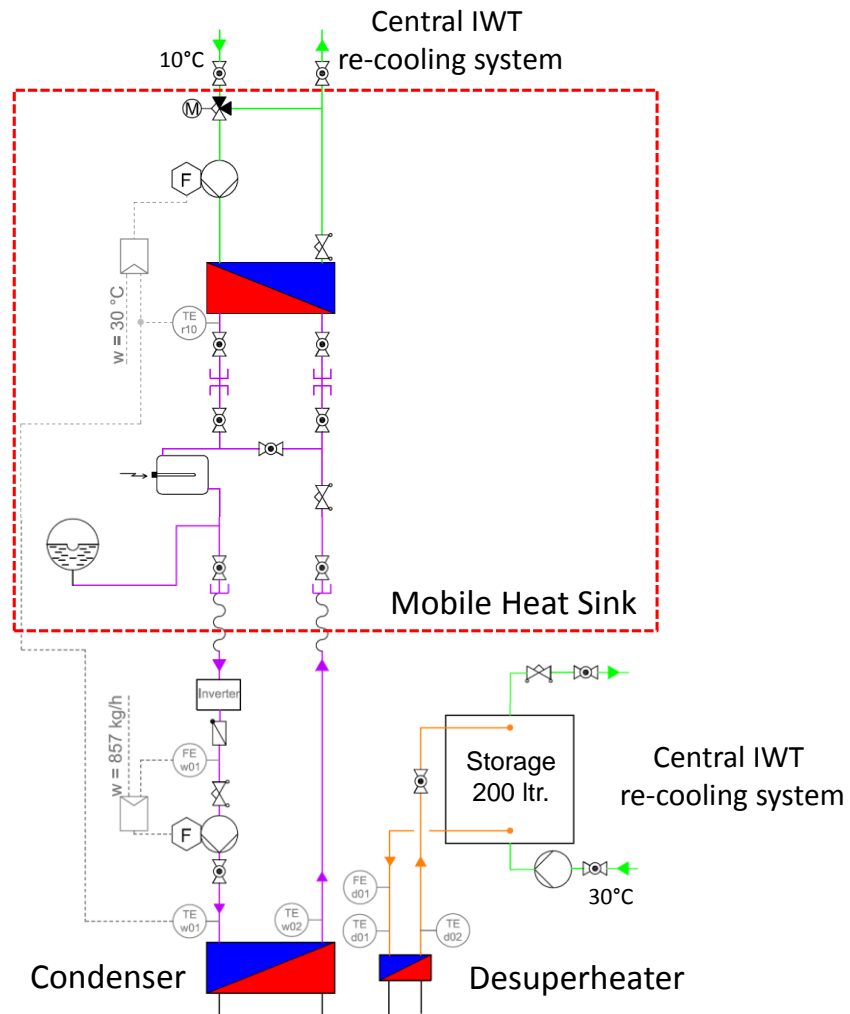


Figure 41: Heat sink, scheme



Figure 42: left: 'Mobile heat sink'; right: Desuperheater storage tank

The water flow rate through the condenser is measured by a magnetic inductive flow meter (Endress + Hauser, Promag 50P, DN15) (FE w01) which is positioned on an additional rack. Also the speed controlled circulation pump (Wilo Stratos 25/1-8) is placed on this rack. The pump provides a constant mass flow rate of 857 kg/h for all steady state measurements. Inlet (TE w01) and outlet temperature (TE w02) of the condenser are measured with two Pt-100 temperature sensors directly at the ports of the heat exchanger.

The desuperheater is realised as a heat exchanger with natural circulation. For this application a storage tank with a volume of 200 litres is installed, which is illustrated in Figure 42 on the right. The heights of the inlet and outlet ports are the same as those in the overall system tests, which were optimised with simulations by the project partner. For cooling purposes the tank is connected to the thermal system of IWT which provided a temperature of about 30 °C for all measurements. This temperature will not be the same for the system tests as both condenser and desuperheater will be connected to the same hydraulic system. However, for the functionality and performance tests that were accomplished in this master thesis the inlet temperature of the desuperheater is reasonable. Moreover, linking the two hydraulic systems would have led to control problems as the volume of the storage tank significantly influences the dynamics of the control.

The inlet (TE d01) and outlet temperature (TE d02) of the desuperheater are measured directly at the ports of the heat exchanger. At first the volume flow rate of the natural circulation was detected with a magnetic inductive flow meter (IFM, SM6004, DN15) which has a high accuracy at low flow rates. However, a high pressure drop came along with the small inner diameter (12 mm) of the measuring device leading to an unrealistic low mass flow rate. So it was decided to disassemble the flow meter in order to achieve a higher mass flow rate. On the other hand the heating capacity of the desuperheater has to be calculated over the refrigerant cycle which leads to a high uncertainty of measurement for the mass flow rate and heating capacity, see Chapter 5.4.

3.4. Design of test rig

The hydraulic optimisation is one potential improvement of the heat pump system. This is realised by coupling the heat pump to the thermal energy storage system, which was investigated and realised by the project partner SPF (Institute of Solar Technology). So the design of the heat pump test rig was strictly linked to the interfaces between the storage system and the heat pump. There are several key aspects that had to be achieved to fulfil the requirements.

One aspect is the stratification of the TES. Therefore, the desuperheater has to be placed at a higher level. The inlet port of the storage is placed at a height of 1750 mm, which is at the top of the TES. The outlet port is placed at a height of 1150 mm. As it can be seen in Figure 43 the desuperheater is placed 200 mm below the upper and 100 mm above the lower port of the storage. The difference in height is proportional to the pressure difference leading to natural circulation. These differences in altitude ($\Delta H_{DES} = 300 \text{ mm}$ and $\Delta H_{tank} = 600 \text{ mm}$) were defined by SPF. In the system test the whole thermal energy storage with a capacity of 763 litres is analysed. The installed storage tank provides a volume of 200 litres for testing the natural circulation of the desuperheater.

The condenser is placed below the desuperheater for a compact design and minimising the length of the copper pipes.

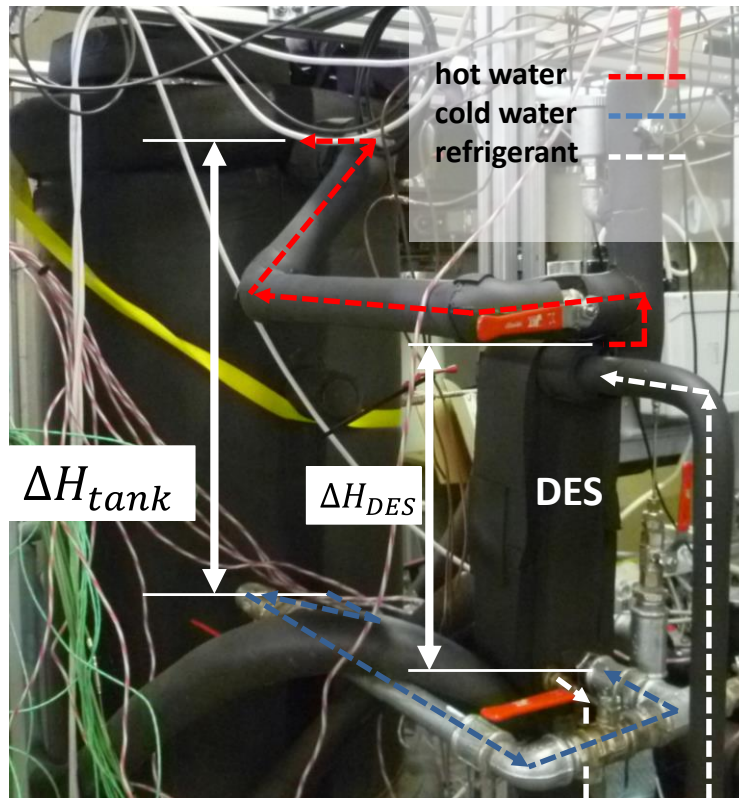


Figure 43: Desuperheater inlet and outlet ports

Another aspect is the insulation of the TES. To reduce the heat losses of the storage, for the overall system test at SPF a vacuum insulated panel (VIP) is accomplished on the upper third of the storage. This insulation minimises the heat losses of the upper, and therefore hotter volume of the storage. As the VIP is more expensive than commonly used insulation material it is necessary to install the heat pump as close as possible to the storage, to reduce the amount of VIP. So there is a maximum distance from the storage to the outer boundary of the heat pump which is not allowed to be exceeded. Also other components for the solar heating system are placed close to the heat pump and the thermal energy storage which has to be considered. This leads to a very compact design of the system and to vertically arranged components.

When the thermal energy storage is fully loaded it has a temperature of up to 95 °C. This means that also the components of the heat pump are faced with high temperatures. As the critical pressure is already reached at a temperature of 72 °C some components of the low pressure side could be damaged. To prevent this, the liquid receiver is placed outside of the vacuum insulation. This is realised by positioning the liquid receiver as low as possible and putting the receiver outside of the insulation. However, the low position of the liquid receiver is disadvantageous regarding the pressure drop in the liquid line. The pressure drop in the liquid line should be kept as small as possible, as the expansion valves should always face liquid refrigerant on the high pressure side, as described in Chapter 3.2.4. Therefore the piping of the liquid line was realised as a falling pipe and all components after the liquid receiver were positioned below it.

So the construction of the heat pump cycle is strictly regulated by the conditions described above. Only if these aspects are assured, the guidelines of Chapter 3.2.7 can be realised:

- Installing the copper piping as smooth as possible to reduce pressure drop.
- Positioning of measurement equipment within or next to the test rig. Further explanation in Chapter 3.5.
- The three connection pipes to the compressor are accomplished as U-bends, see Figure 44. This isolates the other components from the compressors vibrations. Additionally some pipe clamps are installed to reduce the vibrations of the heat pump cycle.

In Figure 45 on the left, the 3D heat pump model (inclusive tank, which is used only at SPF), which was elaborated by the working group of IWT and SPF, is illustrated. On the right, a photo of the constructed heat pump is depicted. In these illustrations the hydraulic components are not shown that only the refrigerant cycle can be seen.



Figure 44: U-bend for preventing vibrations

3.5. Measuring equipment

For the test rig it is necessary to keep the influence of the measuring equipment to the refrigerant circuit as small as possible. Therefore all temperature sensors are installed as contact sensors ('clamp-on'). Thus it is possible to design the piping of the heat pump smoother, as no further installations for the in-stream measurements are needed. However, it makes the control of the system more slowly as the temperature is detected on the surface of the copper pipes instead of directly in the flow of the refrigerant. For measurements of operating points steady state conditions have to be provided and even the dynamic measurements have only moderate changes of temperatures, as the simulated heating profiles correspond to realistic temperature changes over a day. This leads to a sufficient measurement of the temperature by the contact sensors for this application. The temperatures of the heat sink and source are measured in-stream. Guidelines for the installation were already given in Chapter 2.2.1.

The mass flow rate of the refrigerant is measured with a Coriolis mass flow meter and the volume flow rate of brine and water are detected with a magnetic inductive flow meter. The pressure transmitters that are necessary to control the compressor, and which are part of the

integrated Copeland system, are also used for the measurements. In Figure 30 the positions of the measurement devices of the refrigerant circuit are illustrated. Those of the heat sink and source cycle are shown in Figure 40 and Figure 41. The bubbles mark the position of the device and the abbreviation represents its type and consecutive number. The abbreviations are described in the following Table 3: In Table 4 all measurement devices are listed.

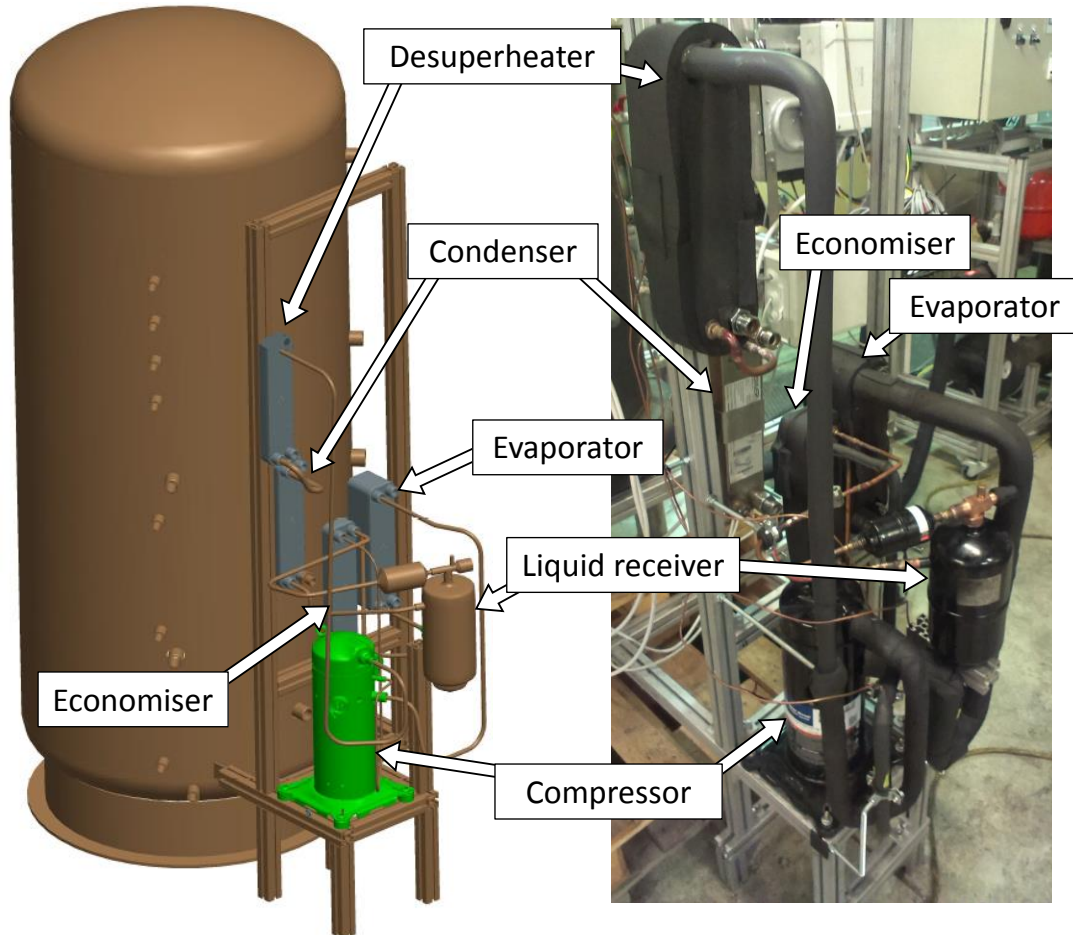


Figure 45: Heat pump test rig left: 3D model (Haller and Mojic, 2014); right: construction

Table 3: Encoding of measurement devices

Physical variable	
TE temperature sensor	PI.....pressure indicator (analog)
FE flow measuring sensor	PSH.....pressure switch (high)
PE pressure sensor	PSLpressure switch (low)
EQE electrical energy meter	
Working fluid	Index
r..... refrigerant	i injection
w water	d desuperheater
b..... brine	

3. DESCRIPTION OF THE TEST RIG

Table 4: Measuring devices

Code	Physical variable	Unity	Position	Measuring device	Measurement range	Max. error of measurement
Heat pump						
TE_r01	Temperature	[°C]	Compressor suction	Thermocouple Type K	-20 to 20 °C	±0.15 K
TE_r02	Temperature	[°C]	Compressor discharge	Thermocouple Type K	40 to 95 °C	±0.15 K
TE_r03	Temperature	[°C]	Desuperheater outlet	Thermocouple Type K	40 to 95 °C	±0.15 K
TE_r04	Temperature	[°C]	Condenser outlet	Thermocouple Type K	20 to 70 °C	±0.15 K
TE_r05	Temperature	[°C]	Liquid line - filter dryer	Thermocouple Type K	20 to 70 °C	±0.15 K
TE_r06	Temperature	[°C]	Liquid line - Economiser inlet	Thermocouple Type K	20 to 70 °C	±0.15 K
TE_r06i	Temperature	[°C]	Injection line - Economiser inlet	Thermocouple Type K	20 to 70 °C	±0.15 K
TE_r07	Temperature	[°C]	Liquid line - Economiser outlet	Thermocouple Type K	20 to 70 °C	±0.15 K
TE_r07i	Temperature	[°C]	Compressor injection	Thermocouple Type K	20 to 70 °C	±0.15 K
TE_r08	Temperature	[°C]	Evaporator inlet	Thermocouple Type K	-20 to 20 °C	±0.15 K
TE_r09	Temperature	[°C]	Evaporator outlet	Thermocouple Type K	-20 to 20 °C	±0.15 K
PE_r01	Pressure	[bar]	Compressor suction	Pressure Transmitter – PT5-18T	0 to 18 bar	0.14 bar
PE_r02	Pressure	[bar]	Compressor discharge	Pressure Transmitter – PT5-50T	0 to 50 bar	0.4 bar
PE_r07i	Pressure	[bar]	Compressor injection	Pressure Transmitter – PT5-30T	0 to 30 bar	0.16 bar
FE_r05	Mass flow	[kg/s]	Liquid line	Promass 83A DN4	0 to 200 kg/h	±0.1 % o.r.
EQE_r01	Electrical meter	[Wh]	Compressor, Inverter, SEC	AC-meter - AAD1	0 to 17 A/230 V	1 %
Heat source						
TE_b01	Temperature	[°C]	Evaporator inlet	Pt-100	-20 to 20 °C	±0.06 K
TE_b02	Temperature	[°C]	Evaporator outlet	Pt-100	-20 to 20 °C	±0.06 K
FE_b01	Volume flow	[m ³ /s]	Evaporator inlet	Promag 50P DN15	400 to 1200 l/h	±0.5 % o.r.
Heat sink						
TE_w01	Temperature	[°C]	Condenser inlet	Pt-100	20 to 70 °C	±0.06 K
TE_w02	Temperature	[°C]	Condenser outlet	Pt-100	20 to 70 °C	±0.06 K
TE_d01	Temperature	[°C]	Desuperheater inlet	Pt-100	40 to 95 °C	±0.06 K
TE_d02	Temperature	[°C]	Desuperheater outlet	Pt-100	40 to 95 °C	±0.06 K
FE_w01	Volume flow	[m ³ /s]	Condenser inlet	Promag 50P DN15	300 to 1000 l/h	±0.5 % o.r.

(o.r. = of reading)

3.5.1. Temperature sensors

All temperature sensors in the refrigerant cycle were realised as contact sensors. The guidelines for the installation of contact sensors were already shown in Figure 19. Thermocouples of Type K with a sensor head diameter either 1.5 mm or 1.0 mm were tightened with wire straps to the pipes. Those straps have to be fixed at the measuring point for a tight contact with the pipe. In Figure 46 the strap at the measuring point is not illustrated for visualising reasons. To prevent air inclusion between the sensor head and the uneven surface of the pipes, which would lead to a lower heat conduction, heat-conductive paste is applied. For pipes that are not insulated an additional insulation was mounted around the sensor to diminish environmental influences.

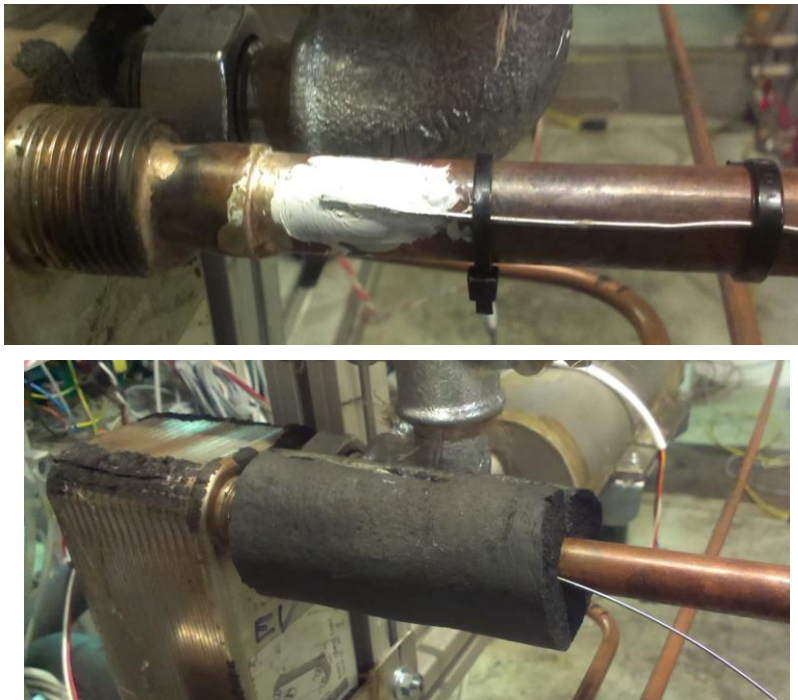


Figure 46: Contact sensor, top: fixation, bottom: insulation

For the heat sink and source Pt-100 resistance thermometer with a diameter of 3 mm are used. They have a higher accuracy compared to thermocouples and they are directly measuring the temperature of the fluid in the pipes. The sensor should be mounted with the measuring head against the flow direction to reduce the influence of the sensor itself at the measurement position (Figure 20). To avoid temperature stratification within the stream a change of direction of the pipe should be accomplished ahead of the position of measurement, as shown in Figure 47. Stratifications can occur at the outlet of plate heat exchangers and in long straight pipes.

All temperature sensors were calibrated with a cryostat which keeps a fluid at a constant temperature and a reference temperature sensor. According to their position in the test rig the sensors were grouped into three temperature ranges:

- Low (-20 to 20 °C),
- Medium (20 to 70 °C) and
- High (40 to 95 °C).

For each range three temperature levels were used for calibrating the sensors. After the calibration factors were determined, repeatability measurements were carried out to get the error of measurement of the temperature sensors. A maximum error of ± 0.15 K was

determined for the thermocouples. Although most of the sensors are much more accurate, the biggest deviation is used for the uncertainty calculation. The same procedure is applied for the Pt-100 sensors which have an error of measurement of ± 0.06 K.

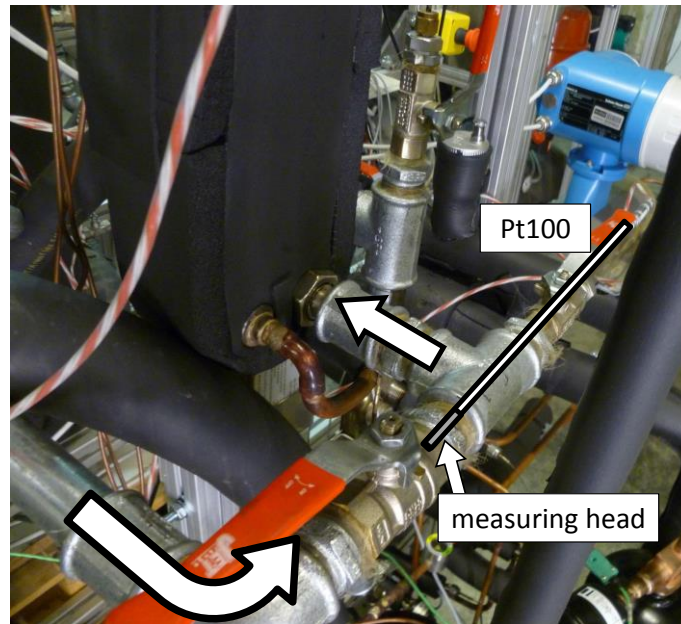


Figure 47: Pt-100 installation at desuperheater inlet port (TE_d01)

Additionally three NTC-temperature sensors had to be installed for the control of the compressor (SEC). The positions of these sensors are equal to those of TE_r01, TE_r07 and TE_r07i, see Figure 30. As these sensors belong to the SEC, no calibration was done for these sensors.

3.5.2. Flow measuring systems

To evaluate the heating capacity of the heat pump test rig, the mass flow rates in all fluid cycles have to be determined. For water and brine, the material properties are well known and data bases are used to get the density and specific heat capacity at different temperatures and constant pressure. Additionally the fluids are operated in liquid state and for small temperature ranges only. So measuring the volume flow rate was sufficient. Also the property data of R410A is available in a data base. However, in the liquid line of the heat pump cycle it is very likely to get into the two-phase area. Therefore it is advantageous to measure the mass flow rate.

Mass flow

As described above the refrigerant mass flow rate on the high pressure side was measured in the liquid line of the heat pump cycle, but not the evaporator and injection mass flow, in order to keep the influence of the measuring equipment on the cycle as small as possible. On the one hand a mass flow meter influences the cycle by requiring place, which is limited because of the compact design of the heat pump. On the other hand an additional pressure drop occurs which can disturb the control of the expansion valve if the high pressure side of it faces two phase refrigerant. The injection mass flow is calculated by using the cooling capacity of the evaporator as described in Equation 33.

A Proline Promass 83A DN4 by Endress+Hauser is used as mass flow meter. It has an operating range from 0 to 450 kg/h while for the measurements within this work a range from

0 to 200 kg/h is used. An error of measurement of 0.1 % of reading (o.r.) is specified by the manufacturer. (E+H, 2012)

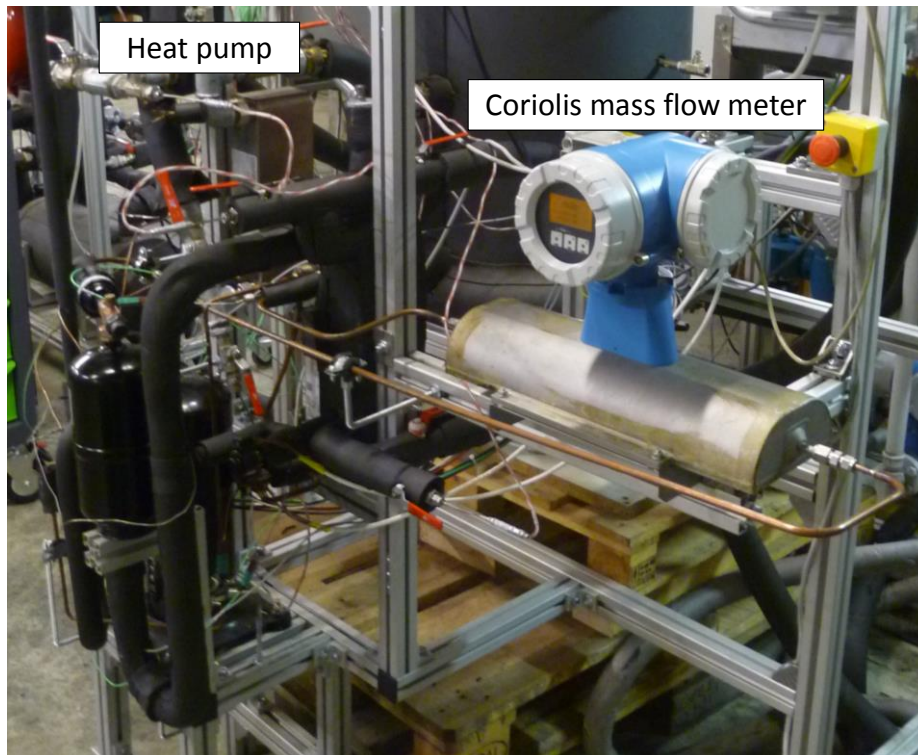


Figure 48: Coriolis mass flow meter

In the system test at the SPF it is not necessary to measure the mass flow rate of the refrigerant, as only the electrical power consumption of the compressor and the heating capacity on the water side are relevant for the evaluation of the overall heating system. Therefore the Coriolis mass flow meter is positioned next to the test rig in a way, to be able to dismount it easily after the measurements. The piping is accomplished as smooth as possible to keep the influence of the measuring device little, as can be seen in Figure 48.

Volume flow

The volume flow rates in the heat sink and source cycle (see Chapter 3.3) have a maximum error of 0.5 % of reading (o.r.) (E+H, 2010). The brine cycle was operated from 400 to 1200 l/h and the sink cycle in a range from 300 to 1000 l/h. Even though the volume flow rates were kept at a constant level for the steady state measurements, they varied during the dynamic measurements.

As described in Chapter 3.3.2 all measurements were carried without measuring the water flow rate of the desuperheater due to optimisation reasons and the heating capacity of the desuperheater was calculated according to Equation 29 instead.

3.5.3. Pressure sensors

For determining the pressure levels of the heat pump cycle the pressure transmitters of the compressor control (SEC) are used. At the suction, injection and discharge pipes, t-pieces (copper fittings) are installed wherefrom capillary tubes are going to the sensors, as illustrated in Figure 49.

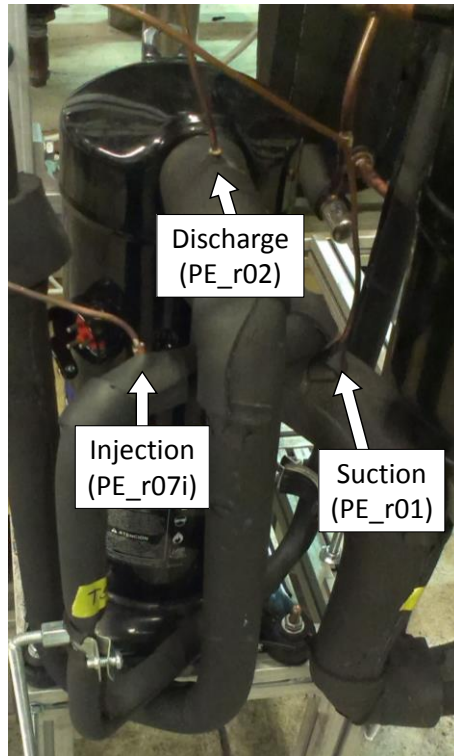


Figure 49: Position of pressure measurement

These relative pressure transmitters have an error of measurement of 1 % full scale (FS) according to the data sheet (Alco Controls, 2013). Additionally the atmospheric pressure has to be considered. In this case, the atmospheric pressure was assumed to be at a constant level of 975 mbar. This assumption is based on an atmospheric pressure measurement in Graz in a course of one year (Meteonorm, 2014). The variation of the atmospheric pressure is from 960 to 980 mbar, which is small in comparison to the error of the relative pressure transmitters. An error of 1 % full scale means for the high pressure sensor with a maximum pressure of 50 bar, that the maximum error can be 500 mbar in any measurement. At a condensation pressure of 35 bar this would lead to a saturation temperature difference of more than 0.5 K. As these pressure transmitters were already installed in combination with more accurate absolute pressure sensors these measurements were used to calibrate the sensors. By this, a maximum error from 0.14 to 0.4 bar was determined (see Table 4).

Additionally to the pressure sensors also three pressure indicators and two pressure switches are installed, depicted in Figure 50. The manometers (PI_r01, PI_r02, PI_r07i) are used to provide a fast evaluation of the pressure levels in the heat pump cycle for the operator. Pressure switches have to be installed for safety reasons. All components of the heat pump cycle are designed for a maximum pressure of 45 bar, when they are installed on the high pressure side. If the high safety pressure, which is slightly below the maximum pressure, is exceeded the high pressure switch (PSH_r02) cuts off the power supply of the compressor. On the other side the compressor is not allowed to be operated below an evaporation temperature of $-30\text{ }^{\circ}\text{C}$ which is equivalent to an evaporation pressure of 2.7 bar. The low pressure switch (PSL_r01) cuts off the power supply if the low safety pressure, which is slightly higher than the minimum pressure, is undercut. After the pressure switch has cut off the power supply, the pressure level within the refrigerant circuit stabilises and when a safety margin to the minimum or maximum pressure is reached, the pressure switch reconnects the power supply to the compressor.

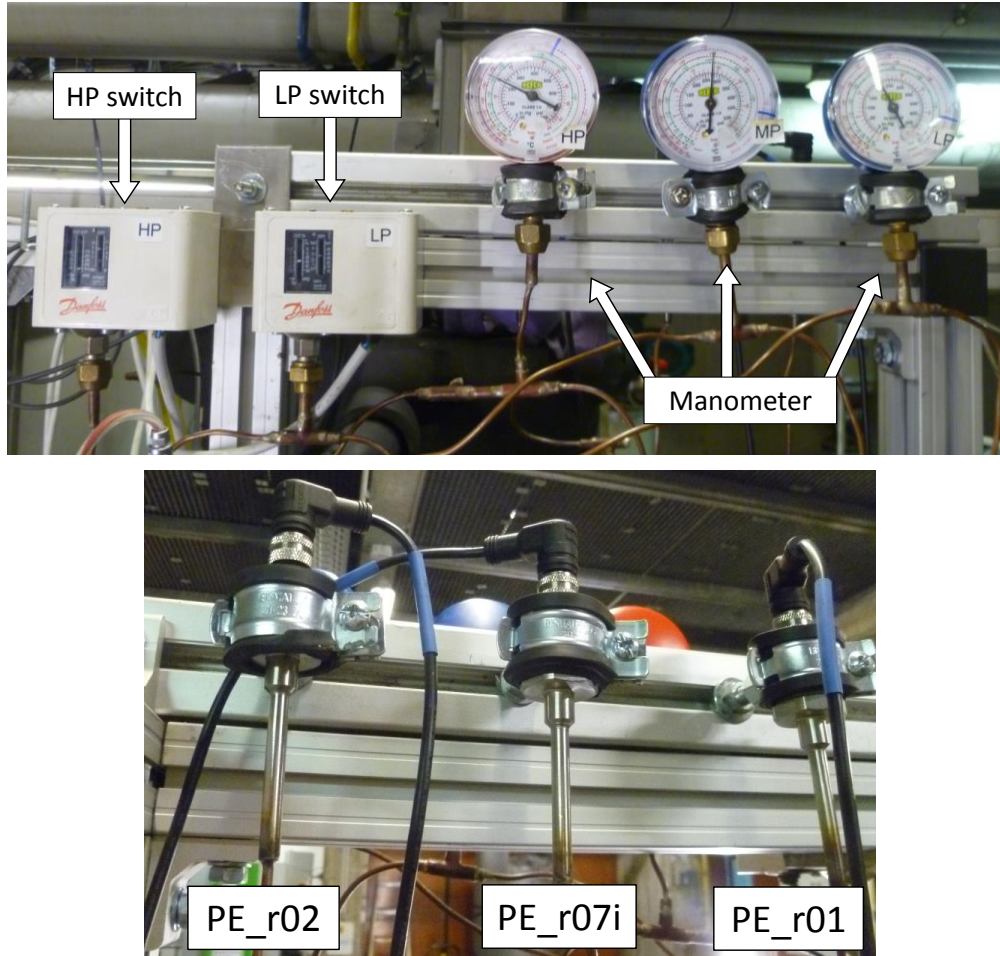


Figure 50: Pressure measurement, top: manometers and switches, bottom: pressure transmitter

3.5.4. Electrical power

For the evaluation of the Coefficient of Performance (COP) the electrical power consumption of the compressor is required. With a speed controlled compressor not only the electricity consumption of the compressor, but also of the inverter drive and the compressor controller (SEC) have to be measured. This is accomplished by means of an electrical meter AAD1 by Saia-Burgess (2014). It measures 1000 pulses per kWh with an accuracy of 1%. The maximum electrical power consumption of the compressor is 4 kW, which means a maximum current of 17 A with a voltage of 230 V. The AAD1 can be operated with a maximum current of 25 A.

An additional error can emerge when starting and stopping the measurement, as it could occur that one or two pulses are not detected. This influence is illustrated in Figure 51. It shows that the error in mean electrical power consumption gets less than 1% when a minimum number of 200 pulses is reached. All measurements are accomplished with a minimum measuring period of 15 minutes to guarantee a steady state condition on the one hand and a sufficient number of pulses on the other hand.

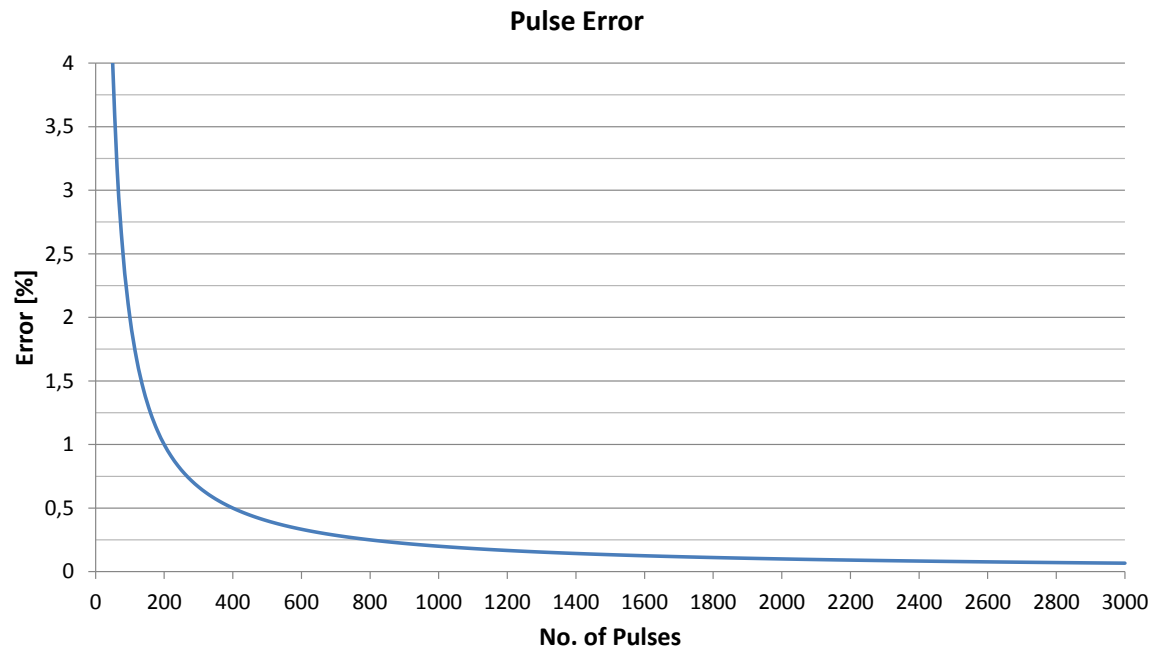


Figure 51: Electrical meter, pulse error electrical power

3.6. Control

The measurement equipment described above is not used for analysing the heat pump system only, but also for controlling different components. Emerson provided the 'Superheat and Envelope Controller' (SEC) for the control of the compressor and inverter drive. The control of the periphery that facilitated the operating conditions for the heat pump test rig was accomplished with LabVIEW (2012). Also the compressor control (SEC) was embedded into the LabVIEW programme.

3.6.1. Hardware

To connect the measuring equipment to the software, hardware modules by National Instruments are used. For this heat pump test rig a NI compactRIO-system ('cRIO') is chosen. The cRio is equipped with a processor for real time application and operates as interface between hardware and software. Each measuring device has different signals and therefore different modules are required.

The NI9208 is an analog-input (AI) module for current which is used for the Coriolis mass flow meter. NI9375 is a digital-input (DI) module where the electrical energy consumption is detected. For temperature sensors there are different modules for Pt-100 and thermocouples (TC), NI9213 for TC and NI9217 for Pt-100.

The SEC sends and receives the compressor data via a Modbus connection. Therefore the module NI9871 is used. To control the heat sink and source the electrical heater and the circulation pump are activated and actuated and the flow rates are detected by modules. These modules (NI9375, NI9208, NI9263 and NI9265) communicate via an EtherCAT connection with the NI cRIO of the heat pump hardware.

The block diagram in Figure 52 shows the connection of the systems.

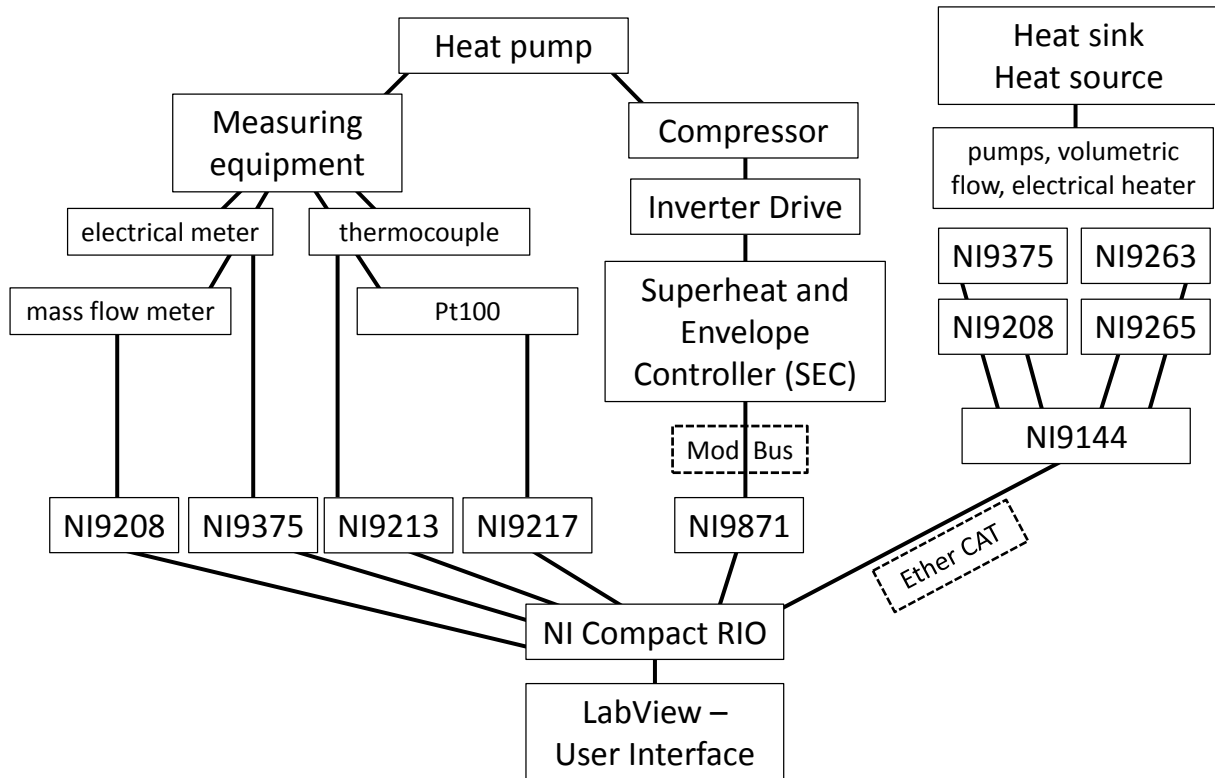


Figure 52: Hardware – Software connection, block diagram

3.6.2. Software

With the software LabVIEW (2012) the entire control of the heat pump cycle is realised. It is separated into a 'Front panel' and a 'Block diagram'. The front panel represents the graphical user interface (GUI) where the heat pump is operated and adjustments to different controllers can be made. In the block diagram the calculations and the programming of the control are accomplished.

Front Panel

The front panel is build up with tab pages, where the following modes can be watched and controlled:

- Compressor data from the Modbus connection to the SEC (MB_Monitoring, MB_Config, MB_Write)
- Heat pump
- Heat sink (Sink Side)
- Heat source (Source Side)
- Graphs (Pressure, Temperature, Flow)
- Data from SEC (Data acquisition)
- Automation control (Automatic)

The SEC delivers information about the state of the compressor, inverter drive and expansion valves. Starting the compressor is either realised by giving it a desired heating capacity, or by setting a fixed speed where the speed limits at 1800 and 5400 rpm have to be considered. The lower limit of 1800 rpm is set by the compressor manufacturer due to oil return issues and minimum heating capacities whereas the upper limit of 5400 rpm is set as no higher heating capacities are necessary for the overall heating system. A maximum speed of 7020 rpm would be possible according to the manufacturer. Different alarm settings of the

3. DESCRIPTION OF THE TEST RIG

compressor control can be evaluated here as well. The Copeland software is already equipped with important safety systems:

When a maximum or minimum pressure is detected by the pressure sensors, the compressor is shut down. If the superheating is low, liquid refrigerant might enter the suction chamber which can cause damage to the compressor. When low superheating is detected by the temperature and pressure sensors the alarm mode induces an immediate shut down of the compressor. Also a maximum discharge temperature is not allowed to be exceeded, as the lubricant is likely to decompose and thereby losing lubrication performance at high temperatures. Another important safety system is the oil return mode. If the compressor is operated at a lower compressor speed than 2200 rpm for a time period of two hours, it is not ensured that the oil is able to pass the entire cycle back to the compressor. Therefore the compressor speed is set to 3000 rpm for at least 120 seconds to improve the oil return. These limits are default values from the compressor control and can be changed if differing setups are required.

On the tab pages 'heat pump', 'heat sink' and 'heat source' the schemes of the circuits with relevant measuring data can be monitored. Also the corresponding PID controllers are placed in those tabs. In Figure 53 the heat pump tab is shown. The heat pump cycle with important monitoring data is visualised here. At the heat sink one PID controller is for the circulation pump on the system side for rejecting the condenser heat. Its control variable is either the temperature sensor at the condenser inlet (TE_w01) or a thermocouple that is positioned right at the heat exchanger of the system (TE_r10). All measurements are carried out with TE_r10 as control variable, for the reasons described in Chapter 3.3.2. The second PID controller is used to keep the mass flow of the water cycle at a desired level for different operating conditions. The signal of the flow meter (FE_w01) is the control variable for the speed controlled circulation pump. For controlling the heat source also two PID controllers are used. The brine inlet temperature (TE_b01) is the control variable of the electrical heaters and the circulation pump is controlled by getting a signal from the volume flow of the brine (FE_b01).

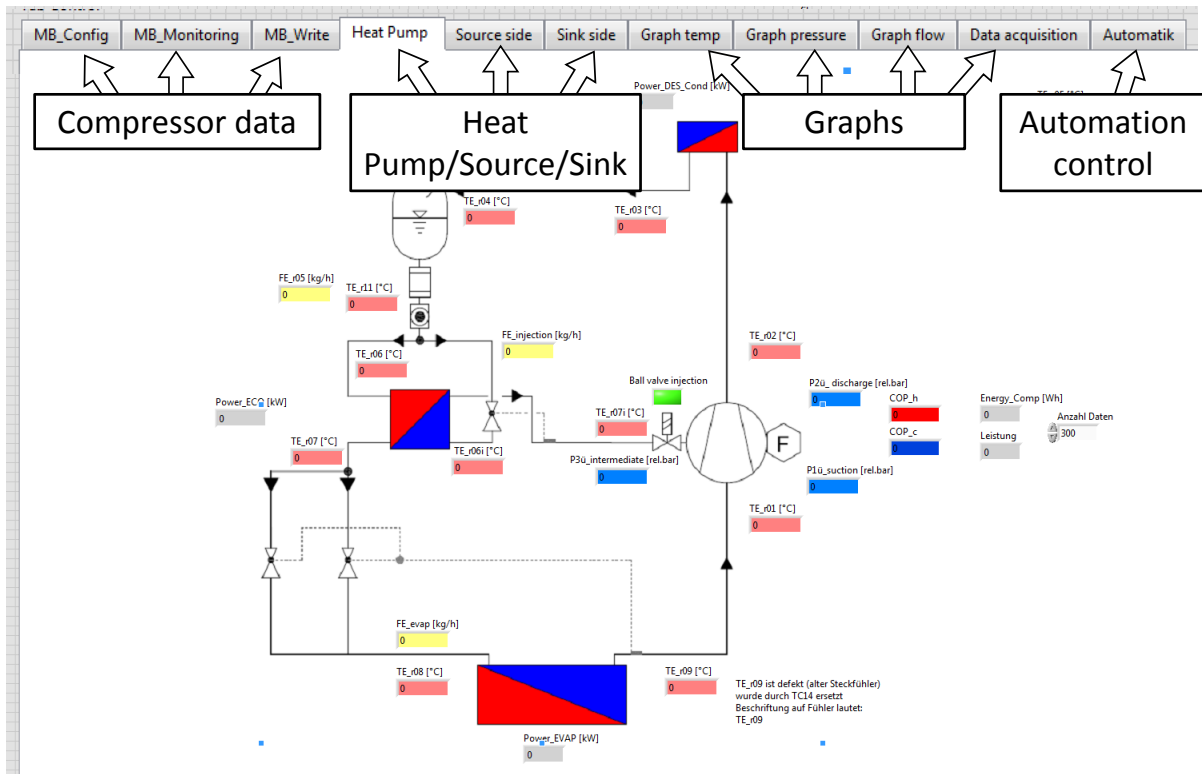


Figure 53: LabVIEW – Front Panel, 'Heat pump'-tab

As also 24 hour tests are performed, the compressor speed has to be controlled as well. Therefore a PID controller, that gets its process variable derived from the heating curve and the ambient temperature of the simulation file, is used. The control variable for this controller is the condenser outlet temperature (TE_w02).

Graphs give an overview of the signals development over a period of time. Different graphs for pressure, temperature and flow data are implemented. Additionally, superheating and opening degrees of expansion valves can be monitored in the tab 'Data acquisition'. The control unit for the automation of the heat pump is described in detail in Chapter 3.6.3.

Simulation file

As 24 hour tests are performed to analyse the problems of the automatic heat pump control, simulation files are read by the software and treated as input values. The simulation files were generated from the data base of the year-round simulations which were carried out within the project MacSheep. Three significant days with different profiles, which will be thoroughly analysed in Chapter 5.3, were chosen:

Day 1.....space heating – long-time runs (3 starts)
Day 2.....space heating – short-time runs (7 starts)
Day 3.....space heating and DHW preparation – (5 SH starts, 1 DWH start)

The simulation file provides the desired heating mode (SH or DHW), the set temperature for inlet of condenser and evaporator, the calculated mass flows of the brine and water circuit and the ambient temperature. With this information the set point for the condenser outlet is calculated according to the heating curve. This information corresponds to the information that will be given to the heat pump system by the project partner's control.

Block Diagram

As already described, the programming of the control is done in the block diagram. It is divided into the following areas, also shown in Figure 54:

- Input
- Graphs and Calculations
- PID controller
- Automation
- Output

The whole LabVIEW control is based on one while loop which activates each programme at every time step. At each iteration loop all data is received and processed according to the implemented programmes. At the beginning of the loop all data is read from the hardware in the 'Input' area. The signals from the sensors shown in Table 4 are detected with the hardware modules. Data of the compressor is determined by the Modbus connection whereas input values of the user are registered directly within the LabVIEW (2012) software. Additionally the simulation file for the 24 hour tests is read in this section.

As the front panel serves as graphical user interface it is important to get a quick overview of the state of the heat pump system. This information is processed in the graphs and calculations area of the block diagram. Here, calculations are proceeded to be able to check operating conditions during operation. The control of the heat sink and source is done in the 'PID controller' section. How the parameters for the controller were determined was already described in Chapter 2.4. For the electrical heater, safety functions are embedded to prevent overheating of the heating coils. The heaters are not enabled until a mass flow of 300 l/h is reached and are disabled when the brine inlet temperature exceeds 30 °C.

3. DESCRIPTION OF THE TEST RIG

At the end of the loop the data is saved and the output values are forwarded to the specific components. As the automation of the heat pump cycle is a main task of this thesis, it will be described in detail in the following chapter.

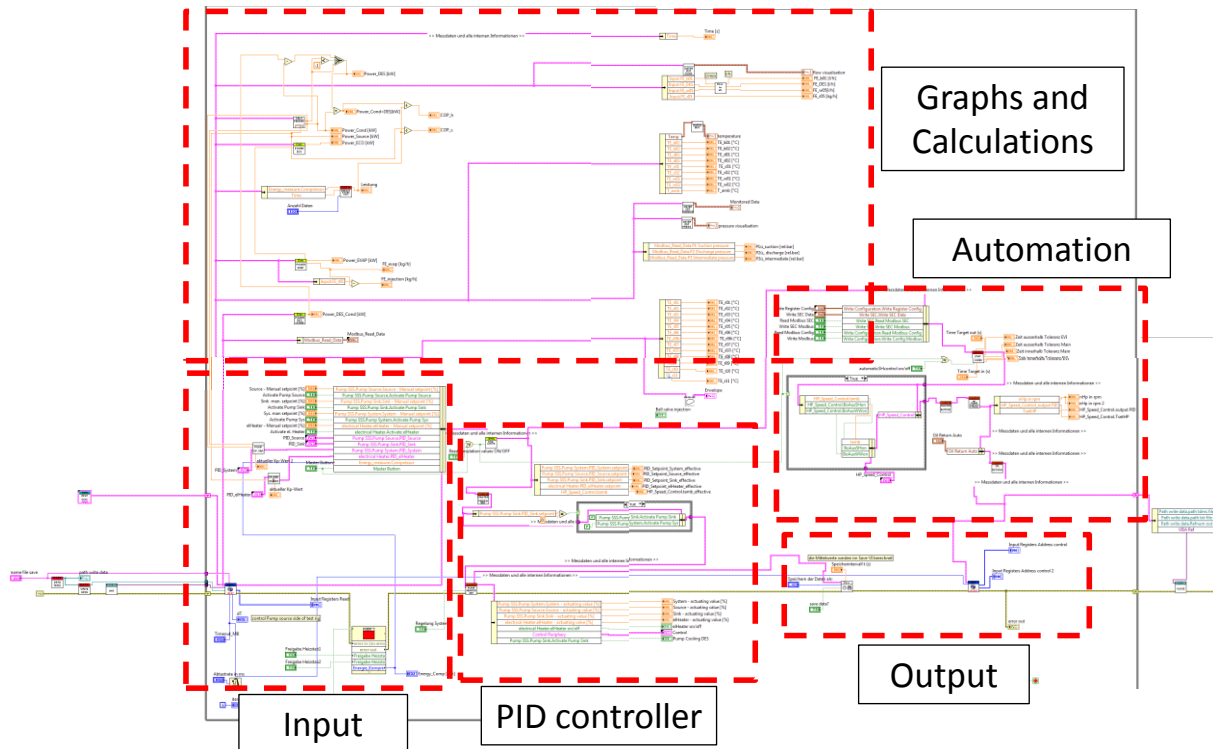


Figure 54: LabVIEW – Block Diagram

3.6.3. Automation of heat pump control

In the system test the heat pump is supposed to get a signal whether it should be operated in space heating (SH) or domestic hot water preparation (DHW) mode. For space heating, additionally a set temperature for the condenser outlet is provided. With this information the heat pump has to be able to run in a stable way and efficiently on its own. The compressor software has already functions embedded which allow a stable operation of the cycle. However, these functions are disabled when the control of the expansion valves is set to manual mode. The manual mode is necessary as the control parameters of the expansion valves have been optimised. Therefore these functions were rebuilt and extended in this software.

To keep the superheating of the suction gas small is a key aspect to get a high efficiency of the heat pump cycle. Lower superheating leads to a higher evaporation pressure and furthermore to a lower pressure ratio. This results in a higher efficiency of the heat pump cycle. However, when the superheating is low the system is vulnerable to oscillations when there is a change of operating conditions. The programme 'Automatic Superheat Control' checks whether the expansion valves are oscillating or not. If they are stable the set point is set 1 K lower, if not, it is set 2 K higher. At higher superheating set points the valves are able to stabilise again. The maximum superheating set point is at 10 K and the minimum superheat of 5 K should be reached as often as possible during operation.

In the programme 'Speed Control Compressor', the input values of the simulation file are processed. Depending on the desired mode, SH or DHW preparation, the compressor speed

has different control variables. When space heating is demanded the compressor speed is controlled by a PID controller in order to reach a set water temperature at the outlet of the condenser according to a heating curve for the system tests. The fundamentals of heating curves are explained in Chapter 2.5. It uses the outlet temperature of the condenser (TE_w02) as control variable. The parameters of the controller are chosen conservatively as the system is rather slow. Additionally, big changes of the speed can lead to instabilities of the control. This instability of the superheating is considered in the DHW preparation mode as well. When there is a demand of DHW the heat pump needs to operate at high speeds as fast as possible. In the worst case the speed of the heat pump changes from 1800 rpm in space heating mode to 5400 rpm in DHW mode. If this step would be done at once the system would get unstable, which would lead to a shutdown of the compressor. Therefore a programme was implemented to increase the speed in moderate steps in DHW mode. Every 120 seconds the speed is increased by 1200 rpm which leads to a maximum time delay of 4 minutes until the desired speed is reached. This delay is accepted as the stability is improved and a shutdown of the compressor would otherwise cause a waiting time of 10 minutes at least.

The compressor speed in DHW mode is set to be linearly dependent on the brine inlet temperature. It is adjusted to the increasing Coefficient of Performance at lower pressure ratios and to density differences of the suction gas. When the brine inlet temperature decreases the suction gas density does as well, which leads to a lower mass flow at constant compressor speed. To work against that, the compressor speed is increased at low brine temperatures, whereas it is reduced at high brine temperatures. Additionally the *COP* is higher at high brine temperatures and the minimum and maximum speeds need to be considered for both modes. The compressor is not allowed to be run under 1800 rpm and a maximum speed of 5400 rpm is set. Another function that is disabled due to operation in manual mode is the oil return which was described in Chapter 3.6.2. As this function is essential for a long-time operation of the compressor it was rebuilt as well. By positioning it at the end of the data stream it is able to overwrite any previous signal. It has the highest priority except for alarm modes of the compressor.

In Figure 55 the sequence of the programmes is shown. The sections (Manual, Automatic Superheat Control, Speed Control Compressor and Automatic Oil Return) are activated in sequence from left to right. If the automation for the heat pump cycle is deactivated the compressor can be controlled manually. The 'Automatic Superheat Control' and the 'Speed Control Compressor' programmes are simultaneously activated with the automation button on the front panel. When the automation is enabled the manual mode is deactivated and input data is read from the simulation file. 'Automatic Oil Return' is activated when the compressor is run below 2200 rpm for a longer period than 2 hours. It is not dependent on the automatic mode and overwrites any previous signal of the speed control when necessary. A detailed description of the software is given in the Appendix A-1. A few programmes from the block diagram as well as the tabs from the front panel are explained there.

3.6.4. Optimization for system test

As the heat pump was supposed to be operated in a system test at the Institute of Solar Technology (SPF), the heat pump test rig as well as the LabVIEW programme had to be adapted after the measurements at the IWT. The measurement devices were reduced to a minimum. All temperature sensors in the heat pump cycle were removed except for the three sensors for the SEC that are used for controlling the expansion valves. Also the mass flow meter was dismantled from the test rig. For the speed control of the compressor only the outlet temperature of the condenser (TE_w02) and the brine inlet temperature (TE_b01) are

3. DESCRIPTION OF THE TEST RIG

measured. For analysis of the heat pump performance the electricity meter is used in the system test as well.

Based on the modifications and the differing tasks also the LabVIEW programme had to be changed. The main task is to communicate with the system of SPF by sending and receiving data. Therefore the heat pump control is embedded into the main control of SPF where all the settings of the overall system are controlled for the system tests. Demand for SH or DHW preparation is determined by the main control of SPF and the information is sent to the heat pump control. Additionally the set temperature for the condenser outlet is provided by the main control of SPF. The main control of SPF needs to decide which mode is best for the current conditions. Therefore it requires information about the status of the heat pump including the following data:

- Status of the heat pump
- Heat Pump blocked
- Heat Pump on/off
- Minimum Run time of Heat Pump exceeded
- Minimum Heating capacity

The status of the heat pump can be either Off, Heating, Alarm, Waiting, Stopping or Manual. It should not be given a signal from the control when the status is either Off, Waiting, Stopping or Manual. In this case the heat pump is blocked and the main control changes into a mode without heat pump. As a minimum run time of 15 minutes and a minimum heating capacity are decision criteria for the main control, this information is sent as well. With this exchange of information and the embedded stability programmes, the heat pump is able to run automatically within the overall heating system.

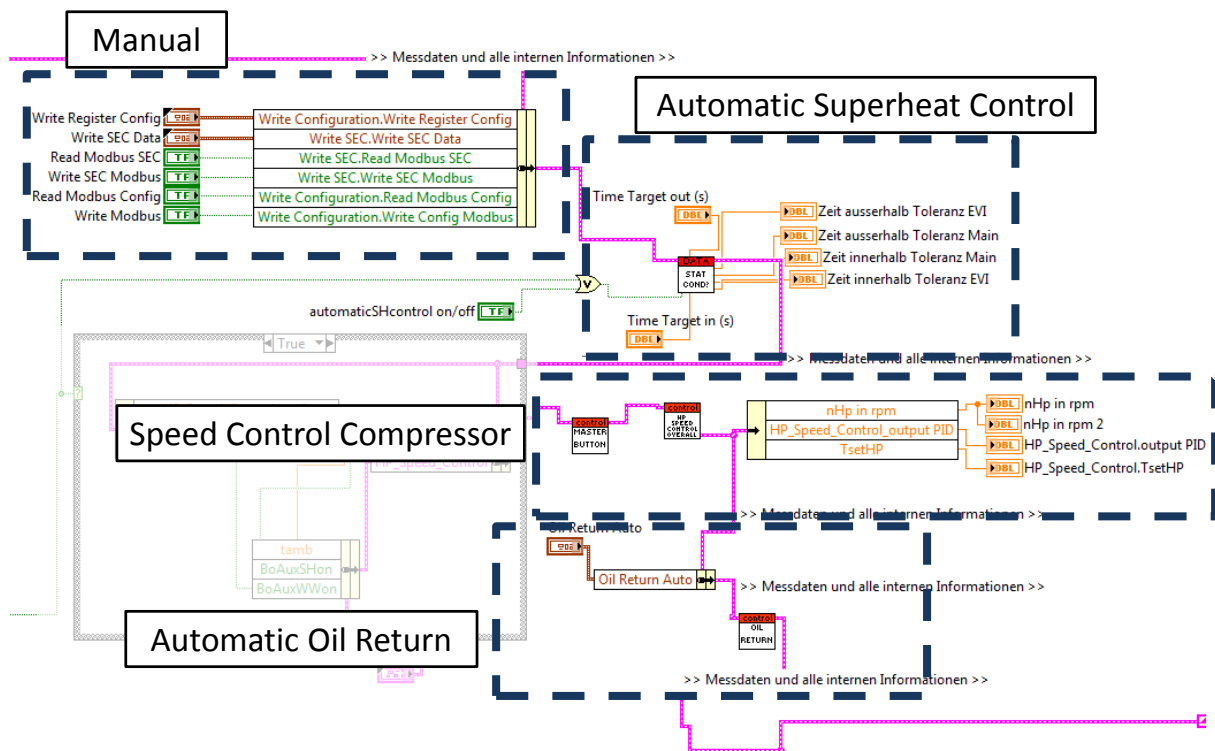


Figure 55: LabVIEW - Automation

4. EVALUATION OF MEASUREMENTS

In this chapter the evaluation of the measured data is explained. All calculations for the analysis of the heat pump cycle are described. The uncertainty propagation for important operating figures is shown at the end of this chapter.

For the evaluation of the compressor 58 operating points were measured with variations of the brine inlet temperature, condenser water inlet temperature and compressor speed. The brine inlet temperature was varied from -15 to +15 °C whereas the condenser inlet temperature was set within a range from 20 to 50 °C. Seven different compressor speeds were examined with a range from 1800 to 5400 rpm. The results of all measurements are listed in the Appendix A-2. In Figure 56 the envelope of the compressor with the different operating points is shown. It needs to be considered, that the envelope's shape depends on the compressor speed and here only the maximum envelope (4500 rpm) is depicted (compare to Figure 33). When looking at the operating points, it can be seen that the condensation temperature increases and the evaporation temperature decreases at higher speeds. This is due to higher temperature differences at the pinch points of the heat exchangers for higher heating capacities. Additionally the higher heating capacities result in a higher temperature difference on the water and brine side, leading to an increased pressure ratio.

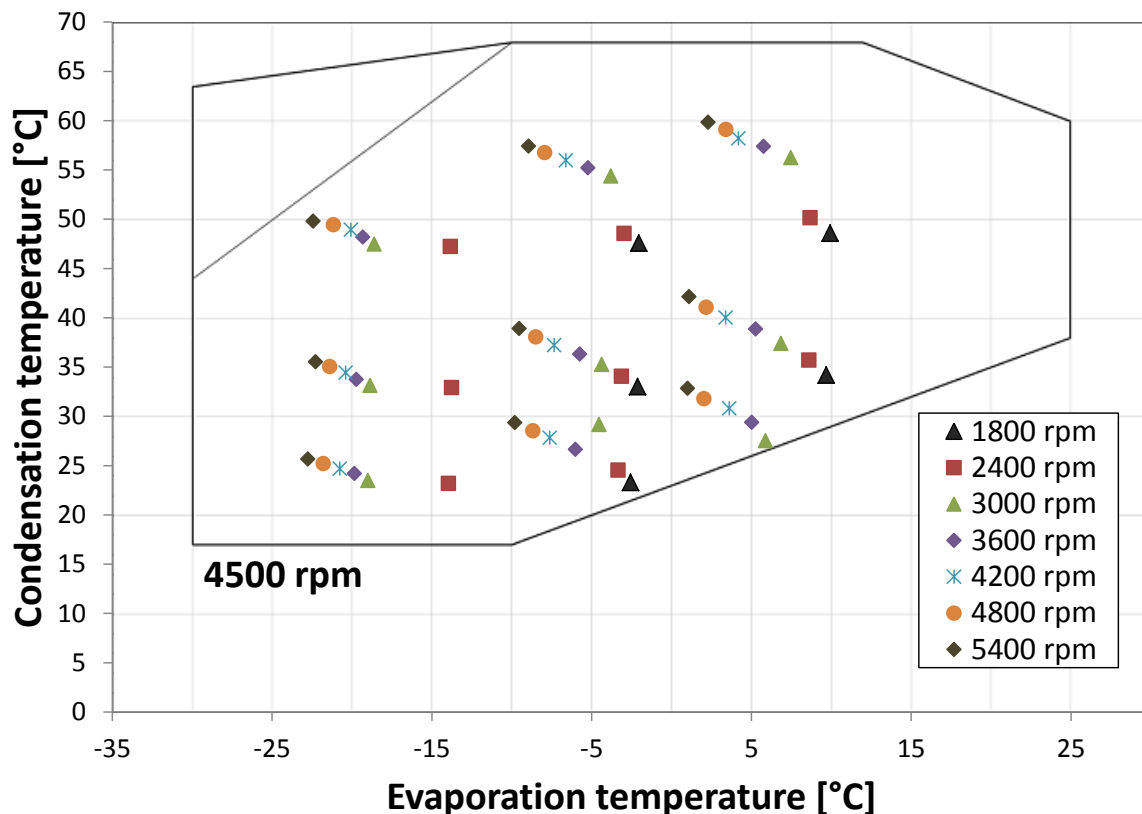


Figure 56: Measured operating points

4.1. Evaluation of heat pump cycle

The arrangement of the measuring equipment was already explained in Chapter 3.5. In Figure 57 on top an exemplary operating point of the heat pump cycle is illustrated in a temperature-enthalpy diagram and below the denotation of the different points is shown in the scheme.

4. EVALUATION OF MEASUREMENTS

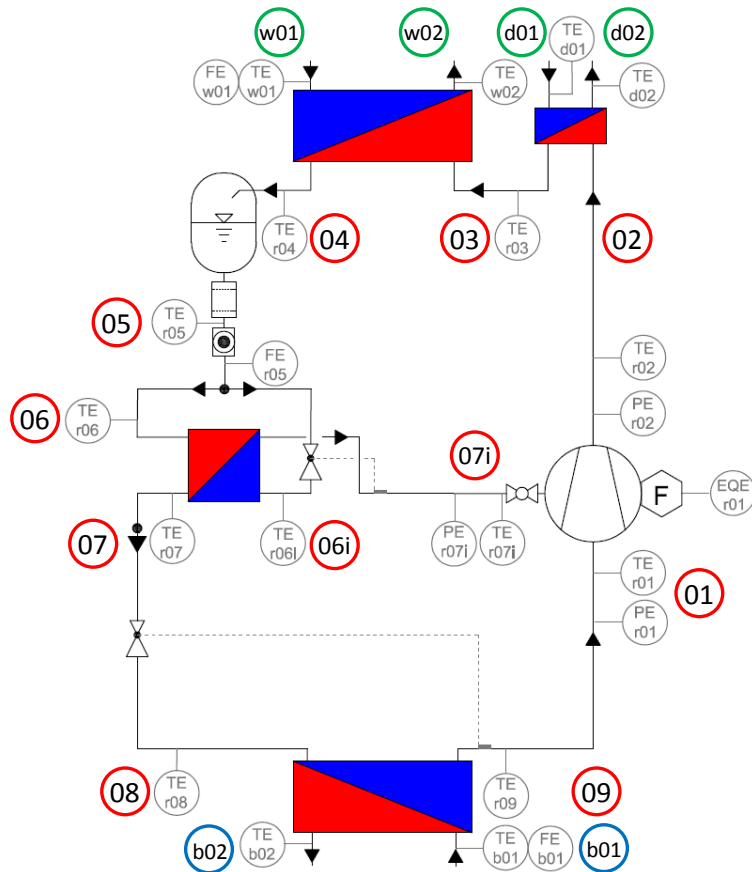
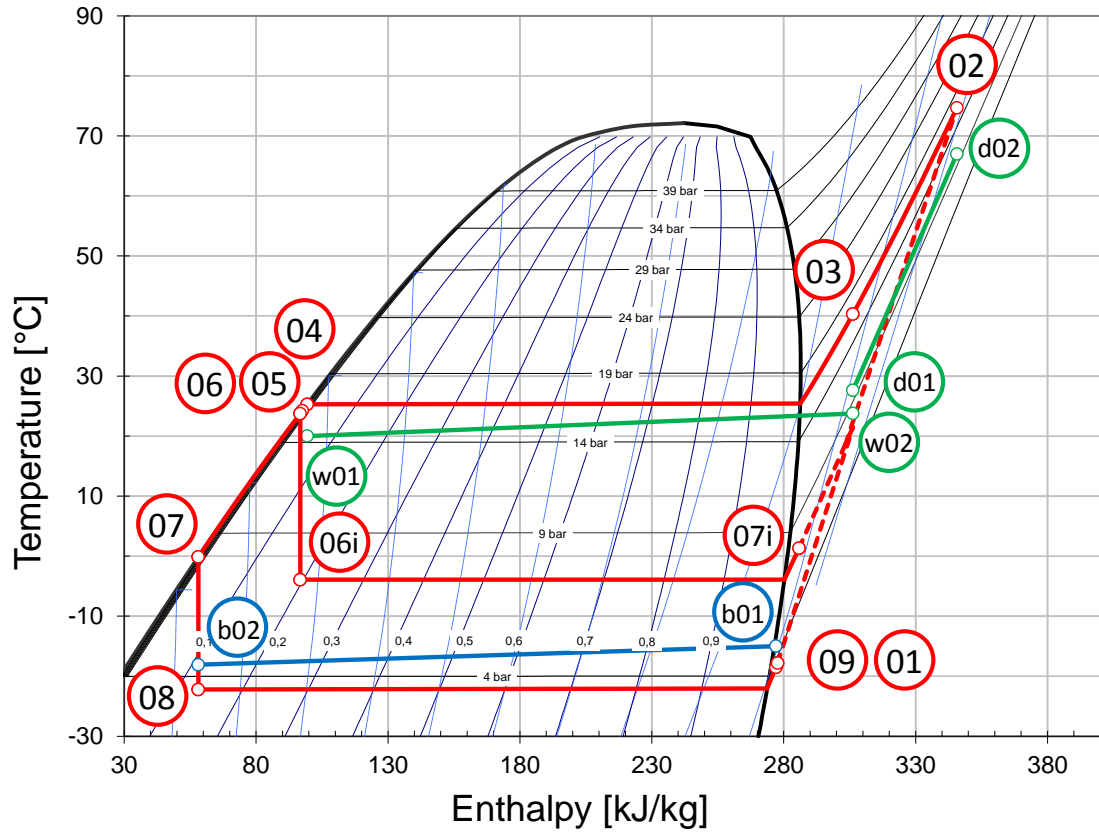


Figure 57: Heat pump denotation, top: t/h-diagram of R410A, bottom: scheme

All equations for the heat pump cycle evaluation are given in Equation 15 to Equation 25 and will be explained in the following paragraphs.

The superheated refrigerant (01) and the injection mass flow (07i) are sucked by the variable speed compressor. All three pressures (p_{r01} , p_{r02} and p_{r07i}) and the corresponding temperatures (T_{r01} , T_{r02} and T_{r07i}) are measured right before and after the compressor. With this data, the enthalpies are calculated via property data tables. This data was generated from the software EES (2015) and a polynomial as a function of pressure and temperature represents the property data.

After the discharge (02) the refrigerant is cooled by the desuperheater (03) and afterwards condensed in the condenser (04). The enthalpy of the desuperheater outlet is detected with a temperature sensor and also on the liquid line three sensors are measuring the refrigerant temperature after the condenser (04), the liquid receiver (05) and before the economiser (06). The enthalpy h_{r04} is evaluated with the condensation pressure p_{r02} (assuming no pressure drop), whereas the enthalpy after the liquid receiver h_{r05} is calculated with the measured temperature and the vapour quality of the refrigerant being zero, as only liquid refrigerant should be present after the receiver. At the high pressure inlet of the economiser (06) the temperature is detected for the evaluation of the heat exchanger. The enthalpy of the subcooled refrigerant at the outlet of the economiser (07) h_{r07} is equal to the enthalpy after the expansion valve (08) h_{r08} on the low pressure side. Directly at the outlet of the evaporator the temperature is detected (09) for the evaluation of the heat exchanger. At the injection expansion valve, the enthalpies are equal before (06) and after (06i) the EEV and the temperatures of (06i) and (07i) are measured. All enthalpies of the refrigerant circuit are calculated as shown in Equation 15 to Equation 25.

$$h_{r01} = h(T_{r01}; p_{r01}) \quad \text{Equation 15}$$

$$h_{r02} = h(T_{r02}; p_{r02}) \quad \text{Equation 16}$$

$$h_{r03} = h(T_{r03}; p_{r02}) \quad \text{Equation 17}$$

$$h_{r04} = h(p_{r02}; x = 0) \quad \text{Equation 18}$$

$$h_{r05} = h(T_{r05}; x = 0) \quad \text{Equation 19}$$

$$h_{r06} = h(T_{r06}; x = 0) \quad \text{Equation 20}$$

$$h_{r07} = h(T_{r07}; x = 0) \quad \text{Equation 21}$$

$$h_{r08} = h_{r07} \quad \text{Equation 22}$$

$$h_{r09} = h(T_{r09}; p_{r01}) \quad \text{Equation 23}$$

$$h_{r06i} = h_{r06} \quad \text{Equation 24}$$

$$h_{r07i} = h(T_{r07i}; p_{r07i}) \quad \text{Equation 25}$$

As the uncertainty of measurements on the water and brine side is smaller than the uncertainty on the refrigerant side, the heat pump cycle is evaluated on the water and brine side. Additionally all temperatures in the refrigerant circuit are contact ('clamp-on') sensors whereas those in the brine and water cycle are installed in-stream. However, as no water volume flow rate is measured over the desuperheater, it is inevitable to use the measured data of the refrigerant circuit for the evaluation. Also for analysing the compressor the data of the refrigerant circuit is very important.

On the high pressure side the refrigerant mass flow over the condenser and desuperheater $\dot{m}_{cond,r}$ (FE_r05) is measured. With the enthalpies explained above, the heating capacity of the heat exchangers can be determined ($\dot{Q}_{cond,r}$ and $\dot{Q}_{des,r}$). For the condenser also the volume flow rate on the water side is detected, which makes it possible to determine the heating capacity in two ways. As the measured data on the water side is assumed to be more accurate, $\dot{Q}_{cond,w}$ is used for the further evaluation. The capacity of the desuperheater $\dot{Q}_{des,w}$ is determined by calculating the total heating capacity of condenser and desuperheater on the refrigerant side $\dot{Q}_{cond,tot,r}$ and subtracting the condenser capacity (Equation 29). This value is preferred compared to the calculation on the refrigerant side $\dot{Q}_{des,r}$ as the measurement uncertainty on the water side is smaller and no pressure drop over the heat exchanger is considered on the refrigerant side. As a simplification for the evaluation, all heat exchangers are assumed to have no heat losses to the ambient, as desuperheater and evaporator are insulated and condenser and economiser do not reach temperatures far away from ambient conditions.

$$\dot{Q}_{cond,w} = \dot{m}_{cond,w} \cdot c_{p,w} \cdot (T_{w02} - T_{w01}) = \dot{V}_{w01} \cdot \rho_w \cdot c_{p,w} \cdot (T_{w02} - T_{w01}) \quad \text{Equation 26}$$

$$\dot{Q}_{cond,r} = \dot{m}_{cond,r} \cdot (h_{r03} - h_{r04}) \quad \text{Equation 27}$$

$$\dot{Q}_{cond,tot,r} = \dot{m}_{cond,r} \cdot (h_{r02} - h_{r04}) \quad \text{Equation 28}$$

$$\dot{Q}_{des,w} = \dot{Q}_{cond,tot,r} - \dot{Q}_{cond,w} \quad \text{Equation 29}$$

$$\dot{Q}_{des,r} = \dot{m}_{cond,r} \cdot (h_{r02} - h_{r03}) \quad \text{Equation 30}$$

$$\dot{m}_{des,w} = \frac{\dot{Q}_{cond,tot,r} - \dot{Q}_{cond,w}}{c_{p,w} \cdot (T_{d02} - T_{d01})} \quad \text{Equation 31}$$

The capacity of the evaporator $\dot{Q}_{evap,b}$ can only be calculated via the brine side as no mass flow is detected on the low pressure side of the refrigerant circuit. It is also used to determine the refrigerant mass flow $\dot{m}_{evap,r}$ and the injection mass flow $\dot{m}_{inj,r}$. The heating capacity of the economiser $\dot{Q}_{eco,HP}$ is evaluated by the liquid line of the internal heat exchanger, as the mass flow is higher and the measured data is assumed to be more accurate than for the two-phase refrigerant.

$$\dot{Q}_{evap,b} = \dot{m}_{evap,b} \cdot c_{p,b} \cdot (T_{b01} - T_{b02}) = \dot{V}_{b01} \cdot \rho_b \cdot c_{p,b} \cdot (T_{b01} - T_{b02}) \quad \text{Equation 32}$$

$$\dot{m}_{evap,r} = \frac{\dot{Q}_{evap,b}}{(h_{r09} - h_{r08})} \quad \text{Equation 33}$$

$$\dot{m}_{inj,r} = \dot{m}_{cond,r} - \dot{m}_{evap,r} \quad \text{Equation 34}$$

$$\dot{Q}_{eco,HP} = \dot{m}_{evap,r} \cdot (h_{r06} - h_{r07}) \quad \text{Equation 35}$$

Thereby all heating capacities are defined. The electrical energy consumption of the compressor ΔE_{comp} is detected with an electrical meter and by having appropriate measuring periods Δt the error of measurement is decreased as shown in Figure 51. With this data the most important coefficient for the evaluation of the heat pump cycle can be determined, the Coefficient of Performance COP . For the heat pump system with desuperheater it is defined as the ratio of total heating capacity to electrical power consumption of the compressor, shown in Equation 37. This is the definition for heating purposes, as for cooling purposes the ratio is defined with the cooling capacity. Another important figure that will be used for further

evaluation is the pressure ratio π , which is defined in Equation 2. For analysing the performance of the cycle for a heating profile over a period the performance factor PF is defined in Equation 38. It is the ratio of the heating energy of the condenser ΔQ_{cond} to the electrical energy consumption of the compressor for the same period of time.

$$P_{el} = \frac{\Delta E_{comp}}{\Delta t} \quad \text{Equation 36}$$

$$COP = \frac{\dot{Q}_{cond,tot,r}}{P_{el}} \quad \text{Equation 37}$$

$$PF = \frac{\Delta Q_{cond}}{\Delta E_{comp}} \quad \text{Equation 38}$$

4.2. Compressor evaluation

To analyse the compressor the system boundary is placed directly around the compressor, as shown in Figure 58. The incoming refrigerant from the evaporator ($\dot{m}_{evap,r} \cdot h_{r01}$) and the injection line ($\dot{m}_{inj,r} \cdot h_{r07i}$), the electrical power input P_{el} and the outgoing refrigerant to the discharge line ($\dot{m}_{cond,r} \cdot h_{r02}$) as well as the heat losses to the ambient $\dot{Q}_{loss,comp}$ are considered. With these factors the efficiency of the compressor can be determined.

Generally there are two coefficients which are used for the compressor evaluation. One is the overall isentropic efficiency $\eta_{is,overall}$ (Equation 4), which takes the losses of the compression into consideration. The other coefficient is the volumetric efficiency η_{vol} (Equation 3), which compares the maximum mass flow of the compressor to the real one. Both of these coefficients are based on several assumptions as the state between the two stages was not measured. This makes it difficult to interpret the results for the compressor evaluation. Nevertheless, the results can be used for the validation of the simulations.

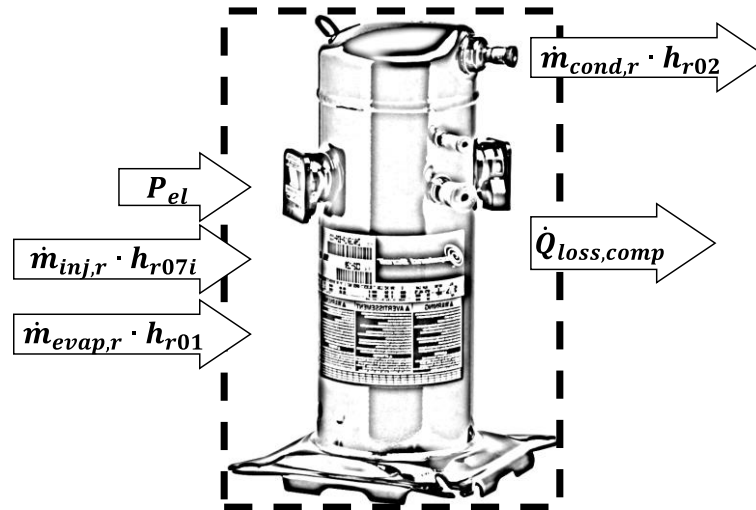


Figure 58: System boundary for compressor evaluation (Copeland, 2011b)

4.2.1. Overall isentropic efficiency

The overall isentropic efficiency compares the real electrical power consumption of compressor, inverter and SEC, to the power that is needed for an isentropic compression at a certain pressure ratio and mass flow, as generally described in Equation 4. Whereas for the one-stage compression the overall isentropic efficiency can be directly derived from the

electrical power consumption, for the two-stage compression several assumptions have to be made, which are explained in the following paragraphs. All losses that occur from the compression itself (inner isentropic efficiency) as well as motor, inverter and mechanical losses are combined by the compressor heat losses $\dot{Q}_{loss,comp}$, which are derived from an energy balance (Equation 39) over the system boundary, defined in Figure 58. The ratio of the compressor heat losses to the electrical power input $f_{comp,loss}$ is given in Equation 40. It is assumed to be the same ratio for both stages of the compressor.

$$\dot{Q}_{loss,comp} = \dot{m}_{evap,r} \cdot h_{r01} + (\dot{m}_{cond,r} - \dot{m}_{evap,r}) \cdot h_{r07i} + P_{el} - \dot{m}_{cond,r} \cdot h_{r02} \quad \text{Equation 39}$$

$$f_{comp,loss} = \frac{\dot{Q}_{loss,comp}}{P_{el}} \quad \text{Equation 40}$$

In Figure 59 the two-stage compression is depicted in a temperature/enthalpy-diagram. The points (1), (7i) and (2) are measured points whereas all other points are calculated points which are needed for solving the equation system. All figures of the first compression are marked with one apostrophe whereas the mixing point at medium pressure is marked with two apostrophes. The isentropic efficiency of both stages is defined as shown in Equation 41 and Equation 42. As the two-stage scroll compressor has its injection ports directly within the scrolls (see Chapter 2.1.2) it is not possible to measure the state of the refrigerant between the two stages. It is assumed that the isentropic efficiency is the same for both stages (Equation 43). The theoretical points are explained in the following paragraphs.

$$\eta_{is1} = \frac{(h_{r02'is} - h_{r01})}{(h_{r02'woloss} - h_{r01})} \quad \text{Equation 41}$$

$$\eta_{is2} = \frac{(h_{r02,is} - h_{r02''})}{(h_{r02,woloss} - h_{r02''})} \quad \text{Equation 42}$$

$$\eta_{is1} = \eta_{is2} \quad \text{Equation 43}$$

The entropy of point (1) s_{r01} is derived from the property table via the measured data of temperature and pressure. Point (2'_{is}) is reached when isentropic compression in the first stage is assumed. With medium pressure p_{r07i} and entropy s_{r01} the enthalpy of this point $h_{r02'is}$ can be calculated. To get the calculated state at the end of the first-stage compression (2'), the compressor losses which were defined above, have to be considered. The compression without losses ($h_{r02'woloss}$) is gained from Equation 46.

$$s_{r01} = s(T_{r01}, p_{r01}) \quad \text{Equation 44}$$

$$h_{r02'is} = h(p_{r07i}, s_{r01}) \quad \text{Equation 45}$$

$$(h_{r02'} - h_{r01}) = (h_{r02'woloss} - h_{r01}) - (h_{r02'woloss} - h_{r01}) \cdot f_{comp,loss} \quad \text{Equation 46}$$

$$h_{r02'woloss} = \frac{(h_{r02'is} - h_{r01}) \cdot f_{comp,loss}}{(1 - f_{comp,loss})} \quad \text{Equation 47}$$

At the injection ports of the fixed scroll the compressed refrigerant of the first stage is cooled with the injection mass flow. The mixing point (2'') is calculated with an energy balance as both input enthalpies ($\dot{m}_{evap,r} \cdot h_{r01}$ and $\dot{m}_{inj,r} \cdot h_{r07i}$) have to result in the state of the mixing point ($h_{r02''}$, $s_{r02''}$). Where the isentropic compression of stage two leads to $h_{r02,is}$, the enthalpy of the compression without losses $h_{r02,woloss}$ is calculated with the measured state at the end of compression h_{r02} and Equation 49. The six unknown variables (η_{is1} , η_{is2} , $h_{r02'woloss}$, $h_{r02'}$, $h_{r02''}$, $h_{r02,woloss}$) can be iteratively solved with the six equations (Equation 41 to Equation 43 and Equation 47 to Equation 49).

$$h_{r02''} = \frac{\dot{m}_{evap,r}h_{r02'} + (\dot{m}_{cond,r} - \dot{m}_{evap,r})h_{r07i}}{\dot{m}_{cond,r}} \quad \text{Equation 48}$$

$$h_{r02,woloss} = \frac{(h_{r02} - h_{r02''} f_{comp,loss})}{(1 - f_{comp,loss})} \quad \text{Equation 49}$$

$$s_{r02''} = s(h_{r02''}, p_{r07i}) \quad \text{Equation 50}$$

$$h_{r02,is} = h(p_{r02}, s_{r02''}) \quad \text{Equation 51}$$

The overall isentropic efficiency of the two-stage compression is calculated as follows:

$$\eta_{is,overall} = \frac{\dot{m}_{evap,r}(h_{r02'is} - h_{r01}) + \dot{m}_{cond,r}(h_{r02,is} - h_{r02''})}{P_{el}} \quad \text{Equation 52}$$

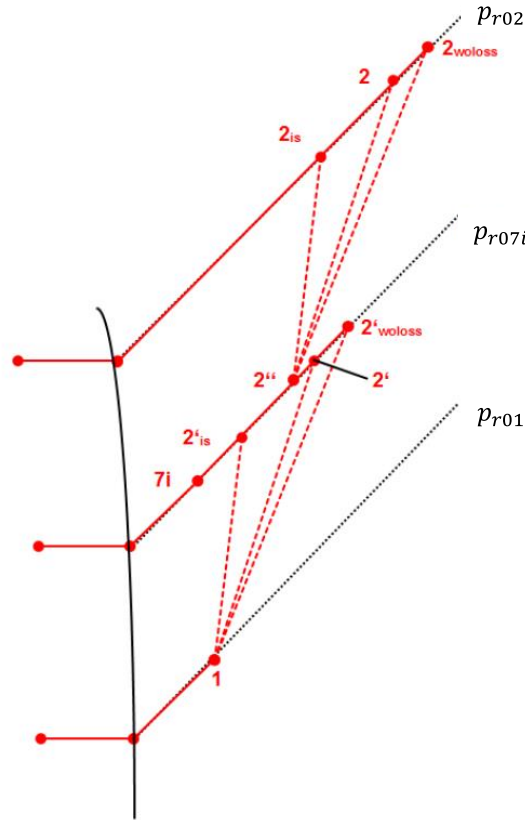


Figure 59: Theoretical two-stage compression for scroll compressor (Baur, 2014)

4.2.2. Volumetric efficiency

The general definition of the volumetric efficiency is given in Equation 3. A fixed swept volume V_{swept} is given by the geometry of the scrolls. For the second stage the swept volume V_{swept2} is smaller, as the injection is executed within the same pair of scrolls (Equation 53 to Equation 54). The factor of 0.71 that correlates these values, was derived with the assumption of equal overall isentropic compressor efficiencies for both stages. The compressor behaviour was simulated and by varying the swept volume of the second stage the results were compared to the values of the software 'Select' from the compressor manufacturer (Copeland, 2013b), which shows the performance of the compressor. The results matched with the factor 0.71.

Due to leakage of refrigerant within the scrolls and re-expansion from the clearance volume the volumetric efficiency is smaller than 1 and will decrease with higher pressure ratios. It is an important coefficient as the leaked refrigerant has to be compressed again and therefore increases the electrical power consumption of the compressor. In Equation 55 and Equation 56 the efficiencies are defined. For the first stage the volume flow rate at the suction port (r_{01}) is divided by the swept volume multiplied by the compressor speed ratio of the real to the nominal speed of $n_{nom} = 3000 \text{ rpm}$. Whereas the volumetric efficiency of the second stage is calculated with the volume flow rate at the mixing point (2'') and the ideal flow rate of the remaining swept volume V_{swept2} .

$$V_{swept} = 2.8 \frac{\text{m}^3}{\text{h}} \text{ at } 50 \text{ Hz} \quad \text{Equation 53}$$

$$V_{swept2} = V_{swept} \cdot 0.71 = 1.99 \frac{\text{m}^3}{\text{h}} \text{ at } 50 \text{ Hz} \quad \text{Equation 54}$$

$$\eta_{vol1} = \frac{\dot{m}_{evap,r} \cdot v_{r01}}{V_{swept} \cdot \frac{n_{comp}}{n_{nom}}} \quad \text{Equation 55}$$

$$\eta_{vol2} = \frac{\dot{m}_{cond,r} \cdot v_{r02''}}{V_{swept} \cdot 0.71 \cdot \frac{n_{comp}}{n_{nom}}} \quad \text{Equation 56}$$

To be able to compare the two-stage scroll compressor with other compressors it is usual to define an overall volumetric efficiency $\eta_{vol,overall}$. Thereby it is necessary to use an appropriate reference value, as the mass flow rate of the two stages varies. For this evaluation a mass-related definition as shown in Equation 57 is used. It is also possible to use other definitions for the volumetric efficiencies. An alternative definition is given in the following paragraph. Nevertheless, it is very important only to compare efficiencies with the identical definition to get valid conclusions.

$$\eta_{vol,overall} = \frac{\dot{m}_{evap,r} \cdot \eta_{vol1} + \dot{m}_{cond,r} \cdot \eta_{vol2}}{\dot{m}_{evap,r} + \dot{m}_{cond,r}} \quad \text{Equation 57}$$

To evaluate the overall volumetric efficiency of a two-stage compressor also the following method could be used. By defining a volumetric efficiency for the suction gas $\eta_{vol,evap}$ (Equation 58) and the injection gas $\eta_{vol,inj}$ (Equation 59), a maximum theoretical mass flow $\dot{m}_{cond,max}$ can be calculated. The volumetric efficiency of the suction gas is identical to the definition in Equation 55. For the injection gas, the real mass flow rate of the injection line is related to the maximum possible mass flow rate. This variant of the overall volumetric efficiency $\eta_{vol,overallVAR}$, is then calculated by comparing the real mass flow rate to the maximum theoretical value (Equation 60). A main disadvantage of this method is that the injection mass flow, which has a high uncertainty of measurement, is needed for the evaluation.

$$\eta_{vol,evap} = \frac{\dot{m}_{evap,real}}{\dot{m}_{evap,max}} \quad \text{Equation 58}$$

$$\eta_{vol,inj} = \frac{\dot{m}_{inj,real}}{\dot{m}_{inj,max}} \quad \text{Equation 59}$$

$$\eta_{vol,overallVAR} = \frac{\dot{m}_{cond,real}}{\dot{m}_{cond,max}} = \frac{\dot{m}_{cond,real}}{\dot{m}_{evap,max} + \dot{m}_{inj,max}} \quad \text{Equation 60}$$

In the following, the evaluation of the overall volumetric efficiency is only executed with the definition in Equation 57.

4.3. Uncertainty propagation

The basics of the uncertainty propagation were already explained in Chapter 2.3. It is necessary as different measuring devices are used for the measurements, which have an influence on the measured value. To be able to evaluate these values, the uncertainty is very important. As for the single measurement devices the errors are already listed in Table 4, in this chapter the uncertainty propagation of calculated values, which are dependent on several measured values, is described. For this purpose the Gaussian propagation of uncertainty (Equation 9) is used. As certain values are gained from property data, which would lead to complex derivations, an approximation as shown in Equation 61 is done. The finite differences method with a small variation $\Delta x_{1,var}$ of Δx_1 leads to a small variation of the function f (Baur, 2014).

$$\frac{\partial f}{\partial x_1} \cdot \Delta x_1 \approx \frac{\Delta f}{\Delta x_{1,var}} \cdot \Delta x_1 \quad \text{Equation 61}$$

For the interpretation of the operating points the most important values are the Coefficient of Performance, the overall isentropic efficiency, the overall volumetric efficiency and the mass flow on the water side of the desuperheater, as these variables are calculated from other measured variables. The method of finite differences is applied for all values in the same way. It will only be exemplarily demonstrated for the total heating capacity of the condenser on the refrigerant side $\dot{Q}_{cond,tot,r}$ (Equation 28).

As the enthalpy is a function of temperature and pressure, which is approximated by a polynomial function, the finite difference method is used, see Equation 62. By using a fictive difference Δp_r , a fictive enthalpy is gained, from which the enthalpy difference Δh_r is derived. With the Gaussian propagation the uncertainty of the enthalpy is calculated. This can then be used for other values such as $\dot{Q}_{cond,tot,r}$. In Equation 63 the derivations of all variables are shown. The error of measurements of the measured variables (T_r , p_r and \dot{m}_{r05}) are taken from Table 4, which represent the unknown systematic deviations.

$$u_{h_r} = \sqrt{\left(\frac{\partial h_r}{\partial p_r}\right)^2 \cdot u_{p_r}^2 + \left(\frac{\partial h_r}{\partial T_r}\right)^2 \cdot u_{T_r}^2} = \sqrt{\left(\frac{\Delta h_r}{\Delta p_r}\right)^2 \cdot u_{p_r}^2 + \left(\frac{\Delta h_r}{\Delta T_r}\right)^2 \cdot u_{T_r}^2} \quad \text{Equation 62}$$

$$\text{with} \quad p_r^* = p_r - \Delta p_r \quad h_r^* = f(p_r^*) \quad \Delta h_r = h_r - h_r^*$$

$$\begin{aligned} u_{\dot{Q}_{cond,tot,r}} &= \\ &\sqrt{\left(\frac{\partial \dot{Q}_{cond,tot,r}}{\partial \dot{m}_{cond,r}}\right)^2 \cdot u_{\dot{m}_{cond,r}}^2 + \left(\frac{\partial \dot{Q}_{cond,tot,r}}{\partial h_{r02}}\right)^2 \cdot u_{h_{r02}}^2 + \left(\frac{\partial \dot{Q}_{cond,tot,r}}{\partial h_{r04}}\right)^2 \cdot u_{h_{r04}}^2} \\ &= \sqrt{(h_{r02} - h_{r04})^2 \cdot u_{\dot{m}_{cond,r}}^2 + (\dot{m}_{cond,r})^2 \cdot u_{h_{r02}}^2 + (-\dot{m}_{cond,r})^2 \cdot u_{h_{r04}}^2} \end{aligned} \quad \text{Equation 63}$$

Most of the uncertainties are calculated like shown above, but a few values are more difficult to solve with the finite difference method. For these the software EES (2015), which has an integrated functionality for uncertainty propagation is used to calculate the deviations. A comparison of these two different calculation approaches was done and it was found out that the ranges are similar. Therefore it will not be mentioned in the following chapter, which calculation was used for the interpretation of the individual results.

5. RESULTS AND DISCUSSION

In this chapter all measured operating points and the measurements of the 24-hour test are analysed. At first the envelope and the efficiency of the compressor are discussed. Afterwards the heat pump cycle is studied by interpreting the COP depending on several variables. An analysis of the heat exchangers will not be executed as this was already done by Baur (2014). An emphasis is put on the dynamic measurements, as they are important for the further operation of the heat pump integrated within the whole system, which is carried out in the laboratory of the project partner.

The nomenclature of the operating points is defined with the brine inlet temperature T_{b01} , which is an indicator for the temperature level of the heat source such as ground source or ambient air temperature, followed by the condenser inlet temperature T_{w01} , which is the control variable of the water circuit and thereby representing the return temperature of the heating cycle. For heating applications it is preferred to indicate the outlet temperature of the condenser T_{w02} , as this is the provided temperature level for the heating system. Nevertheless, the control behaviour of the water circuit is better when T_{w01} is used as control variable for the measurements. The last figure indicates the compressor speed in revolutions per minute (rpm) at a certain operating point. Thus the abbreviation of an operating point with a brine inlet temperature of $-15\text{ }^{\circ}\text{C}$, a condenser inlet temperature of $30\text{ }^{\circ}\text{C}$, measured at a compressor speed of 3600 rpm is '-15/30/3600'.

All steady state measurements were performed with a mass flow rate of 1078 kg/h on the brine cycle and 857 kg/h on the water cycle (see Chapter 3.3). The superheating of the suction and injection gas is set to a value of 5 K and the storage temperature for the natural circulation of the desuperheater is $30\text{ }^{\circ}\text{C}$. During the measurements the mass flow meter on the refrigerant side (FE_{r05}) displayed implausible values for all operating points of 15/20, where the pressure ratio is at its minimum. The reason for the mass flow meter showing implausible values could not be detected within this thesis and the error could not be eliminated. Therefore the mass flow rate was calculated with Equation 26 and Equation 27, which leads to a higher inaccuracy for these measuring points. These uncertainties are shown at the end of this chapter.

5.1. Compressor

The compressor performance has a big influence on the efficiency of the overall heat pump system. There are several limiting factors, which are evaluated in the following paragraphs. Some of these factors are the heat losses to the ambient, inner compression losses and leakage within the scrolls.

In Figure 60 the ratio of the heat losses to the electrical power input $f_{loss,comp}$ (see Equation 40) is shown as a function of the compressor speed n . Different operating points are plotted and a second order polynomial fit-curve is inserted to visualise the progression of the values. The relative compressor losses decrease with increasing compressor speed for all operating points. Minimum losses are reached within a range of 4200 to 5400 rpm, depending on the operating point. As only measurements with a maximum speed of 5400 rpm were carried out, an optimum for the heat losses at even higher speeds cannot be ruled out, considering that the maximum possible speed of the compressor is at 7020 rpm. The gradient of the curves is getting smaller with higher compressor speeds and similar operating conditions. This can be explained by the higher discharge temperatures at higher speeds. Thereby also the temperature of the compressor shell rises and the heat losses to the ambient increase. This seems to have a bigger impact on the progression of the curve than the electrical power consumption of the compressor, which also increases at higher speeds. It can also be derived from this figure that the compressor heat losses are increasing with the pressure

ratio. The operating points (-15/45, -15/30 and -15/20) show the highest relative losses when comparing it to operating points with the same compressor speed. Low pressure ratios as for 2/20 and 2/30 are almost equal and show the lowest losses for a wide range of speeds. For 2/30 the compressor losses increase again at speeds higher than 4200 rpm. The minimum measured loss of 6 % is at 2/20/5400 whereas the maximum loss of 14.5 % is at 2/30/1800.

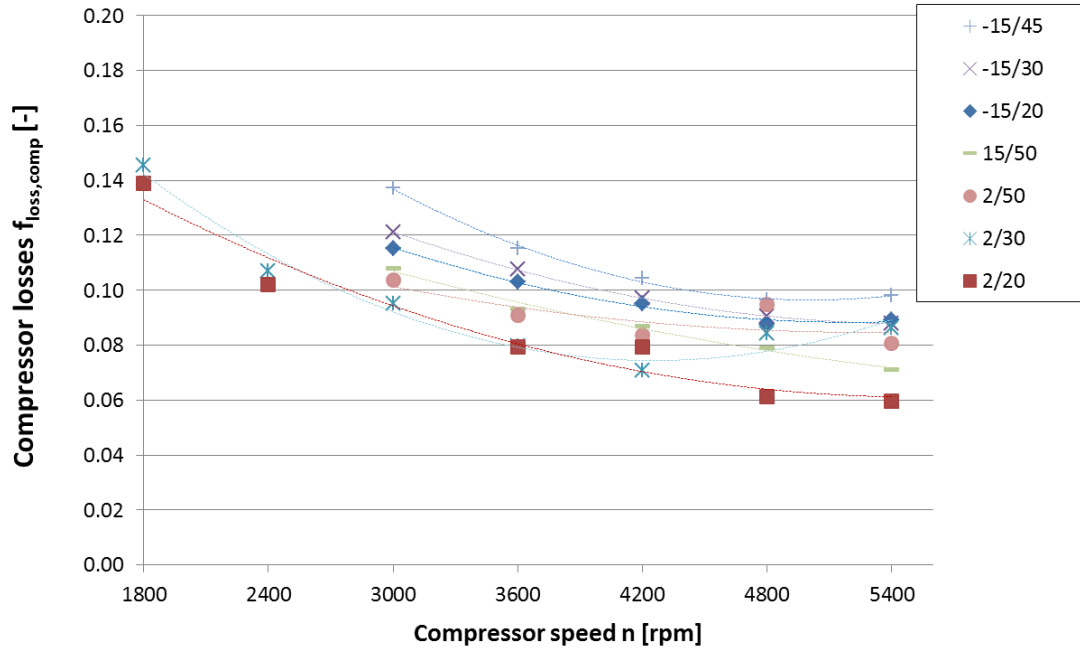


Figure 60: Heat losses of compressor $f_{loss,comp}$ for different operating points as a function of the compressor speed n

5.1.1. Overall isentropic efficiency

With the definition of the heat losses, the overall isentropic efficiency for the two stage compression can be determined. It is defined as described in Equation 52. The operating points with different compressor speeds from 1800 to 5400 rpm are illustrated in Figure 61. Although the operating points stay constant, the pressure ratio increases with higher speeds due to a higher capacity at the heat exchangers, which leads to a higher temperature difference in the pinch point and therefore rising condensation and decreasing evaporation pressure. Additionally the temperature difference both on the water and brine side (condenser or evaporator) increases, because the mass flow rate on the water or brine cycle is constant. This leads to a rise of the pressure ratio as well.

At operating points with low evaporation temperatures (-15/45, -15/30 and -15/20) (causing high pressure ratios) the overall isentropic efficiency is low. 2/20, 2/30, 15/20 and 15/30 show best efficiencies at compressor speeds between 3600 and 5400 rpm. With lower speeds the efficiency decreases tremendously for these operating conditions. At the operating point 15/30 the highest overall isentropic efficiency of 64 % is reached at a compressor speed of 4800 rpm. This value decreases to 53 % at a speed of 1800 rpm. The lowest efficiency of 51.5 % is achieved at the highest pressure ratio of 8.5 at the operating point -15/45 and a compressor speed of 5400 rpm. The operating points of Figure 61 are also plotted in Figure 62, where the efficiency is shown as a function of the compressor speed. It can be seen that the efficiency is low at low compressor speeds, afterwards it rises to a maximum which is within a range of 3600 to 4800 rpm and then slowly decreases again with higher speeds. Looking at the progression of -15/20 and -15/30 the wide range of compressor speed, where only a slight change of efficiency occurs, can be seen.

Generally it can be said that each operating point has maximum in the overall isentropic efficiency at a certain 'optimum' speed, which is within a range of 3500 to 5400 rpm. Several components have an influence on the progression of the overall isentropic efficiency over the compressor speed. The efficiencies of the brushless electric motor and the inverter drive, as well as the mechanical losses vary with the compressor speed. However, the impact of single components was not analysed within this thesis. At low compressor speeds the discharge temperatures are lower, leading to lower losses from the refrigerant to the ambient. This is vice versa for higher compressor speeds. Due to the fixed volume ratio of the scroll compressor, the overall isentropic efficiency decreases besides the optimum pressure ratio, as compression losses occur due to over- and under-compression (Figure 7).

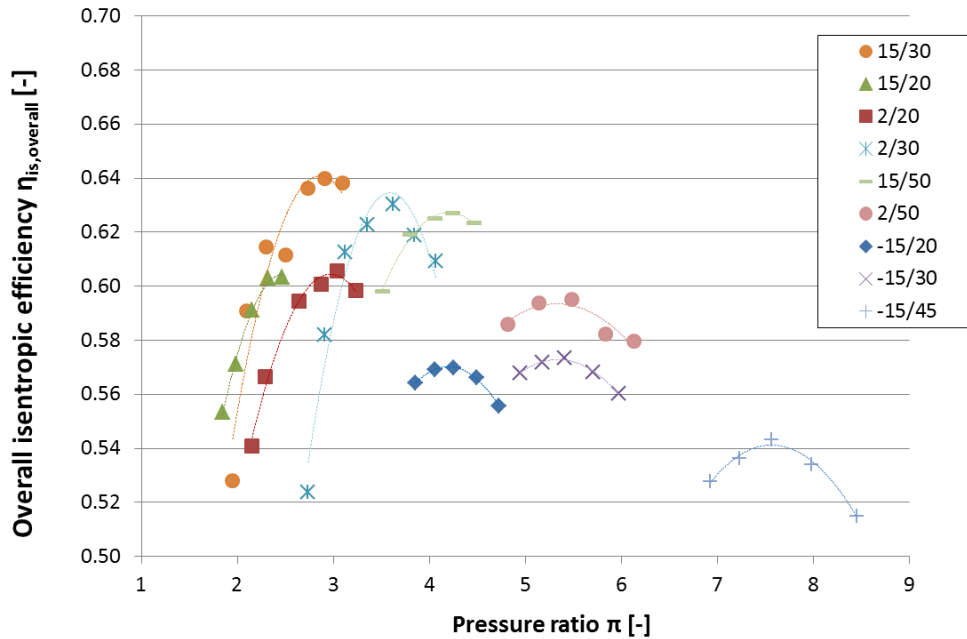


Figure 61: Overall isentropic efficiency $\eta_{is,overall}$ for different operating points as a function of pressure ratio π

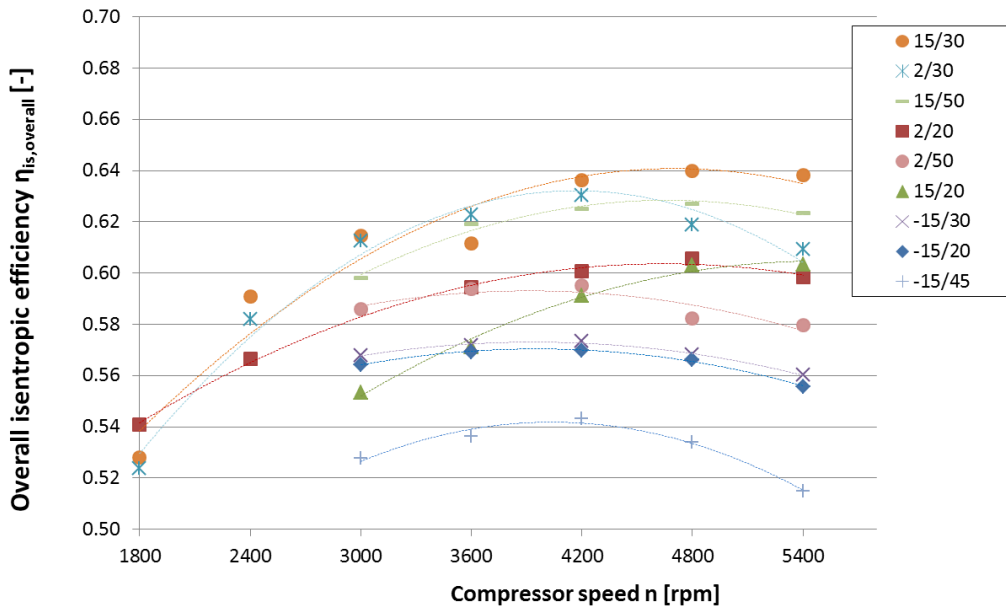


Figure 62: Overall isentropic efficiency $\eta_{is,overall}$ for different operating points as a function of compressor speed n

5.1.2. Volumetric efficiency

The overall volumetric efficiency is defined as described in Equation 57. This efficiency is plotted as a function of the pressure ratio for several operating points and different compressor speeds in Figure 63. It shows that within one operating condition, where the pressure ratio rises due to increasing compressor speeds, the overall volumetric efficiency has an optimum. The highest efficiency of 97 % is reached at 15/20/4200, whereas the lowest measured efficiency of 78 % is achieved at 2/20/1800. Leakage within the scrolls increases with increasing pressure difference. Operating points with high pressure ratios (-15/20, -15/30, 2/50 and -15/50) have a much lower overall volumetric efficiency than operating points with low pressure ratios, such as 15/20, 15/30, 2/20 and 2/30.

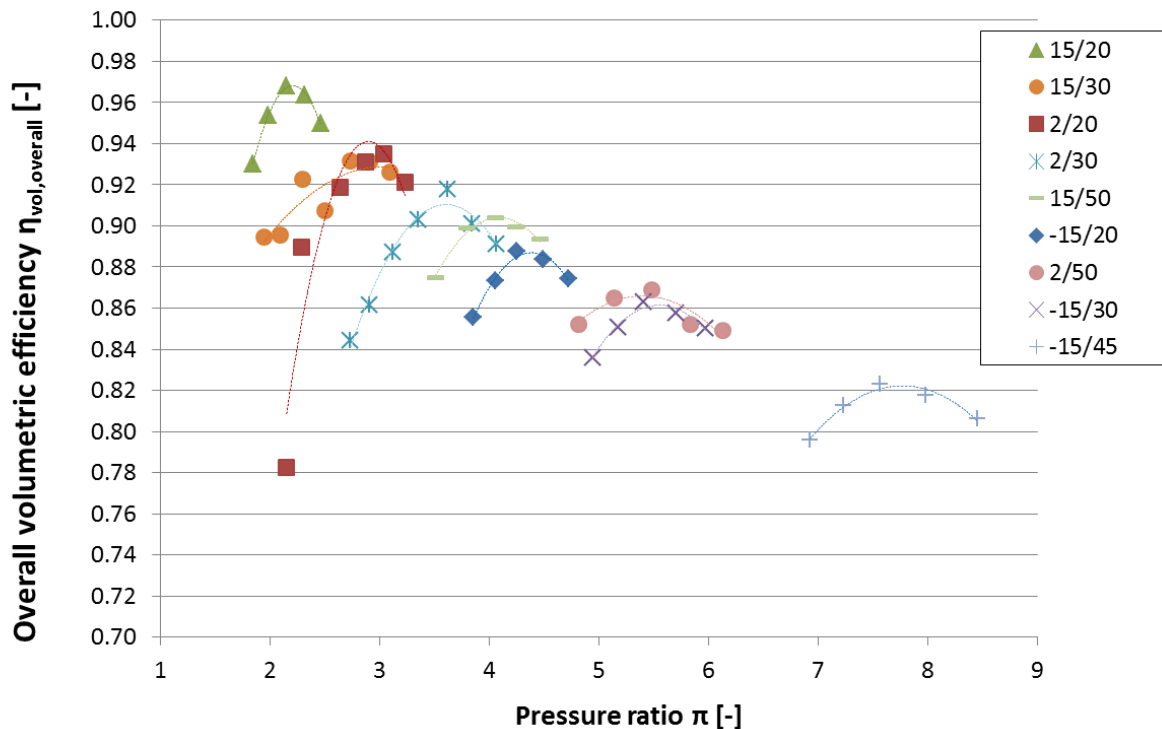


Figure 63: Overall volumetric efficiency $\eta_{vol,overall}$ for different operating points as a function of pressure ratio π

In Figure 64 the same measurements are illustrated but being grouped with identical compressor speeds. It shows that the overall volumetric efficiency is linearly dependent on the pressure ratio for given compressor speeds. The efficiency decreases with increasing pressure ratio. Best efficiencies for each pressure ratio are reached with compressor speeds of 4200 and 5400 rpm.

The mass-related definition of the overall volumetric efficiency (Equation 57) is based on several assumptions, which are explained in Chapter 4.2.2. In Figure 65 the volumetric efficiencies of each stage are compared with each other. On the left side of this figure the first stage is plotted (η_{vol1} - Equation 55) whereas the second stage is on the right side (η_{vol2} - Equation 56). The gradient of the decrease of efficiency over a rising pressure ratio is slightly higher for the second stage. Also for lower compressor speeds the first stage reaches higher efficiencies compared to the second stage. Where the best efficiency at 2400 rpm is 92 % for the first stage, it is only 88 % for the second stage. Altogether the first stage compression shows slightly higher efficiencies than the second stage compression. When comparing the two stages it has to be considered that the volumetric efficiency of the second

stage is calculated by using the fictive mixing point (2''). This point is based on the assumption that the overall isentropic efficiency is the same for both stages.

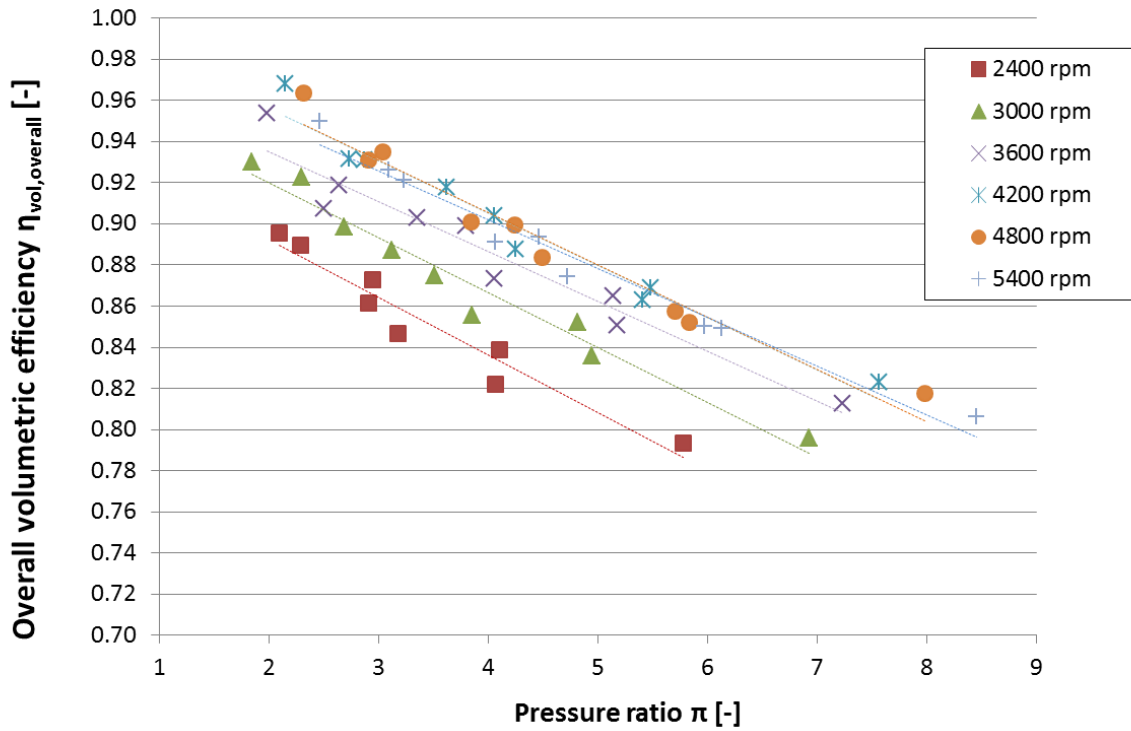


Figure 64: Overall volumetric efficiency $\eta_{vol,overall}$ for different compressor speeds as a function of pressure ratio π

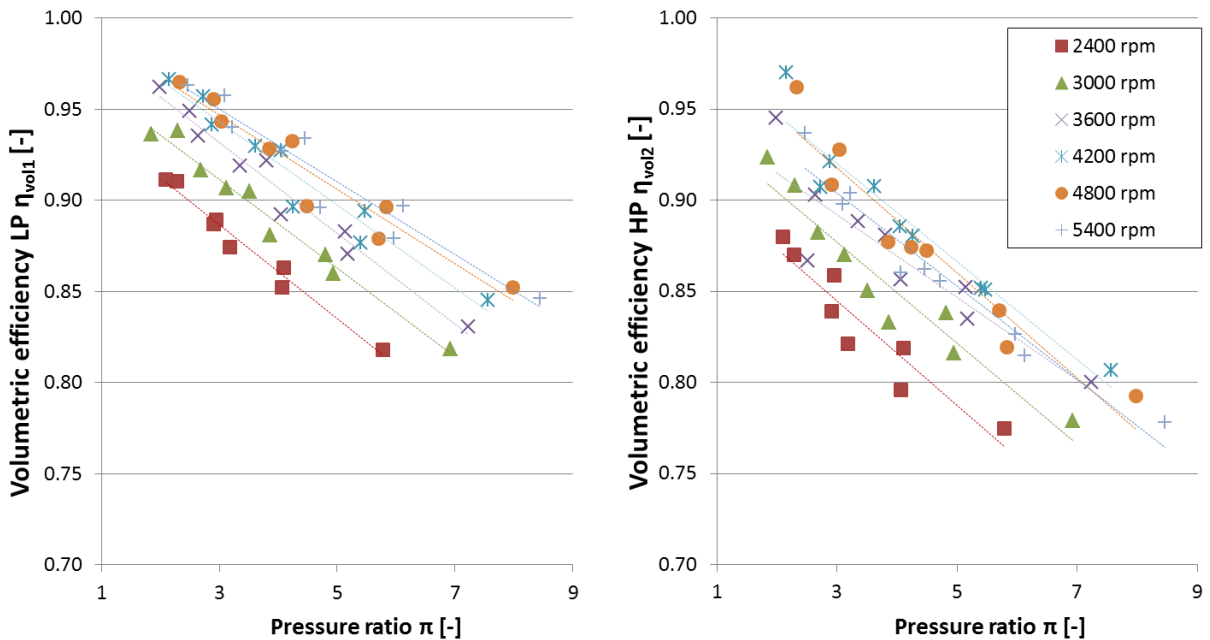


Figure 65: Volumetric efficiency for different compressor speeds as a function of pressure ratio π ; left: first stage compression η_{vol1} ; right: second stage compression η_{vol2}

5.2. Heat pump system

For the heat pump system the Coefficient of Performance (COP) is a very important value for the comparison of different systems at certain operating points. It is defined as shown in Equation 37 and is only valid for one operating point at a specific speed. The COP is severely influenced by the compressor efficiencies, but also additional components as heat exchangers have an impact on the cycle performance. This impact of the heat exchangers is thoroughly analysed in Riedler (2015) and is only summarised in this master thesis. A main conclusion of the analysis is that with higher compressor speeds and brine inlet temperatures the mass flow over the condenser and therefore the heating capacity increases. The overall heat transfer coefficient of the heat exchanger (UA -value) has an optimum for a certain heating capacity or operating condition. When this capacity is exceeded, the temperature difference in the pinch point of the heat exchanger increases significantly and thereby also the pressure ratio, as explained in Chapter 2.1.3.

In Figure 66 the COP of different operating points with various speeds is plotted over the pressure ratio π . The COP decreases with rising pressure ratio, whereby the highest value of 6.99 is reached at 15/20/3000 and the lowest value of 2.13 at -15/45/5400. All measured points are along the fit-curve, which was inserted to visualise the progression of the coefficient, except for the operating points of 15/50, which have a slight deviation to the fit-curve. The highest values for the cycle performance are reached with the operating points at 15/20. As already mentioned at the beginning of Chapter 5 the mass flow meter showed implausible values for these operating points and therefore the mass flow had to be calculated, which leads to a higher uncertainty of measurement for these points. In the Appendix A-2 all measurements are listed with their uncertainty of measurement.

Generally the highest COP is reached at low pressure ratios, which can be explained by the compressor efficiencies shown above. Both the overall isentropic and the volumetric efficiency show the highest values for low pressure ratios. Nevertheless, some operating points also show a decrease of performance at low compressor speeds, which is depicted for the COP in Figure 67. The complete range of compressor speeds from 1800 to 5400 rpm could only be measured for small pressure ratios, as for higher ratios lower compressor speeds are not within the compressor envelope. Also for the measuring points of the smallest pressure ratio (15/20) not all points are in the compressor envelope. Therefore in Figure 67 only the operating points 15/30, 2/20, 2/30, 15/50 and 2/50 are illustrated. It can be seen that not for all operating points the highest value of COP is reached at the lowest compressor speed. Whereas 15/30 and 2/20 show their maximum at 1800 rpm, the operating points of 2/30, 2/50 and 15/50 have their maximum at 2400 rpm. With higher compressor speeds the Coefficient of Performance slightly decreases for all operating points.

All in all there are two different effects that affect the heat pump cycle performance. On the one hand a rising pressure ratio leads to a decrease of the COP and on the other hand the compressor efficiency is higher for compressor speeds at a range between 3600 and 4800 rpm due to the effects explained in Chapter 5.1. As the progression of the COP in Figure 67 decreases steadily with higher compressor speeds, it can be concluded that the impact of these two effects varies. At low compressor speeds the impact of the pressure ratio is less dominant than it is at high speeds. The influence of the compressor efficiency flattens the decrease of the COP at higher speeds. Both the pressure ratio and the compressor efficiency show a negative influence on the COP at the maximum speed of 5400 rpm.

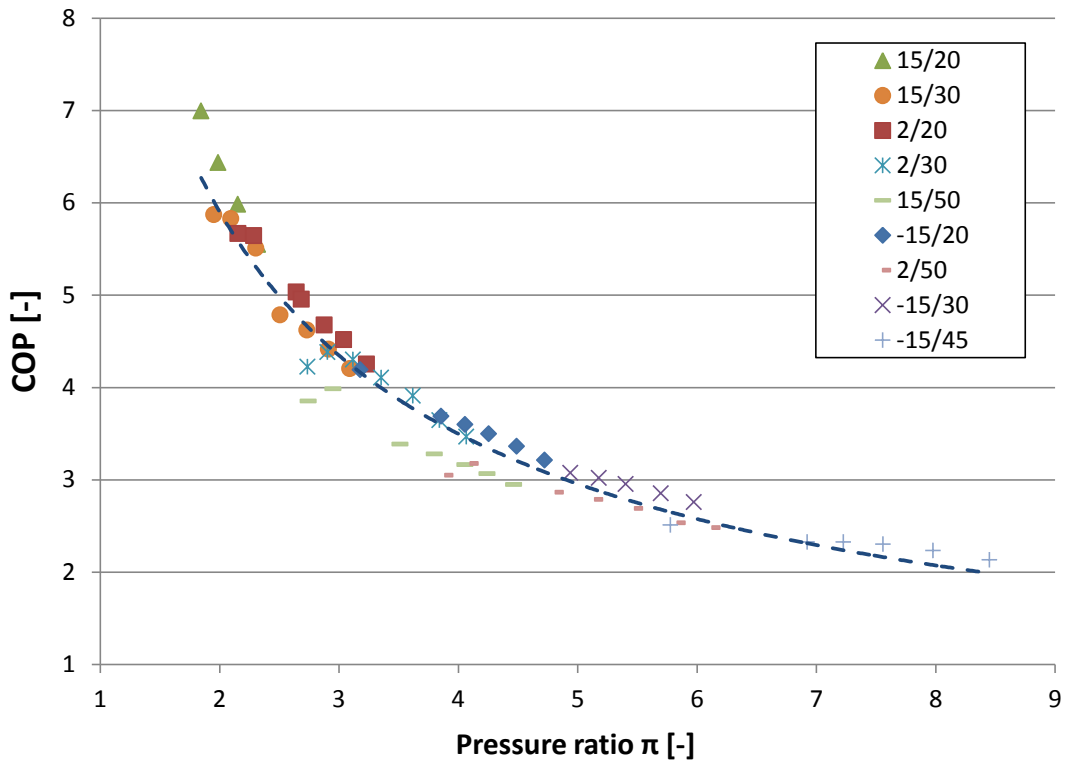


Figure 66: Coefficient of Performance COP for different operating points as a function of pressure ratio π

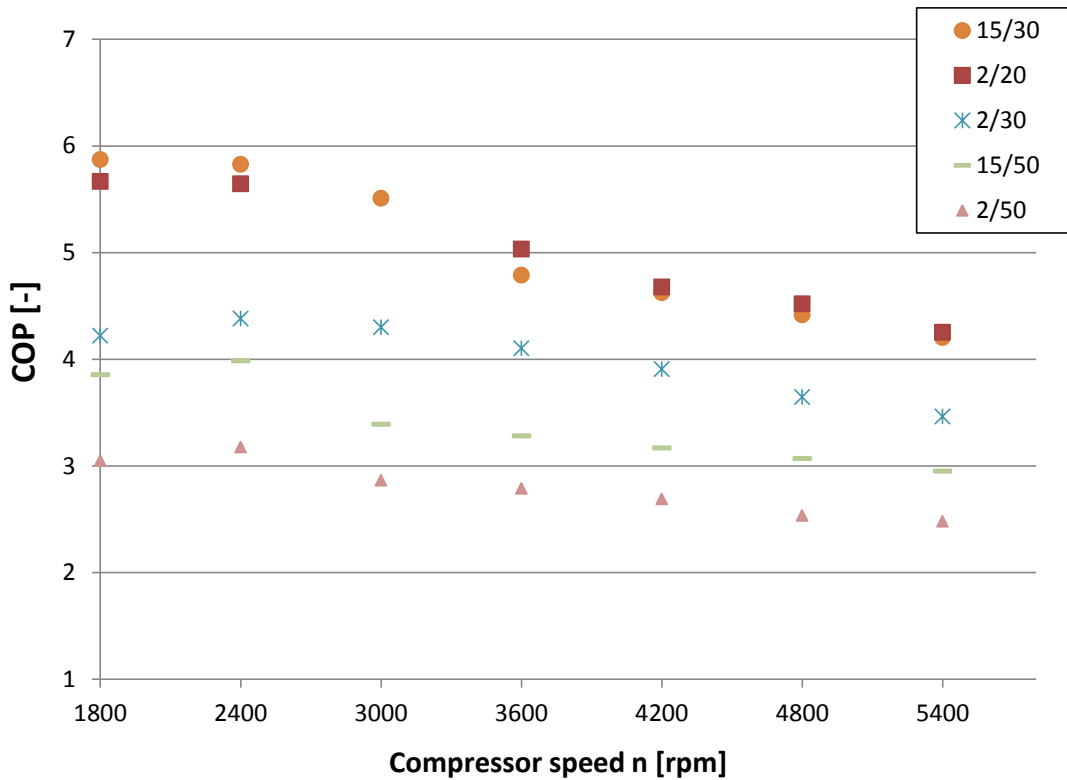


Figure 67: Coefficient of Performance COP for different operating points as a function of compressor speed n

For the application of the heat pump system it is also very important to know the behaviour of the cycle performance at different heating temperature levels and ambient conditions. Usually a heating system is designed for an operating point with a certain temperature level that is supposed to provide space heating. In this case the heat pump system is also supposed to provide domestic hot water at a high temperature level.

In Figure 68 different operating points (T_{b01} from -15 to 15 °C and n from 2400 to 5400 rpm) are shown with their COP at different condenser inlet temperatures T_{w01} . It can be seen that the cycle performance is at its best for low condenser inlet temperatures and therefore low pressure ratios. From 20 to 30 °C the performance decreases more rapidly than it does from 40 to 50 °C for operating points with a brine inlet temperature of 15 °C. Operating points with lower brine inlet temperatures show an almost linear decrease over the rising condenser inlet temperature. Also the progression of these operating points at higher condenser inlet temperatures is flatter compared to operating points with brine inlet temperatures of 15 °C. The influence of the economiser to this progression increases with increasing pressure ratio. It also has to be considered, that the economiser increases the refrigerant mass flow over the condenser, which can lead to a higher temperature difference in the pinch point of the condenser and thereby to an increased pressure ratio. This figure shows that low temperature level heating systems have to be considered for heat pump systems to gain a maximum efficiency. Heating systems with a high temperature level show lower values for the COP . For DHW preparation the temperature level of the condenser inlet temperature is high as well. Compared to the temperature level of space heating, the cycle performance is much lower. This is the reason for the use of a desuperheater that continuously provides energy for DHW, while space heating demand is provided at lower condensation temperatures. The heat pump cycle is showing a better performance compared to operating points where only DHW preparation is done.

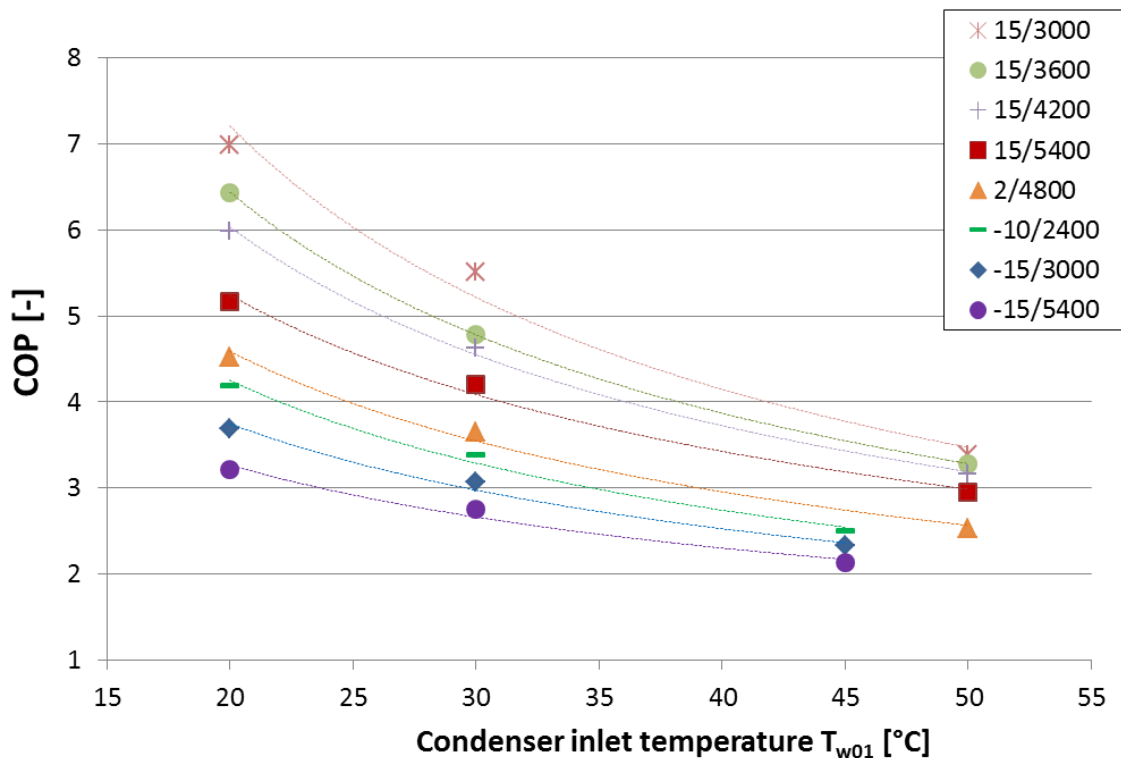


Figure 68: Coefficient of Performance COP for different operating points as a function of condenser inlet temperature T_{w01}

The temperature level of the heat source is also an important factor for the heat pump system. When ground source is used the temperature changes are much lower compared to the use of ambient air. Figure 69 illustrates the cycle performance of different operating points (T_{w01} from 20 to 45 °C and n from 2400 to 5400 rpm) at different brine inlet temperatures. The best performance is reached with brine inlet temperatures at 15 °C as the pressure ratio is low for these operating conditions. All measuring points show an almost linear progression of the COP with rising brine inlet temperature. Operating points with a condenser inlet temperature of 20 °C have a steeper progression of performance than operating points with 30 and 45 °C.

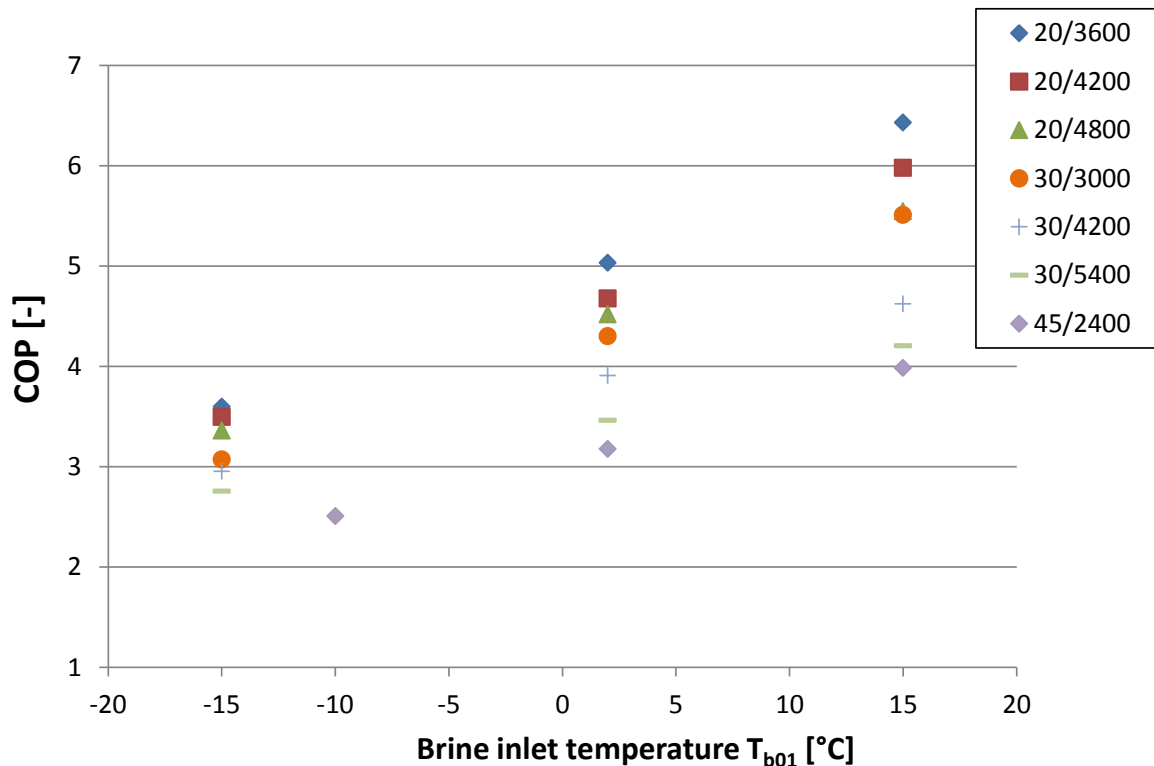


Figure 69: Coefficient of Performance COP for different operating points as a function of brine inlet temperature T_{b01}

The desuperheater which is accomplished with natural circulation is a key part for the energy savings of the heat pump system. At the system tests the desuperheater is directly connected to the upper ports of the thermal energy storage. For the measurements within this thesis the natural circulation was accomplished by separating the water circuit of the desuperheater from the water circuit of the condenser. The desuperheater was connected to a small storage tank (Figure 43) as already explained in Chapter 3.3.2.

All measurements that were analysed so far were executed with a storage temperature of 30 °C. These measurements proved the functionality of the natural circulation, as a sufficient water mass flow over the desuperheater was provided. Nevertheless, the storage temperature of 30 °C is not realistic for all operating points and therefore 9 more measuring points with different storage temperatures (40, 45 and 50 °C) were performed for three different operating conditions (-15/30, 2/30 and 15/30). The operating point 2/30 was operated with a compressor speed of 4200 rpm, due to stability problems, whereas the operating points -15/30 and 15/30 were operated with a speed of 3600 rpm. By using a small range of the compressor speeds, it is tried to keep the impact of the refrigerant mass flow rate on the evaluations small. The changes of the water mass flow of the desuperheater

$\dot{m}_{des,w}$ are plotted as a function of the storage temperature T_{st} in Figure 70. The mass flow over the desuperheater was calculated according to Equation 31. As the compressor discharge temperatures are much higher for low brine inlet temperatures, this leads to a higher mass flow over the desuperheater for the operating points -15/30 and 2/30 compared to 15/30. With rising storage temperatures the mass flow decreases, as the density difference, which is the driving force for the pressure difference in the water circuit decreases as well. It has to be mentioned that the uncertainty of the desuperheater mass flow is high as it is a calculated value. The uncertainty is explained at the end of this chapter.

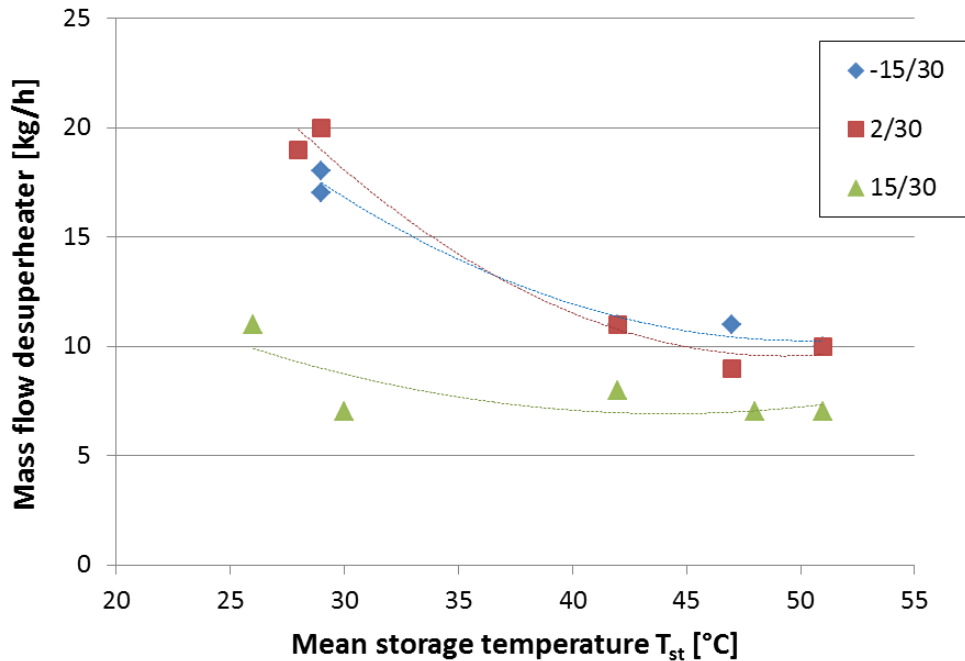


Figure 70: Mass flow desuperheater $\dot{m}_{des,w}$ as a function of the mean storage temperature T_{st}

5.3. 24-hour measurements

After the steady state behaviour of the heat pump system was determined, the dynamic behaviour was analysed. This is the main task of this master thesis, as the heat pump system is supposed to operate automatically in the system tests, which are performed in the laboratory of the project partner. Therefore the software was adjusted and security as well as stability programmes were implemented to ensure a stable behaviour. These programmes were already described in Chapter 3.6.3.

On the contrary to stationary measurements, the dynamic behaviour is influenced by many factors, which cannot be always foreseen. Therefore it is impossible to counteract against these problems in advance. To see the problems that can occur during operation, relevant temperature and heating profiles of a whole day were simulated. Three different simulation days were chosen to cover as many different operating conditions as possible.

- Day 1: space heating – long-time runs
- Day 2: space heating – short-time runs
- Day 3: space heating and DHW preparation

The profile of Day 1 is illustrated in Figure 71. In the diagram the profile is divided into three parts. In the upper part the heating mode (space heating or DHW preparation) and the compressor speed are plotted over the time and the diagram in the middle shows the superheating of the main expansion valve and the volume flow rate of the water cycle at the condenser. The volume flow of the brine cycle is kept at a constant level (1040 l/h) for all profiles. At the bottom of the diagram the temperature profile of the simulation day is illustrated. The heating state 'Space heating' shows whether space heating is provided (state '1') or not (state '0'). It can be seen that space heating is provided from 0:00 to 11:00 and the heat pump is shut down until 19:00. After a short activation the heat pump is then started again at 20:00 for the night hours. The compressor speed is always at a level of about 2500 rpm for the whole measuring period. When the heat pump is stopped, the compressor speed shows a value of about 1000 rpm or less. This is a default value of the control and means that the compressor is not operating. The superheating is illustrated at the diagram in the middle (dotted line). From 0:00 to 5:00 heavy oscillations of the control can be seen. After that period the control keeps the superheating stable at a level of 5 K. On the right axis of this diagram also the volume flow rate of the heat sink is depicted. This value is read from the simulation file and is derived from the demanded heating capacity. From 09:00 to 12:00 the flow rate is steadily decreased, as the heating demand decreases as well. At the bottom of Figure 71 the dotted lines show the values of the simulation file, which were used as reference variables for the controllers. The condenser inlet temperature ($t_{\text{cond_in_simul}}$) and the evaporator inlet temperature ($t_{\text{evap_in_simul}}$) as well as the ambient temperature ($t_{\text{amb_simul}}$) are read from the simulation file. The outlet temperature of the condenser ($t_{\text{cond_out_calc}}$) is calculated with a heating curve for low temperature level heating systems and is used as reference variable for the compressor speed. A slight deviation of the measured condenser inlet temperature to the simulated one can be seen. It is explained by a little temperature offset of the controller, which originates from the position of the temperature sensor, as described in Chapter 3.6.2.

Even though the ambient temperature decreases, the evaporator inlet temperature rises at about 9:00. This clearly shows that the simulated heat source of the heat pump is provided by unglazed solar collectors, where ambient air as well as solar radiation is used as heat source. The influence of the solar radiation is strong on this day. This leads to a steady rise of the brine inlet temperature from $-10\text{ }^{\circ}\text{C}$ to $25\text{ }^{\circ}\text{C}$ within three hours. With the rising evaporation temperature also the density of the suction gas rises, leading to a higher heating capacity. The compressor speed is slowly decreased from 2500 rpm to the minimum speed of 1800 rpm to reduce the heating capacity. When the minimum speed is already reached and the evaporation temperature still rises, the condenser outlet temperature has to increase as the water flow rate decreases. In the system tests the software of the project partner would stop the heat pump as soon as too much heating capacity is provided. This was not implemented for these measurements, as the heat pump test rig was not coupled to the overall heating system. After a longer stopping period and a short on-period, the heat pump is activated again and keeps its condenser outlet temperature at a steady temperature level of $30\text{ }^{\circ}\text{C}$, by increasing the compressor speed as evaporation temperature decreases overnight.

The second profile of the 24 hour tests represents Day 2 and is illustrated in Figure 72. On the upper diagram again the heating state and the compressor speed are plotted. Compared to the profile of Day 1 it can be seen that the heat pump is much more often switched on and off. Also there is no such long stopping period as solar radiation is low for this simulation day.

When looking at the compressor speed it is seen that the heating capacity is very low all day long as the speed is mainly at 1800 rpm. The steady progression of the compressor speed is interrupted five times (at time 2:15, 4:15, 6:15, 10:30 and 22:30) by a peak of 3000 rpm. This is the embedded oil return function which is activated, if the compressor is operated for a longer period at a low speed (see Chapter 3.6.2). Also in the profile of Day 2 the superheating shows oscillations, which seem to be initiated by the first start of the oil return

function. After the second start of the oil return function the superheating is stabilised by the control and is kept at a constant level of 5 K. The volume flow rate of the water cycle is varied between 240 and 400 l/h in this profile. When the other parameters are kept at a constant level, a decreasing water flow rate leads to an increasing condenser outlet temperature. This can be seen in the temperature profile at the bottom of Figure 72 at about 6:30. The controller is not able to reduce the outlet temperature afterwards, as the minimum speed of 1800 rpm is already reached. In the diagram at the bottom it can also be seen that solar radiation is low for this day, as the evaporator inlet temperature only increases slightly between 10:00 and 13:00 and the temperature fluctuates a lot. The inlet temperature of the condenser is kept at the predetermined temperature level by the controller, besides the little offset, for the whole day. The activation of the oil return safety mode can be seen by little temperature peaks of the condenser outlet temperature.

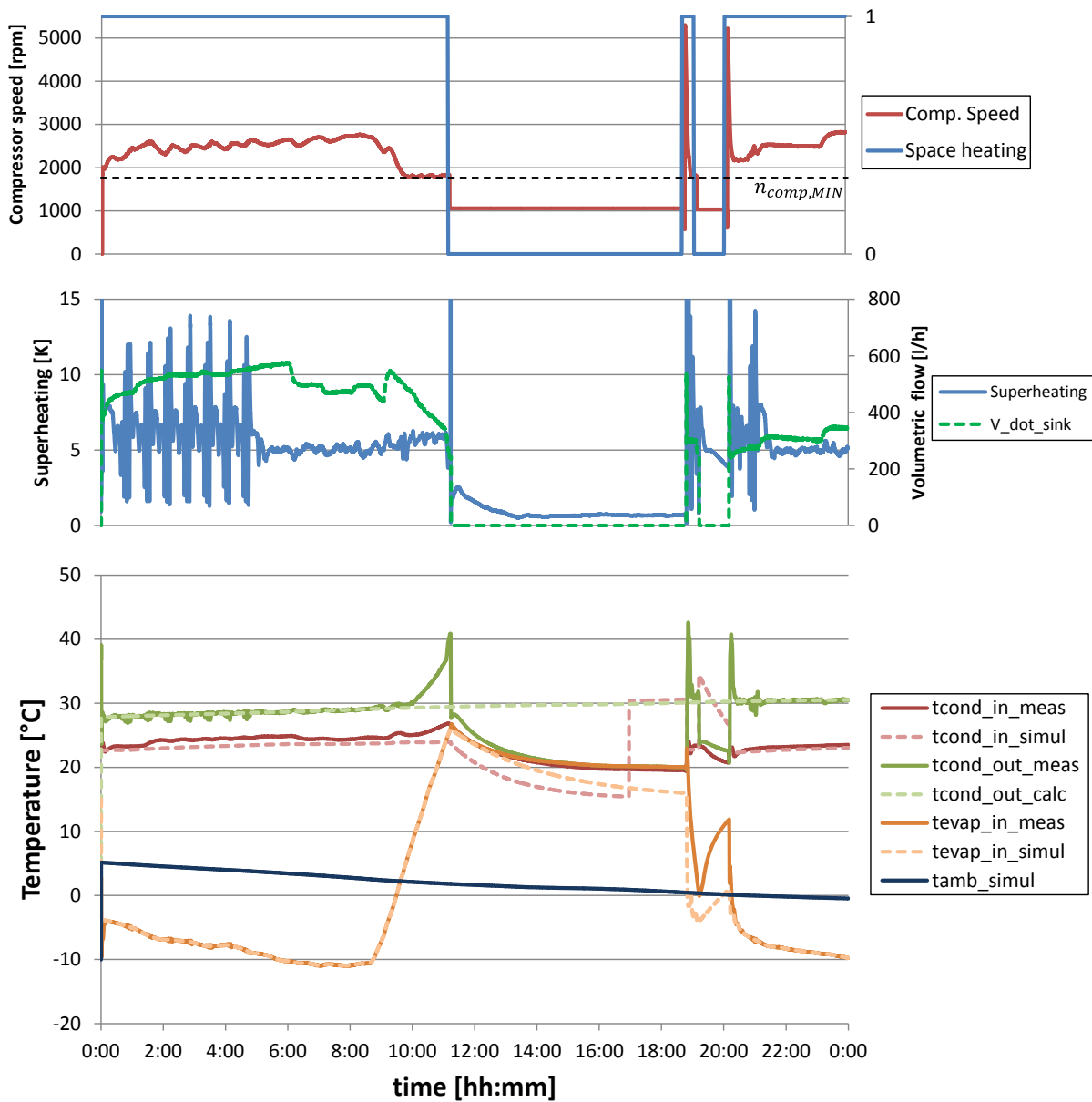


Figure 71: 24-hour measurement – Day 1

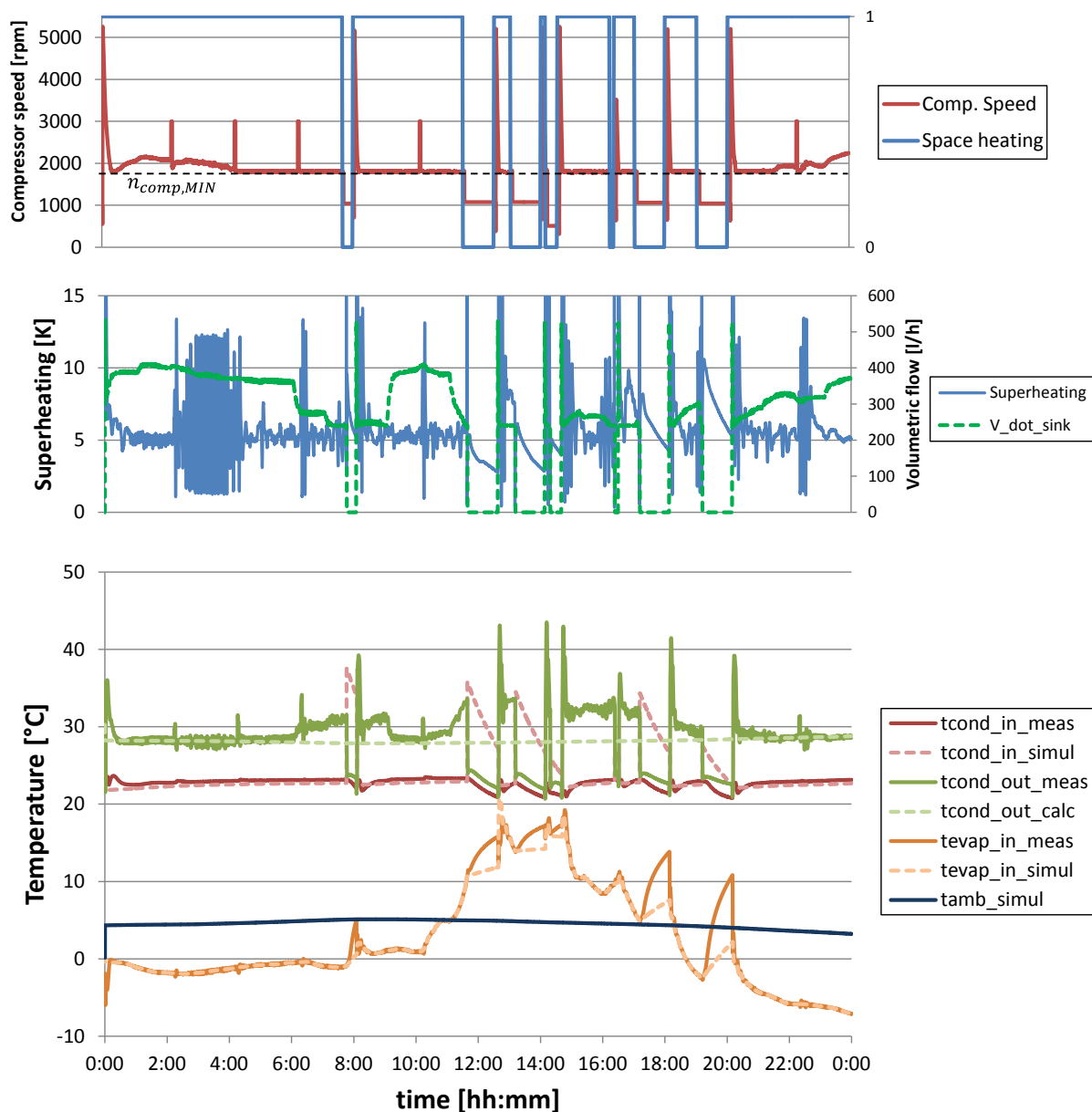


Figure 72: 24-hour measurement – Day 2

The last profile (Day 3) includes DHW preparation and is illustrated in Figure 73. Generally the heating periods (Space heating) are shorter at this simulation day and the heating capacity is low as ambient temperature is above 0 °C and the compressor speed is at the minimum speed of 1800 rpm throughout. During the first heating period from 2:00 to 5:00 the oil return function is activated. The new operating condition of this profile is the DHW preparation at 12:00 as the heating state 'DHW preparation' is activated. At this time both heating states, space heating and DHW preparation, are activated but it is programmed that DHW preparation is prioritised. For this state an additional function was embedded to stabilise the heat pump system. This function will be thoroughly explained after the analysis of this profile. During DHW preparation the desuperheater is not operated with natural circulation in the system tests. There the desuperheater is coupled to the water circuit of the condenser.

The temperature profile of Day 3 shows that the heating capacity is too high for this simulation data as the condenser outlet temperature is about 3 K higher than the set point.

Nevertheless, for analysing the heat pump behaviour this is no problem. When the DHW preparation starts, the outlet temperature, calculated with the heating curve, is not used as reference variable for the compressor speed controller. The compressor speed is set as a function of the brine inlet temperature. The outlet temperature rises to a temperature level above 50 °C. Before a steady state is reached, the DHW mode is stopped.

The correlation of the ambient temperature and the set temperature of the condenser outlet can be seen when comparing the graphs of t_{amb_simul} and $t_{cond_out_calc}$. Where the ambient temperature slightly decreases, the set temperature increases the same way as the heating capacity of the building rises. This correlation was already explained in Chapter 2.5. The superheating is illustrated in the diagram in the middle. When the compressor starts at about 2:00 oscillations of the control can be seen. These oscillations are reduced and the superheating is kept at a constant level of 5 K until 5:00. The superheating during DHW mode is explained in the following paragraphs in detail.

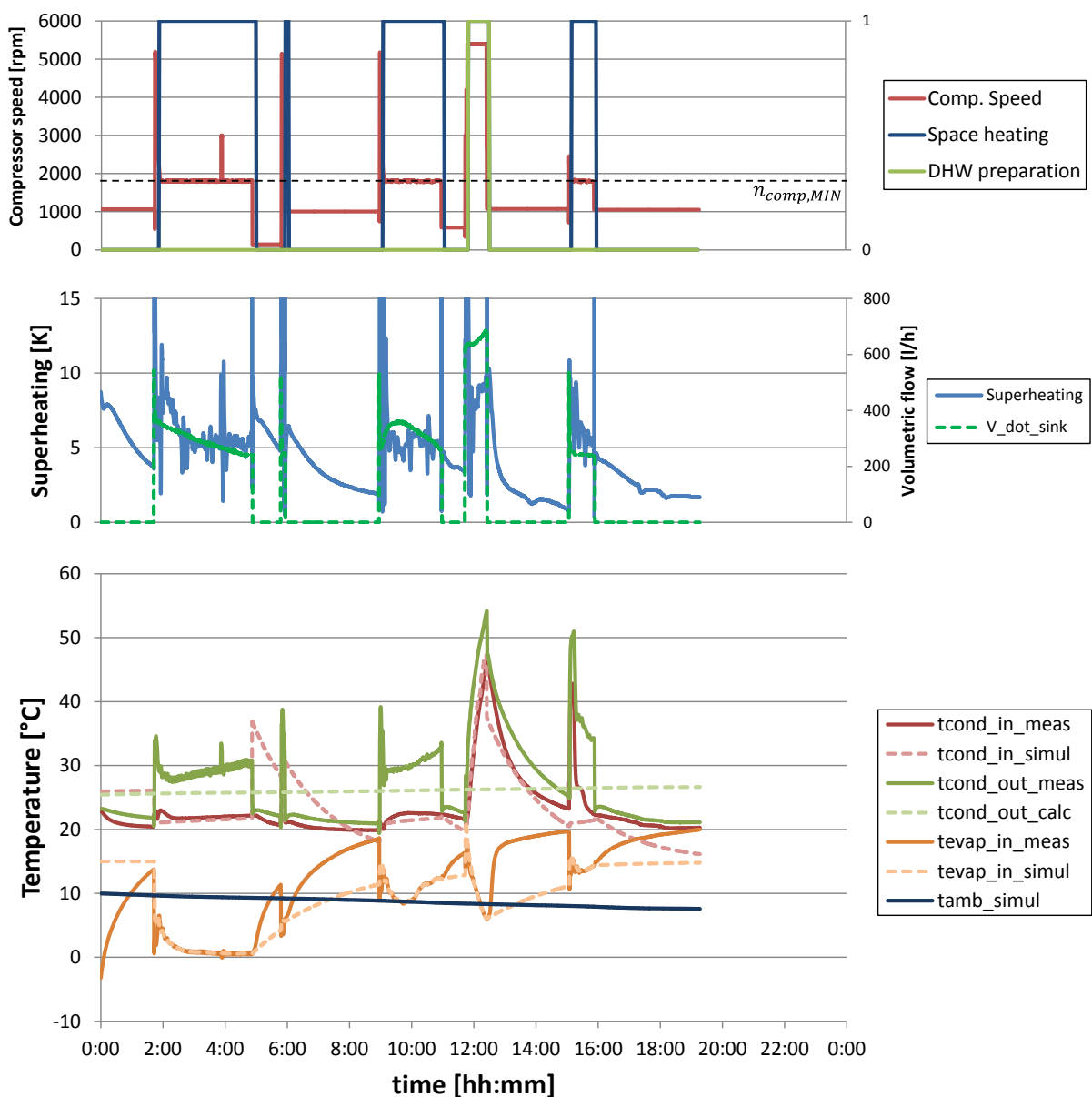


Figure 73: 24-hour measurement – Day 3

Low Superheating

A problem that occurred at the DHW preparation was that the compressor speed is increased to a high value within a short time period. In the worst case the space heating is provided at the minimum speed of 1800 rpm and at the next moment, when DHW preparation is demanded, the compressor speed is increased to 5400 rpm (at low brine temperatures) within seconds. In Figure 74 on top a similar case is illustrated. After a stopping period, the heat pump system is supposed to start DHW preparation. The superheating of the main expansion valve (Heating superheat) is plotted as a blue line, whereas the set point for the superheating (Compressor Superheat Setpoint) is shown as dashed line. On the right axis the compressor speed is shown as a red line. Shortly before 11:45 the heat pump gets the signal to start with DHW preparation. The compressor speed is immediately increased to 5400 rpm. At the beginning the control of the expansion valve tries to stabilise the superheating but at 11:50 it drops to values below 3 K. If the superheating stays for several seconds below 3 K the compressor's safety system starts a hard shut-down, to prevent suction of liquid refrigerant. This also occurred during this measurement. After a hard shut-down the compressor is in 'Waiting' mode for 10 minutes and is started again afterwards. The compressor starts again and after a too long period below 3 K the compressor initiates another hard shut-down. This shows the difficulty of the problem, as the control of the expansion valves is very sensitive to immediate and big changes of the heating capacity.

As the main problem of the control of the expansion valve is that the changes happen too quickly when DHW preparation is demanded, a function which makes the changes more decent was embedded. At the bottom of Figure 74 the same starting point with the same demand on DHW preparation is plotted. The only difference is the embedded function that is initiated when DHW mode is demanded. This function gradually increases the compressor speed to stabilise the expansion valve control. Depending on the previous compressor speed the function allows the compressor only to make a speed step of 1200 rpm. When the compressor is initially started, the first stabilising point is at 3000 rpm. For 120 seconds this speed is kept constant and is then increased again to 4200 rpm. After another 120 seconds the maximum speed of 5400 rpm is reached. Within these steps, where the speed is constant, the control of the expansion valve is able to adjust to the heating capacity. Looking at the diagram on top, the superheating is at its highest at 25 K and then drops to 2 K. Stabilisation of the superheating is not possible. With the embedded function the superheating does not rise that high at the beginning, as it has time to stabilise in between. Additionally when the highest compressor speed is reached the superheating is at 18 K and then drops to 2 K. After some fluctuations at the beginning the control is able to stabilise the superheating. Although the moderate rise of the compressor speed endures a few minutes where the heat pump cannot be operated with the maximum heating capacity, this function promotes stabilisation of the expansion valve control and prevents the compressor of a hard shut-down. The waiting time that occurs after a hard shut-down is much longer than the time that is required for a smooth increase of the compressor speed. In the system tests an electrical heater is switched on for DHW preparation in this situation, which leads to a low efficiency of the system.

In Figure 74 at the bottom, also the 'Automatic Superheat Control' programme is shown. When the superheating of the expansion valve is oscillating or has an offset to the desired value the superheat set point is increased. If the fluctuation endures longer than 15 minutes the set point is increased by 2 K. This goes on until the maximum set point of 10 K is reached. When the superheating stabilises, the set point is reduced by 1 K. This ensures a stable reduction of the superheating without risking further fluctuations. The minimum set point that is targeted for every operating point is 5 K. A lower superheating set point with stable control is not possible for this set up of expansion valve and control.

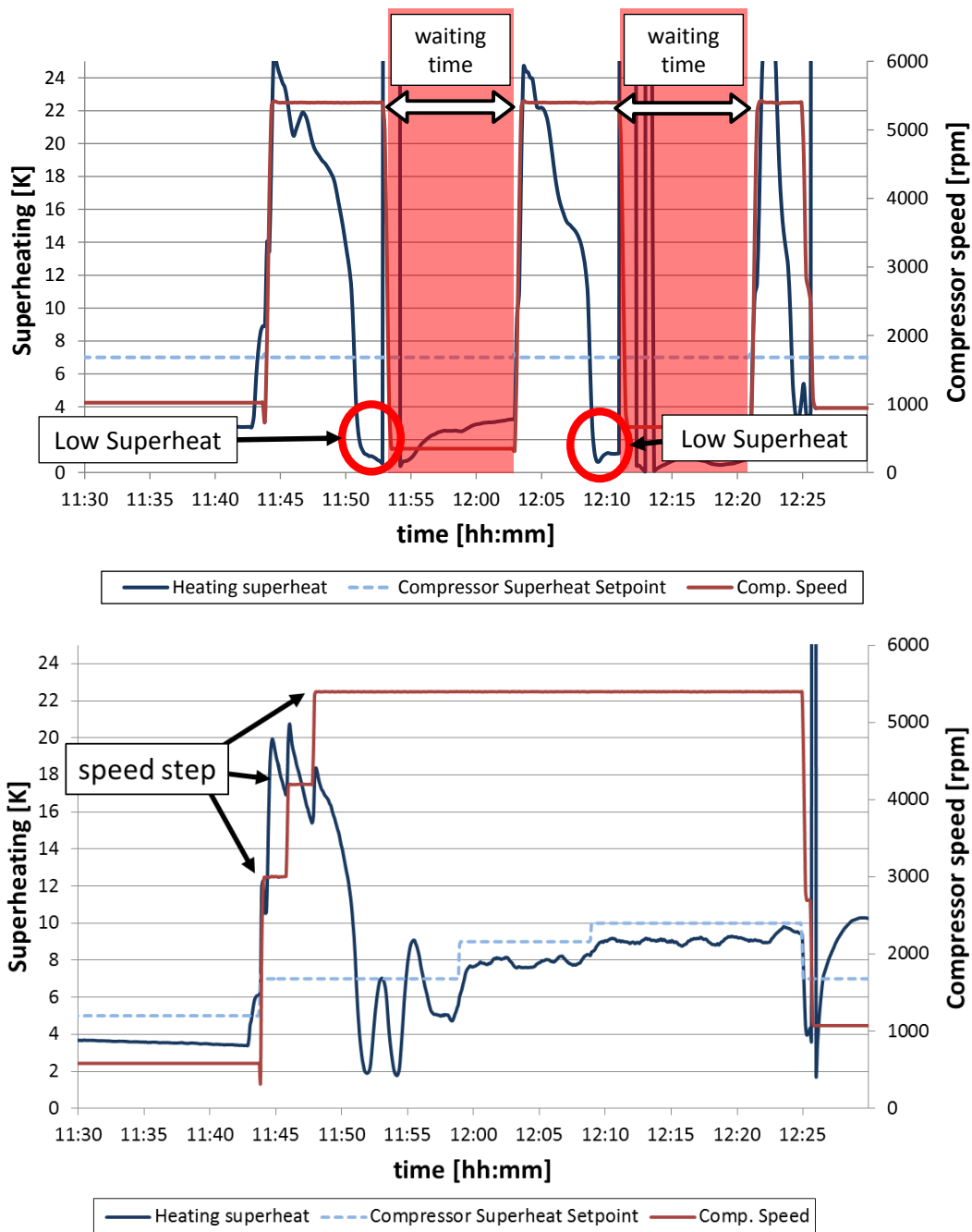


Figure 74: Low Superheat at DHW preparation; top: without optimised software; bottom: with optimised software

Economiser

The 24-hour simulation of Day 2 was accomplished with and without economiser. For the measurement without economiser the ball valve shortly before the injection inlet of the compressor (see Figure 30) was closed, thus no refrigerant was able to enter the compressor. In Figure 75 these two measurements are compared in envelope diagrams. Each dot marks an operating point at a certain time. All dots together represent all measurement values during the 24-hour test. The red line within the overall envelope at 4500 rpm marks the envelope for a compressor speed of 1800 rpm. The compressor is operated at different compressor speeds and therefore different envelopes are valid. On the top the measurement without economiser is plotted and the diagram at the bottom shows the measurements with economiser.

As already shown in the profile of Day 2 (Figure 72), the compressor mainly operates at a speed of 1800 rpm. The oil return mode is responsible for the few breakaways to higher condensation temperatures. A dotted line is inserted at a condensation temperature of 25 °C to illustrate the slight differences. An economiser increases the mass flow rate over the condenser and increases the *COP*, which was measured by Baur (2014). The increased heating capacity at the condenser also increases the temperature difference on the water side of the heat exchanger, which leads to higher condensation pressures. It can be seen that the condensation temperatures of the measurements without economiser are slightly lower compared to the measurements with economiser. Also lower evaporation temperatures are measured with economiser. A comparison of the performance factor (*PF*), which relates the provided energy of condenser and desuperheater to the electrical energy consumption of the compressor system (Equation 38) was carried out. It shows that the operation with economiser is more efficient ($PF_{wECO} = 4.7, PF_{woECO} = 4.35$).

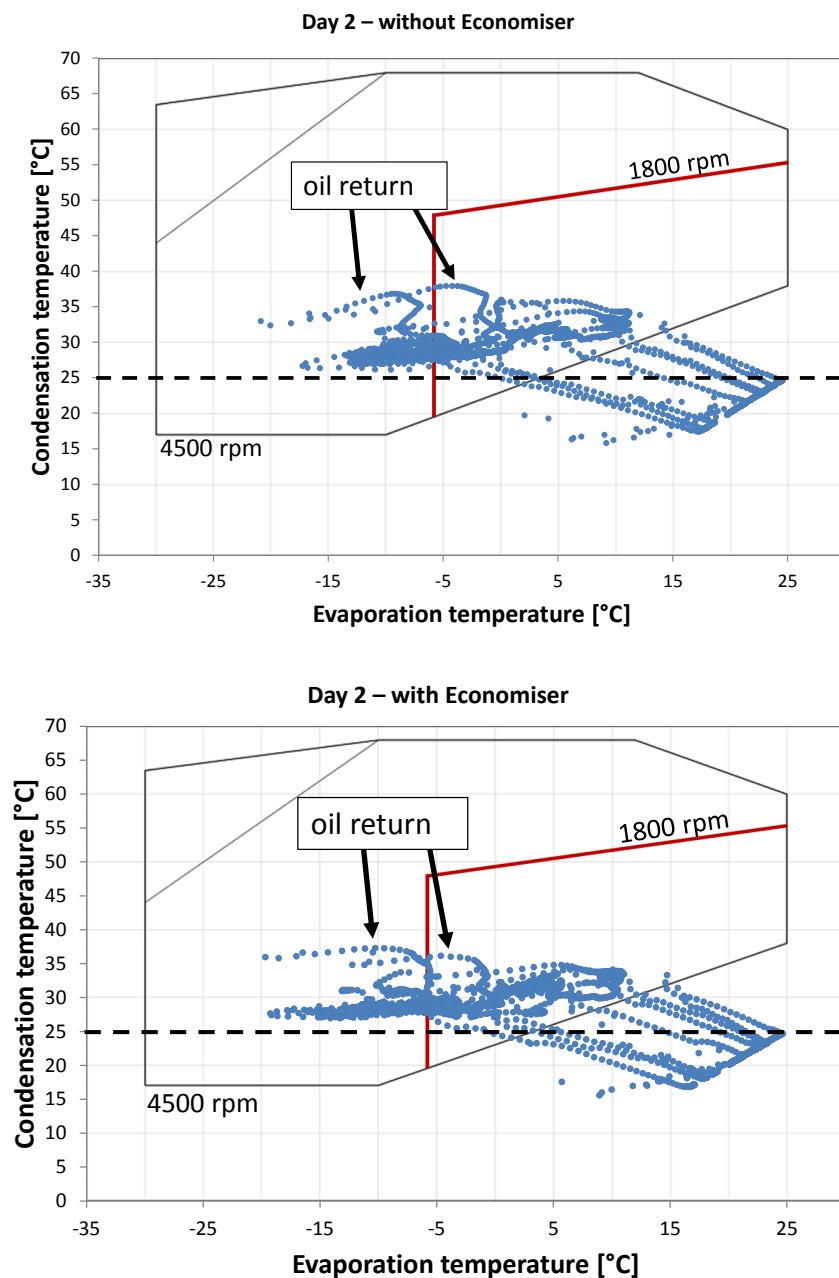


Figure 75: Comparison Day 2 – without and with economiser

5.4. Results of uncertainty propagation

The maximum errors of the measurement devices were already discussed in Chapter 3.5. In this chapter the uncertainty of the results is described. Table 5 shows the five values that were evaluated above with their minimum, maximum and average relative uncertainty of all measurements. As already explained, the measurement equipment of this test rig was reduced compared to the measurements that were performed by Baur (2014). The main focus was on a minimised pressure drop of the cycle and the optimisation of the software to maximise the performance of the overall heating system. Nevertheless, the indication of the uncertainty of measurements is important for evaluating the results of measurement.

The COP has a maximum uncertainty of $\pm 5\%$ and an uncertainty of at least $\pm 1.8\%$. A maximum uncertainty of $\pm 6.3\%$ is calculated for the overall isentropic efficiency and the highest uncertainty of the overall volumetric efficiency is $\pm 3.5\%$. Both mass flow rates of desuperheater and injection show very high uncertainties, as the absolute values are small and both values are dependent on several measurement devices. The maximum values of $\pm 42.1\%$ for the desuperheater mass flow and $\pm 63.8\%$ for the injection mass flow are for very small absolute values. Both mean uncertainties are much lower at ± 14.1 and $\pm 17.7\%$. In Figure 76 the results of the overall efficiencies with their uncertainties are illustrated.

Table 5: Results of Uncertainty

Measurement value	Minimum uncertainty [%]	Maximum uncertainty [%]	Mean uncertainty [%]
COP	1.8	5.0	2.9
$\eta_{is,overall}$	2.0	6.3	3.2
$\eta_{vol,overall}$	1.4	3.5	2.3
$\dot{m}_{des,w}$	4.2	42.1	14.1
$\dot{m}_{inj,r}$	4.6	63.8	17.7

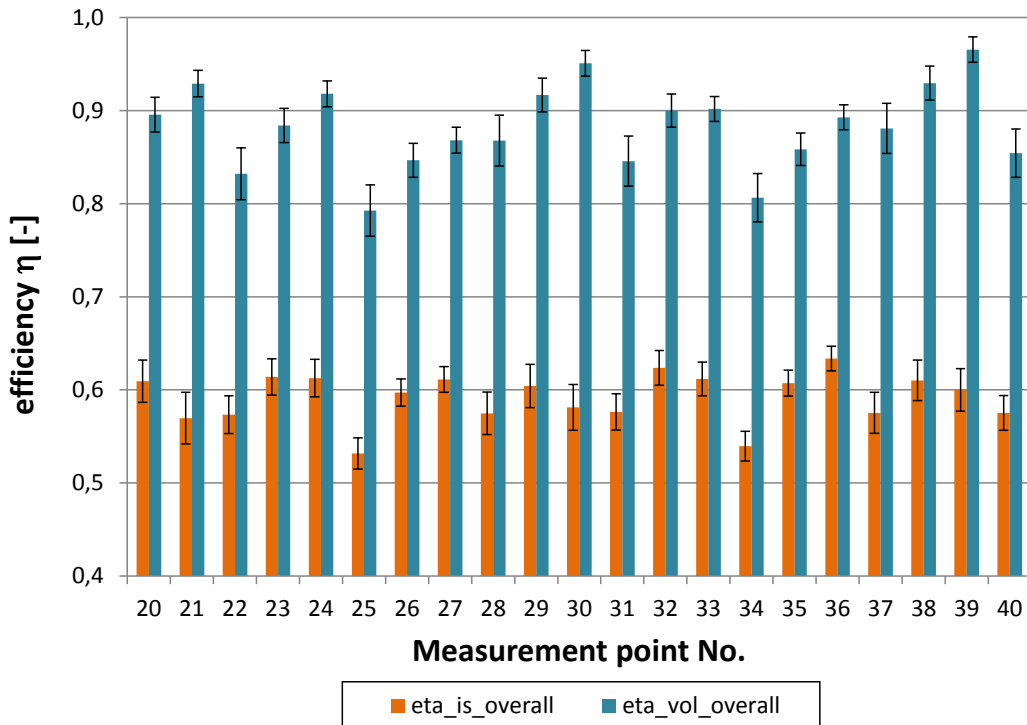


Figure 76: Results of $\eta_{is,overall}$ and $\eta_{vol,overall}$ with uncertainty of measurements No. 20-40

6. CONCLUSION

The main objective of the project MacSheep, which is carried out within the *European Union's Seventh Framework Programme*, is the reduction of the overall electrical energy consumption of a heating system by 25 %. The investigated heat pump system is one part of the overall heating system besides solar collectors and a thermal energy storage (TES). All promising technologies as desuperheater, economiser and speed controlled compressor were already analysed within the master thesis of Baur (2014).

Within this master thesis the evaluated components of the heat pump system were rearranged on the test rig, in order to optimise the piping between the TES and the heat exchangers of the heat pump system. Thereby an increase of the *COP* is expected due to reduced pressure drops and reduced heat losses. Besides the optimisation of the hardware also the software was adapted to ensure an easy and secure operation of the heat pump system and communication between both systems. Additionally measurements were carried out to evaluate the performance after the reconstruction of the heat pump test rig.

At first the requirements for the overall heating system were defined. Those requirements mean that the heat pump system was supposed to be built as compact as possible as the insulation of the TES and heat pump system is cost-intensive and that the heat exchangers had to be arranged vertically to keep the piping to the ports of the stratified TES as short as possible. Therefore the desuperheater was placed at the highest point to provide the upper volume of the storage with domestic hot water and to keep the length of the piping short. Below the desuperheater the condenser was positioned and the remaining components were placed at almost the same height level of the compressor ports. The overall heating system also requested natural water circulation over the desuperheater to minimise parasitic energy consumption of circulating pumps, during space heating mode. To simulate the natural circulation within this test rig the desuperheater was connected to a separate water circuit with a small storage tank. Thereby the functionality was tested and sufficient mass flow rates over the desuperheater were detected. Another important aspect of the construction of the test rig was the smooth piping to minimise the pressure drops in the refrigerant circuit. To minimise vibrations of the whole test rig, U-bends were installed before and after the compressor ports to absorb most of the vibrations.

The software of the heat pump test rig was not only optimised for the measurements of stationary operating points but also for measurements of the dynamic behaviour of the heat pump system. For the operation within the overall heating system (TES, solar collector, heat pump) the heat pump is supposed to operate automatically. When getting a signal that either space heating or DHW preparation is required the heat pump has to switch to the demanded mode and has to run in a stable way. Additionally the heat pump has to be operated with the maximum efficiency for each operating point. These requirements were fulfilled by embedding different safety and stability programmes into the software. The main problem of stability was the sensitivity of the expansion valve control. When operating conditions are changed quickly the expansion valve control tends to oscillate. As the reference variable of the expansion valves is the superheating at the evaporator and economiser outlet, the control is also responsible for the efficiency of the heat pump cycle. Each Kelvin the superheating is reduced means an increase in *COP* as the pressure ratio for the compressor decreases. For each operating point a minimum superheating of 5 K shall be achieved and a maximum of 10 K is allowed ('Automatic Superheat Control').

When DHW preparation is demanded, the condensation temperature and compressor speed are increased to a maximum, which leads to stability problems if the step is too abrupt. Therefore a function was embedded that increases the compressor speed in moderate (1200 rpm) steps and keeps the speed constant for a short period. This ensures a stable switch between space heating and DHW mode. As the speed controlled compressor is able

to operate in part load, it can occur that a low compressor speed is held for longer periods. This could lead to the problem that the oil return is not guaranteed, which results in a damage of the compressor. To prevent this, the 'Oil Return' programme was embedded. This programme already existed in the compressor software. Nevertheless, it was deactivated, as some parameters of the software were optimised manually and therefore the programme had to be redesigned. No matter which heating capacity is required, if the compressor runs for a period of two hours below 2200 rpm the speed is raised to 3000 rpm for 120 seconds.

For the communication with the software of the project partner an interface was defined. The system software decides, which operation mode is required and sends signals to all involved components. The heat pump communicates the availability of the heat pump itself and measurement data to the system software, which further processes the data for decision criteria.

Measurements were carried out to evaluate the performance of the heat pump. However, the limited measuring equipment led to higher uncertainties of the analysed data. The overall isentropic efficiency $\eta_{is,overall}$ showed values from 51 to 64 % where an equal isentropic efficiency of both stages was assumed. Best efficiency was reached at the operating point 15/30 with a compressor speed of 4800 rpm, whereas lowest efficiency was measured at a pressure ratio of 8.5. Generally best efficiencies were detected at compressor speeds between 3500 and 5400 rpm and for operating points with low pressure ratios. The overall volumetric efficiency $\eta_{vol,overall}$ also shows best efficiencies for low pressure ratios and compressor speeds between 4200 and 5400 rpm. At 15/20/4200 the highest efficiency of 97 % was measured whereas the lowest efficiency of 78 % was detected at the measuring point 2/20/1800. As the overall isentropic efficiency also the overall volumetric efficiency decreases strongly with high pressure ratios and low compressor speeds. The evaluation of the heat pump system was accomplished by analysing the Coefficient of Performance COP as a function of different variables. As the compressor efficiency has a big impact on the performance of the heat pump cycle, the results of the COP show a similar progression. Best performance of 6.99 is reached at the operating point 15/20 and a compressor speed of 3000 rpm whereas the lowest value of 2.13 was measured at -15/45/5400.

Finally 24-hour measurements were performed to analyse the dynamic behaviour of the heat pump system. Three different profiles were measured to monitor the automatic operation of the heat pump on the one hand and to evaluate the dynamic behaviour on the other hand. Thereby the embedded stability and safety functions were developed and optimised.

It can be concluded that the performance of the heat pump system has not suffered from rearranging the components. Even though a few efficiency values are slightly higher than those of the previous measurements performed (Baur, 2014), an improvement of the heat pump cycle cannot be reasoned from that, as the uncertainties are also higher due to the reduced measuring equipment. The two-stage compression with vapour injection makes operating points with high pressure ratios more efficient. The desuperheater provides domestic hot water continuously without decreasing the performance of the heat pump. By using the sensible heat of the superheated refrigerant a high temperature level for DHW is reached while the condensation temperature stays at a low level. This reduces operating times where only DHW is provided which requires condensation temperatures of about 50 °C and thereby having a low COP .

For the automation of the heat pump system several functions were embedded which guarantee a stable and safe operation for the system tests. The heat pump is able to stabilise on its own, when difficult operating conditions occur. Additionally it aims to operate with a superheating of 5 K, to maximise the heat pump performance for all operating points.

REFERENCES

- Alco Controls (2012). *Elektrische Regelventile Baureihe EXM/EXL*. Emerson Climate Technologies, Senefelder Str. 3, DE-63477 Maintal; http://www.emersonclimate.com/europe/ProductDocuments/AlcoLiterature/EN_EXML_TB.pdf, 20.01.2015.
- Alco Controls (2013). *Drucktransmitter PT5 - Datenblatt*. Emerson Climate Technologies, Senefelder Str. 3, DE-63477 Maintal; http://www.emersonclimate.com/europe/ProductDocuments/AlcoLiterature/DE_PT5_TB.pdf, 20.01.2015.
- AVL (2014). AVL LIST GmbH - Probability Density Function. Hans-List-Platz 1, 8020 Graz; <https://www.avl.com/construction-equipment>, 06.09.2015.
- Baur, G. (2014). Experimental analysis of a brine/water heat pump with speed control and vapour injection. Master's thesis, Institute of Thermal Engineering, Graz University of Technology.
- Bitzer (2015). *Kältemittel Report 18*. Bitzer Kühlmaschinenbau GmbH, Eschenbrunnlestraße 15, 71065 Sindelfingen, Germany; https://www.bitzer.de/shared_media/documentation/a-500-18.pdf, 14.10.2015.
- Chen, Y., Halm, N. P., Groll, E. A., and Braun, J. E. (2002). Mathematical Modeling Of Scroll Compressors - Part I: Compression Process Modeling. *International Journal of Refrigeration*, 25(6):731 – 750.
- Clariant (2015). *Heat Transfer Fluids - Antifrogen N*. Clariant International Ltd, Rothausstrasse 61, 4132 Muttenz, Switzerland; <http://www.clariant.com>, 05.09.2015.
- Copeland (2011a). *Vapour Injection Scroll Compressors for Heat Pumps - Technical Information*. Ref. C7.4.3/1107-1111/E. Emerson Climate Technologies, Senefelder Str. 3, DE-63477 Maintal.
- Copeland (2011b). *Variable Speed Solutions For Heat Pump Applications*. Ref. C6.2.25/0812-0313/E. Emerson Climate Technologies, Senefelder Str. 3, DE-63477 Maintal.
- Copeland (2013a). *Emerson Inverter Drives For ZHW and ZPV Compressors - Technical Information*. Ref. C7.8.7/0212-0313/E. Emerson Climate Technologies, Senefelder Str. 3, DE-63477 Maintal.
- Copeland (2013b). *Select Software 7.7*. Emerson Climate Technologies, Senefelder Str. 3, DE-63477 Maintal.
- Danfoss (2008). Filtertrockner und Schaugläser. *Kälte Klima Aktuell, Volume 6/2008*. Danfoss A/S, DK-6430 Nordborg, Denmark; http://www.danfoss.com/NR/rdonlyres/03C9ECB6-5186-485D-8749-39009D3C1033/0/Filterdriers_DE.pdf, 16.09.2014.
- EES (2015). *Engineering Equation Solver - Academic Professional V9.901*. F-Chart Software, Box 44042, Madison WI 53744, USA.

- E+H (2010). *Proline Promag 50P Magnetisch-induktives Durchfluss-Messsystem - Technische Information*. Endress+Hauser GmbH, Lehnergasse 4, 1230 Wien, Österreich; https://portal.endress.com/wa001/dla/5000319/0454/000/04/TI047DDE_1109.pdf, 16.09.2014.
- E+H (2012). *Proline Promass 83A Coriolis-Massedurchfluss-Messsystem - Technische Information*. Endress+Hauser GmbH, Lehnergasse 4, 1230 Wien, Österreich; https://portal.endress.com/wa001/dla/5000319/0464/000/07/TI00054DDE_1312.pdf, 15.09.2014.
- Görtler, G. (2010). *Angewandte Messtechnik*. Script, Fachhochschul-Studienzentrum Pinkafeld.
- Guggenberger, M. (2013). *Energie- und umwelttechnisches Mess- und Versuchswesen - Hydraulische Strömungsmaschinen*. Script, Institute of Hydraulic Fluid Machinery, Graz University of Technology.
- Haller, M. and Mojic, I. (2014). 3-D Model of Thermal Storage with Heat Pump. European Union's Seventh Framework Programme FP7/2007-2011 under grant agreement n° 282825 – Acronym MacSheep.
- Heinz, A., Hengel, F., Haller, M. Y., and Mojic, I. (2014). System Overview. Project Report. European Union's Seventh Framework Programme FP7/2007-2011 under grant agreement n° 282825 – Acronym MacSheep.
- Heinz, A., Hengel, F., Haller, M. Y., Mojic, I., Matuska, T., Simek, P., Sedlar, J., Poppi, S., and Bales, C. (2013). System Simulations and Cost Analysis for Breakthroughs in Advanced Heat Pumps and Heat Pump Cycles - Deliverable 4.2. *European Union's Seventh Framework Programme FP7/2007-2011 under grant agreement n° 282825 – Acronym MacSheep*.
- Jungnickel, H., Agsten, R., and Kraus, E. (1990). *Grundlagen der Kältetechnik*. Verlag Technik GmbH Berlin, 3rd edition.
- LabVIEW (2012). *LabVIEW Professional Development System - Version 12.0*. National Instruments GmbH, Plainbachstr. 12, A-5101 Salzburg, Austria.
- Meteonorm (2014). *Luftdruck-Jahresverlauf für Graz*. Global Meteorological Database, Version 7.1, Meteotest, Fabrikstrasse 14, 3012 Bern, Schweiz.
- Pohlmann (2010). *Taschenbuch der Kältetechnik*. VDE Verlag GmbH, 20th edition.
- Recknagel and Sprenger (2007). *Taschenbuch für Heizung und Klimatechnik*. Oldenburg Industrieverlag München, 73rd edition.
- Rieberer, R. (2013). *Heizungs-, Lüftungs- und Klimatechnik VO*. Script, Institute of Thermal Engineering, Graz University of Technology.
- Rieberer, R. (2014). *Heizungs-, Lüftungs- und Klimatechnik VA*. Script, Institute of Thermal Engineering, Graz University of Technology.
- Rieberer, R., Droscher, A., and Prieler, R. (2013a). *Energie- und umwelttechnische Messverfahren - Wärme*. Script, Institute of Thermal Engineering, Graz University of Technology.
- Rieberer, R., Moser, H., and Halozan, H. (2013b). *Wärmepumpentechnik VO*. Script, Institute of Thermal Engineering, Graz University of Technology.

Riedler, J. (2015). Messtechnische Analyse einer Sole/Wasser-Wärmepumpe mit Enthitzer und Economizer. Master's thesis, Institute of Thermal Engineering, Graz University of Technology.

Saia-Burgess (2014). *Energiezähler - AAD1 D5E*. Saia-Burgess Controls AG, Bahnhofstr. 18, 3280 Murten, Switzerland;
<http://idec.de/produkte/distribution/energiezaehler/Energiezaehler.pdf>, 18.09.2014, cc-katalog edition.

Samal, E. and Becker, W. (2000). *Grundriss der praktischen Regelungstechnik*. Oldenbourg Verlag München Wien, 20th edition.

SWEP (2014). *Installations- und Wartungshandbuch für Hartgelötete Plattenwärmetauscher*. SWEP International AB, Rosenstr. 14, 90762 Fürth, Germany;
http://www.swep.net/Documents/Service%20and%20support/Installation%20manuals/92110_DE.pdf, 16.09.2014.

Wang, B., Shi, W., Han, L., and Li, X. (2009). Optimization of refrigeration system with gas-injected scroll compressor. *International Journal of Refrigeration*, 32(7):1544 – 1554.

LIST OF ILLUSTRATIONS

Figure 1: MacSheep heating system (version with ice storage) (Heinz et al., 2014).....	2
Figure 2: Refrigerant circuit, left: scheme; right: t/h-diagram R410A	4
Figure 3: Economiser circuit, left: scheme; right: log p/h-diagram (Copeland, 2011a).....	6
Figure 4: Heat pump cycle with economiser and desuperheater, left: scheme; right: t/h- diagram (Copeland, 2011a).....	7
Figure 5: Absorption of moisture in POE oil and mineral oil in ppm by weight at 25°C and 50% relative humidity (h=hours) (Copeland, 2011b)	9
Figure 6: Working principle of a scroll compressor (Chen et al., 2002)	10
Figure 7: Idealised pressure/volume-diagram of compression (Jungnickel et al., 1990).....	11
Figure 8: Types of leakage (Chen et al., 2002).....	11
Figure 9: Injection port location, left: optimisation (Wang et al., 2009); right: disassembled compressor.....	12
Figure 10: Heating demand and heating capacity of a heat pump with variable speed compressor (Copeland, 2011b)	13
Figure 11: Hourly values of the heating capacity: radiator (Pheat), HP in SH mode (PCondSH) and DHW mode (PCondDHW); left: without speed control, right: with speed control (Heinz et al., 2013).....	13
Figure 12: Block diagram of Inverter drive	14
Figure 13: Pinch points of Evaporator, Condenser and Desuperheater	15
Figure 14: Plate heat exchanger SWEP (SWEP, 2014).....	15
Figure 15: Electronic Expansion Valve; left: scheme (Recknagel and Sprenger, 2007), right: ALCO valve EXM/EXL series (Alco Controls, 2012)	16
Figure 16: Liquid receiver - refrigerant charge (Rieberer et al., 2013b).....	17
Figure 17: Thermocouple standard circuit (Rieberer et al., 2013a)	19
Figure 18: Resistance thermometer, four-wire configuration (Rieberer et al., 2013a).....	19
Figure 19: Contact sensor (Rieberer et al., 2013a).....	20
Figure 20: In-stream installation (Rieberer et al., 2013a)	20
Figure 21: Electromagnetic flow meter; left: scheme; right: Proline Promag 50P (E+H, 2010).....	21
Figure 22: Measuring principle of Coriolis mass flow meter (Guggenberger, 2013)	21
Figure 23: Piezo-resistive pressure transmitter; left: scheme (Guggenberger, 2013); right: ALCO PT5-xxT (Alco Controls, 2013).....	22
Figure 24: Probability density function (AVL, 2014)	23
Figure 25: Control circuit (Rieberer, 2014).....	24
Figure 26: Step response of PID-Controller (Samal and Becker, 2000).....	26
Figure 27: Heating curve (Rieberer, 2013).....	27
Figure 28: Test rig – Heat pump	28
Figure 29: Scheme of whole test rig	29
Figure 30: Heat pump cycle, scheme	30

Figure 31: Scroll compressor ZHW 08 K1 P – 1 E9, left: Chassis (Copeland, 2011b), right: dismantled scrolls.....	31
Figure 32: Cross sections of scroll compressor (Copeland, 2011b).....	32
Figure 33: Envelopes, left: 1800 to 4500 rpm, right: 4500 to 7020 rpm (Copeland, 2013b).....	33
Figure 34: Inverter cooling.....	34
Figure 35: Port configuration, left: evaporator, right: condenser (SWEF, 2014).....	36
Figure 36: Distribution pipe of evaporator.....	36
Figure 37: Expansion valves.....	37
Figure 38: Positioning of expansion valve (Copeland, 2011a).....	38
Figure 39: Filter dryer and sight glass.....	38
Figure 40: ‘Mobile heat source’, left: scheme; right: picture.....	40
Figure 41: Heat sink, scheme.....	41
Figure 42: left: ‘Mobile heat sink’; right: Desuperheater storage tank.....	41
Figure 43: Desuperheater inlet and outlet ports.....	43
Figure 44: U-bend for preventing vibrations.....	44
Figure 45: Heat pump test rig left: 3D model (Haller and Mojic, 2014); right: construction.....	45
Figure 46: Contact sensor, top: fixation, bottom: insulation.....	47
Figure 47: Pt-100 installation at desuperheater inlet port (TE_d01).....	48
Figure 48: Coriolis mass flow meter.....	49
Figure 49: Position of pressure measurement.....	50
Figure 50: Pressure measurement, top: manometers and switches, bottom: pressure transmitter.....	51
Figure 51: Electrical meter, pulse error electrical power.....	52
Figure 52: Hardware – Software connection, block diagram.....	53
Figure 53: LabVIEW – Front Panel, 'Heat pump'-tab.....	54
Figure 54: LabVIEW – Block Diagram.....	56
Figure 55: LabVIEW - Automation.....	58
Figure 56: Measured operating points.....	59
Figure 57: Heat pump denotation, top: t/h-diagram of R410A, bottom: scheme.....	60
Figure 58: System boundary for compressor evaluation (Copeland, 2011b).....	63
Figure 59: Theoretical two-stage compression for scroll compressor (Baur, 2014).....	65
Figure 60: Heat losses of compressor $f_{loss, comp}$ for different operating points as a function of the compressor speed n	69
Figure 61: Overall isentropic efficiency $\eta_{is, overall}$ for different operating points as a function of pressure ratio π	70
Figure 62: Overall isentropic efficiency $\eta_{is, overall}$ for different operating points as a function of compressor speed n	70
Figure 63: Overall volumetric efficiency $\eta_{vol, overall}$ for different operating points as a function of pressure ratio π	71

Figure 64: Overall volumetric efficiency $\eta_{vol, overall}$ for different compressor speeds as a function of pressure ratio π	72
Figure 65: Volumetric efficiency for different compressor speeds as a function of pressure ratio π ; left: first stage compression η_{vol1} ; right: second stage compression η_{vol2}	72
Figure 66: Coefficient of Performance COP for different operating points as a function of pressure ratio π	74
Figure 67: Coefficient of Performance COP for different operating points as a function of compressor speed n	74
Figure 68: Coefficient of Performance COP for different operating points as a function of condenser inlet temperature T_{w01}	75
Figure 69: Coefficient of Performance COP for different operating points as a function of brine inlet temperature T_{b01}	76
Figure 70: Mass flow desuperheater $m_{des, w}$ as a function of the mean storage temperature T_{st}	77
Figure 71: 24-hour measurement – Day 1	79
Figure 72: 24-hour measurement – Day 2	80
Figure 73: 24-hour measurement – Day 3	81
Figure 74: Low Superheat at DHW preparation; top: without optimised software; bottom: with optimised software	83
Figure 75: Comparison Day 2 – without and with economiser	84
Figure 76: Results of $\eta_{is, overall}$ and $\eta_{vol, overall}$ with uncertainty of measurements No. 20-40	85
Figure A-1: Block Diagram – Input.vi	A-1
Figure A-2: Block Diagram – electrical_Heater_control.vi	A-2
Figure A-3: Block Diagram – Oil_return.vi	A-3
Figure A-4: Front Panel – Overview	A-4
Figure A-5: Front Panel – MB_Config	A-5
Figure A-6: Front Panel – MB_Monitoring	A-5
Figure A-7: Front Panel – MB_Write	A-6
Figure A-8: Front Panel – Heat Pump	A-7
Figure A-9: Front Panel – Source side	A-8
Figure A-10: Front Panel – Sink side	A-8
Figure A-11: Front Panel – Automation	A-9

APPENDIX

A-1 Software heat pump system

In Chapter 3.6 the most important parts of the heat pump software were already described. Now the single parts will be explained more detailed. Each programme of the LabView Software is called 'Virtual Instrument' (VI). It can be individually designed and adapted and usually consists of several other programmes at lower levels, which are called 'SubVI'. Those VI's can be programmed in the 'Block Diagram' and their in- and outputs can be connected to the 'Front Panel' which serves as user interface.

First of all the 'Block diagram', where the programming of the software is accomplished, is explained. The whole 'Block diagram' was already divided into several areas, as shown in Figure 54. Within the 'Input'-area all measurement devices are read and data of the compressor control is collected. This happens in the programme Input.vi depicted in Figure A-1. At the beginning the data of the Superheat and Envelope Controller (SEC) is read via a ModBus connection. The measurement data of the temperature sensors, volume and mass flow meters is collected with the hardware of National Instruments. Within the SubVI's of the measurement devices the calibration is directly processed and only the corrected values are used for further calculations and controls. All data is collected in the so called 'Data Cluster', the pink line.

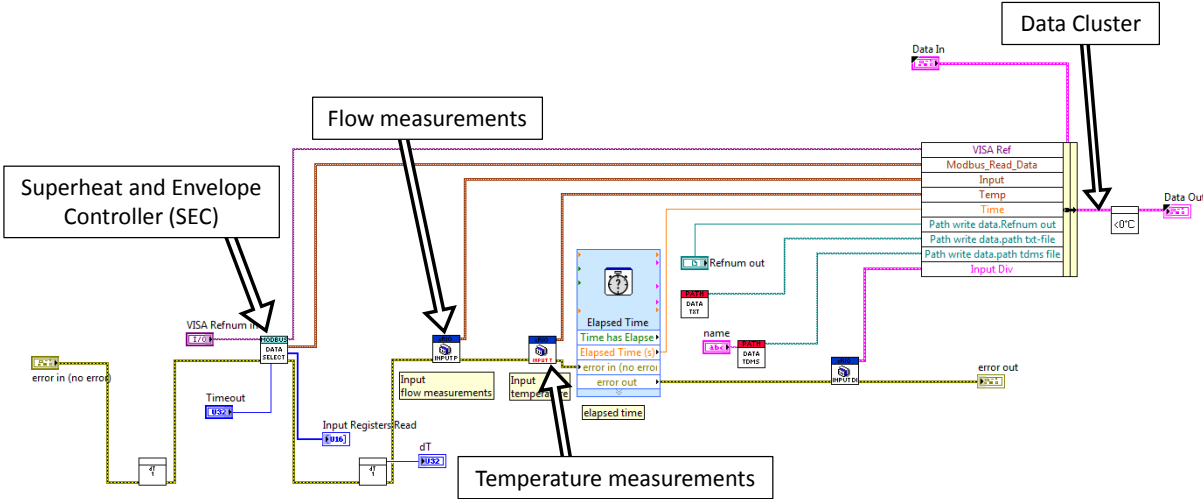


Figure A-1: Block Diagram – Input.vi

The entire data is collected each loop iteration as the whole programme is executed in one while-loop. After the 'Input.vi' is executed the data is further processed in several programmes. As can be seen in Figure 54 the 'Data Cluster' leads to the areas 'Graphs and Calculations', 'PID controller' as well as to 'Automation'. In 'Graphs and Calculations' no specific SubVI's are necessary as it is mainly for the visualisation in the 'Front Panel'. Therefore this area will not be discussed explicitly. Nevertheless, in the area 'PID controller' all controls of the periphery are placed. Each circulating pump and electrical heater is controlled in these SubVI's.

To give an example, the SubVI (electrical_Heater_control.vi) of the control of the electrical heater on the source side is depicted in Figure A-2. A case structure (true or false) is the basis of this programme. A Boolean operator sets the case of the structure. For the electrical heater several conditions have to be satisfied to set it active, due to safety reasons. A

minimum mass flow rate of 300 litres per hour has to be reached and a maximum brine temperature of 30 °C is not allowed to be exceeded. Additionally the controller for the electrical heater has to be set active manually. Only if all three conditions are fulfilled the case structure is set 'true'. Within this case the PID controller, which is accomplished as an individual VI, is executed. The output values of the PID controller are then forwarded to the actuator of the electrical heater, by giving it an actuating value between 0 and 100 % of the maximum heating power. Within the 'Data Cluster' the set point value and the values for the three parameters proportionality factor K_p , reset time T_n and derivative time T_v (Chapter 2.4) are provided for the PID controller. Also an output range for the controller can be set.

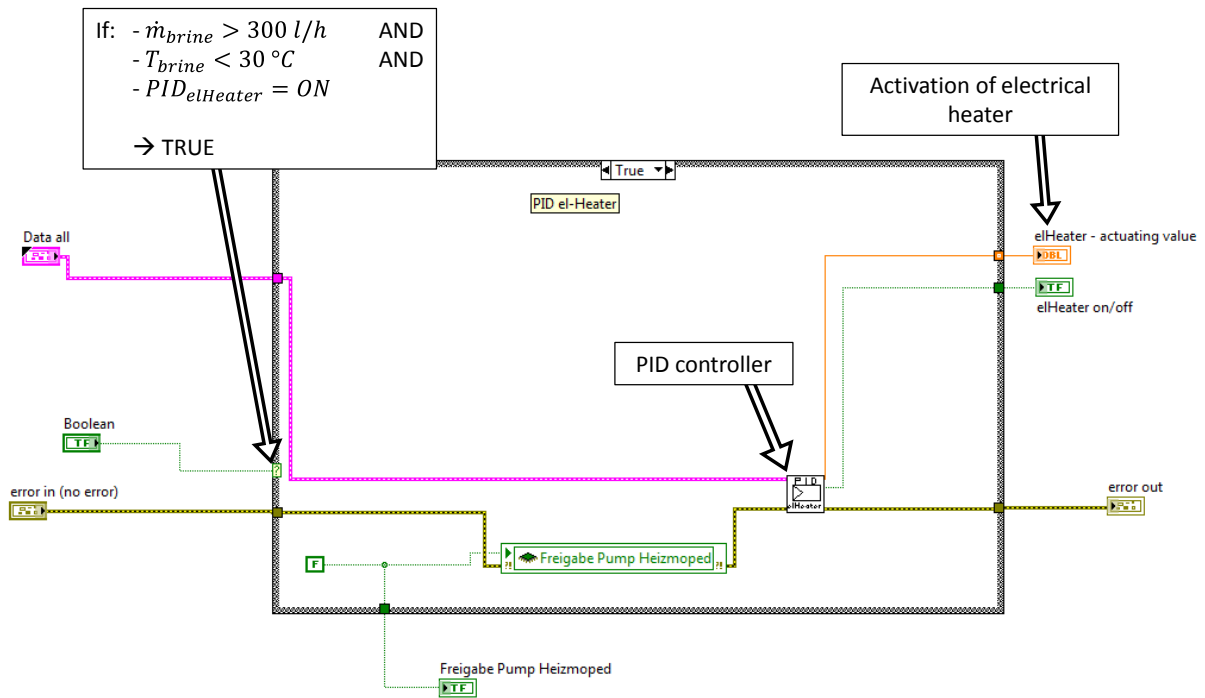


Figure A-2: Block Diagram – electrical_Heater_control.vi

'Automation' is the most important area for the independent operation of the heat pump. The single programmes in this area are shown in Figure 55. Manual input values are overwritten as soon as the automation is started. The 'Automatic Superheat Control' regulates the maximum superheating at the evaporator and economiser outlet. It is implemented to stabilise the system when oscillations occur and to gain a high efficiency by keeping superheating as small as possible.

In the programme 'Speed Control Compressor' the compressor speed is either controlled by a PID controller (space heating) or is set by a function of the evaporation temperature (DHW preparation), depending on the heating mode. These SubVI's are very big and complex and will therefore not be explained in this thesis. Nevertheless, the 'Automatic Oil Return' will be discussed in the following paragraphs, as this is a very important safety function.

In Figure A-3 the SubVI of the automatic oil return programme (Oil_return.vi) is depicted. It is separated and afterwards vertically rearranged for a better visualisation. The VI is based on two case structures (true or false), where the outer structure only checks whether the heat pump is operating or not (1). Also the 'Data Cluster' leads into the structure at the beginning. At point (2) the actual compressor speed from the ModBus connection is compared to the speed limit that can be individually set at the 'Front Panel'. As default setting the VI checks if the compressor speed is below 2200 rpm (Oil return threshold speed). This information is then processed to point (3) where the SubVI 'Elapsed Time' is activated each time the compressor speed is below the limit of 2200 rpm.

If this state lasts longer than the default time of 7200 seconds (Oil return threshold duration) the SubVI sends a Boolean signal to the inner case structure (4). If this case structure is set true, the compressor speed, which is determined by the VI 'Speed Control Compressor', is overwritten with the default value of 3000 rpm (Oil return speed). By using the local variable 'Oil Return Start' it is possible to stay within this case, although the compressor speed exceeds now the threshold of 2200 rpm. Only when the default time of 120 seconds (Oil return duration) is finished, the local variable is set to 'false' by the SubVI 'Elapsed Time' at point (5). Afterwards also the case is set to 'false' and the compressor speed is not overwritten anymore by the oil return programme.

A local variable is able to be either used as reading and writing item within one VI. When using different cases this is necessary to be able to change the case again. Nevertheless a local variable has to be used carefully, as it is written and read at the same time step on the same variable. The sequence of data processing has to be considered.

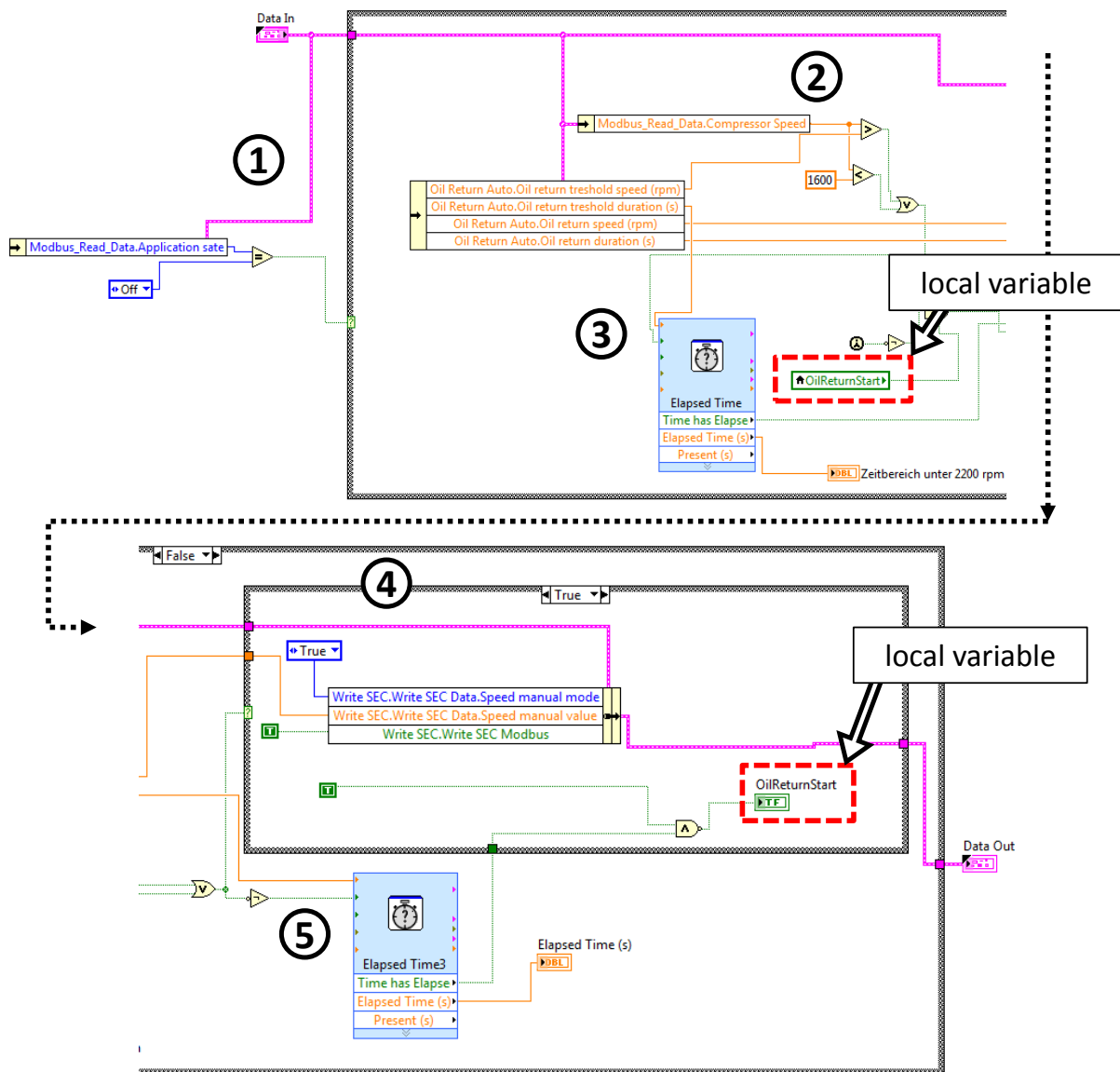


Figure A-3: Block Diagram – Oil_return.vi

The 'Front Panel' represents the user interface of the programmes in the 'Block Diagram'. Certain input values are defined and the heat pump system is monitored here. It is structured as shown in Figure A-4. The main part is the 'Tab Control Area' where different tabs can be chosen for each part of the heat pump system. Each tab will be described in the following paragraphs. In the 'Tab Control Area' only the activated tab can be seen, but it is also necessary to have certain monitoring elements always in sight when operating the heat pump. These elements are placed in the 'Overall Control Area' around the tab window.

With the elements of the 'Overall Control Area' the heat pump software can be stopped, the output value of the error cluster is monitored and an indicator light for each pump and electrical heater can be seen. Thereby it is possible to see which component is active or not without being in the corresponding tab. Also the actual compressor speed and the running time of the software are illustrated. Before starting the heat pump software, a file name, its location and a saving interval can be specified at the right upper part of the 'Overall Control Area'.



Figure A-4: Front Panel – Overview

The first three tabs 'MB_Config', 'MB_Monitoring' and 'MB_Write' represent in- and output values of the SEC, the control of the compressor. All configuration parameters are set according to the manual of the compressor in the tab 'MB_Config' (Figure A-5). Besides defining the types of compressor and pressure transmitters, all default values for the expansion valves as well as for safety programmes are set here. It needs to be considered that by changing these default values, the behaviour of the heat pump system is influenced. To be able to change parameters for the expansion valve's PID controller, the heating control mode of the electronic expansion valve was set 'Manual'. This led to a deactivation of the oil return function. Therefore an additional panel for setting the default values of the oil return mode was placed in this tab on the right.

In the tab 'MB_Monitoring' all values that are processed by the control of the compressor are monitored. If problems with the compressor and its control occur, these can be seen immediately in this tab, which is illustrated in Figure A-6.

APPENDIX

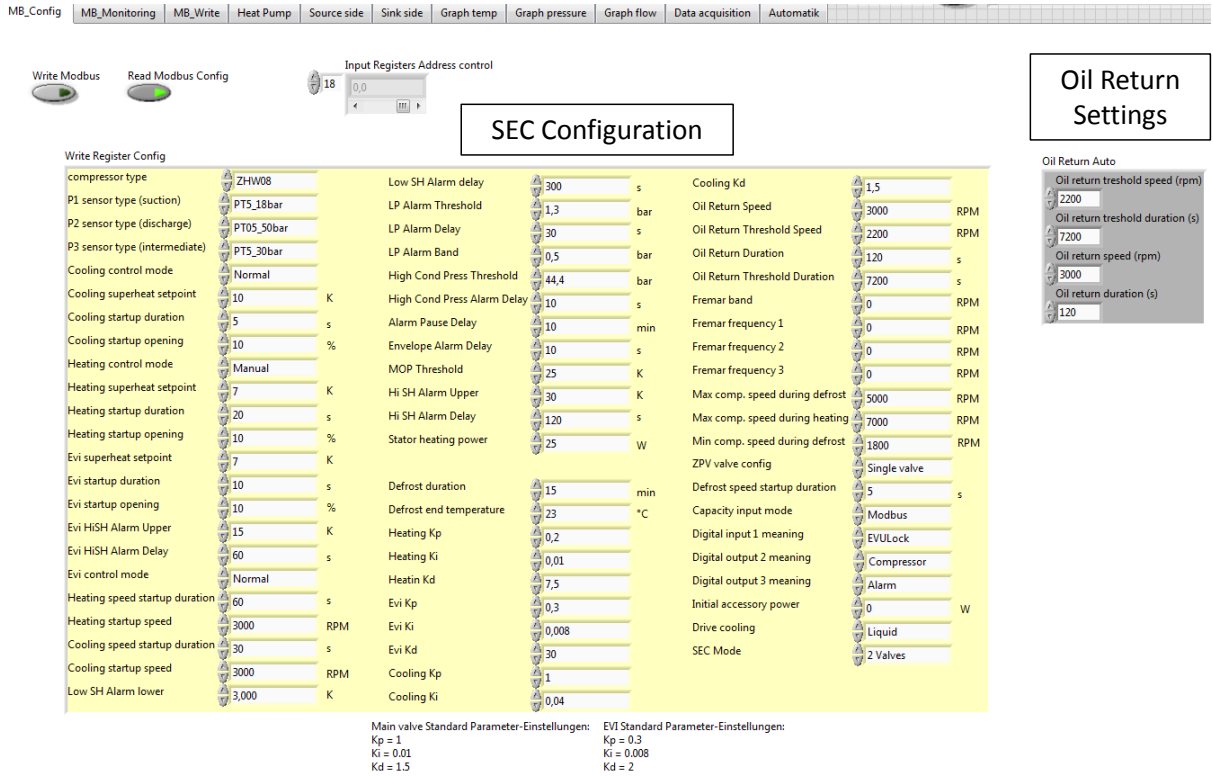


Figure A-5: Front Panel – MB_Config

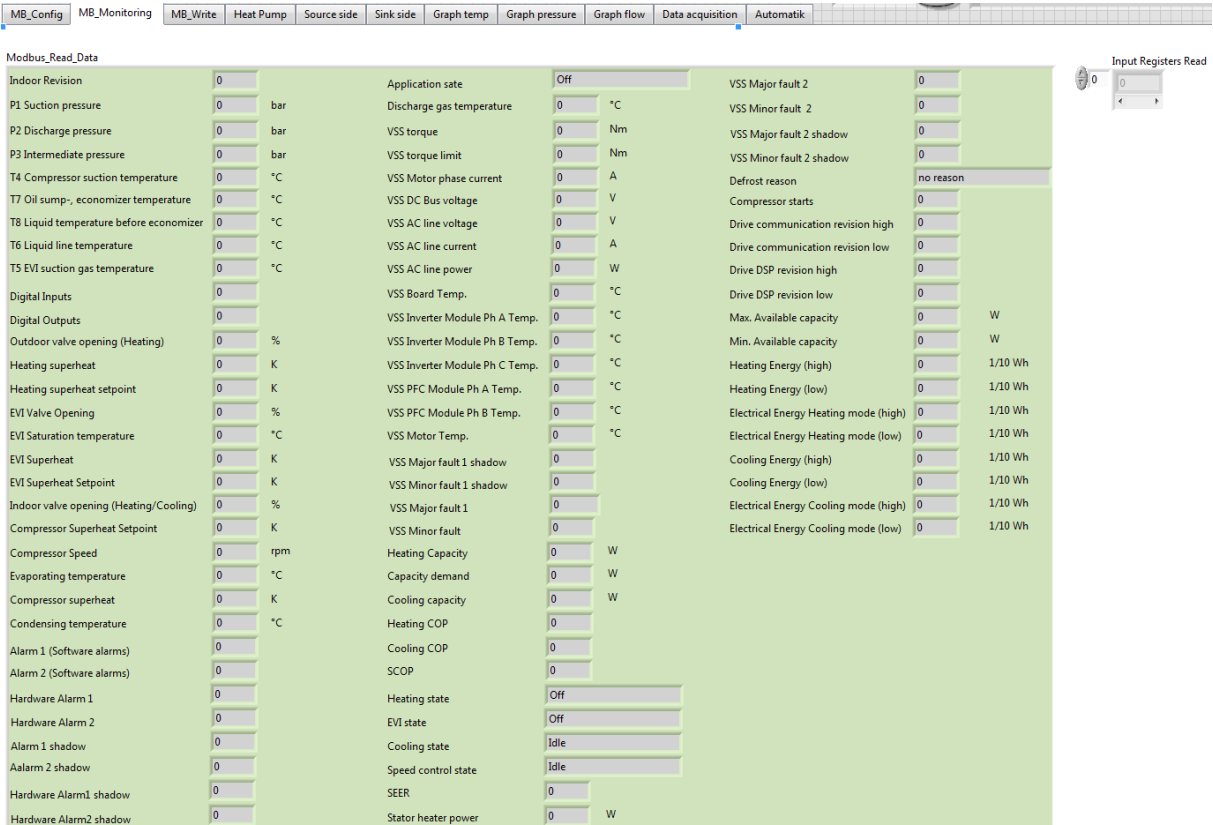


Figure A-6: Front Panel – MB_Monitoring

All pressure levels and temperatures of the refrigerant circuit, as well as the superheating and opening degree of the expansion valves are listed. Additionally all alarm notifications and measurement values as torque and temperatures of motor and inverter are shown. As all values are listed at once, this tab is very important for monitoring the behaviour of the heat pump at critical operating conditions. For monitoring the behaviour over longer periods the graphs of temperature, pressure and flow are useful. In the tab 'Data acquisition' values of the SEC are plotted. Here the superheating and the opening degree of the expansion valves are monitored. Also the progression of the compressor speed is shown in this graph. None of the tabs where graphs are shown will be discussed explicitly.

The tab 'MB_Write' represents the control panel of the compressor (Figure A-7). Here the operating modes 'Off', 'Heating' or 'Manual' can be set. When heating mode is activated the compressor can either be started by giving it a fixed compressor speed or a desired heating capacity. When manual mode is activated all safety functions are disabled, therefore it has to be operated carefully in this mode. Nevertheless, this mode should be avoided as the safety functions are essential for a long-time operation of the compressor. All programmes that were embedded for the automatic operation of the heat pump system, write their values directly to the SEC. Those values are not visualised in this tab and cannot be influenced by writing into this tab when automation is activated.

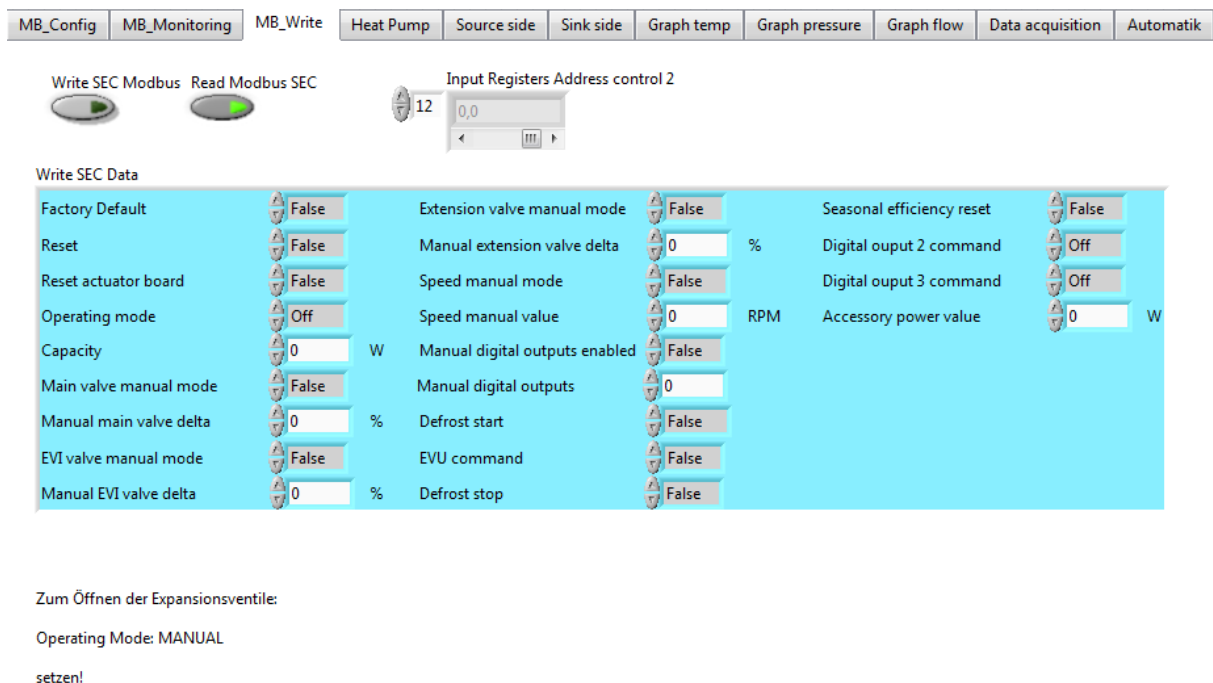


Figure A-7: Front Panel – MB_Write

For monitoring the refrigerant circuit the tab 'Heat Pump' can be activated. A scheme of the cycle with the current measurement values being placed according to their position on the test rig gives an immediate overview of the state of the cycle. Measurement values can be checked concerning their plausibility and displaced or damaged sensors are detected instantly. Additionally calculated values are shown for an on-line evaluation of the operating point. Therefore the COP and the electrical power consumption of the compressor P_{el} are displayed. The heating capacities of the heat exchangers are shown as well. This information helps to detect problems within the cycle and measuring devices and also gives a tendency when a change of operating conditions has to be evaluated.

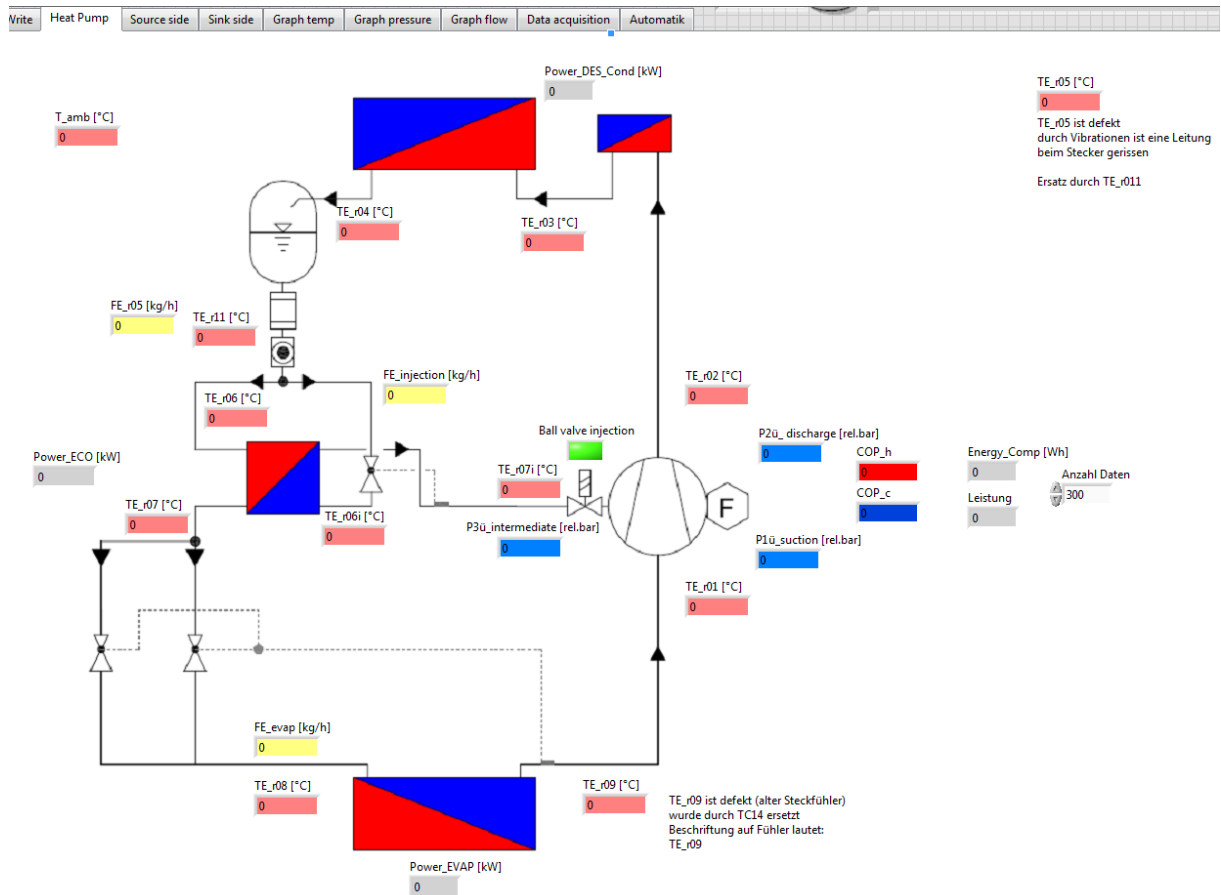


Figure A-8: Front Panel – Heat Pump

Figure A-9 shows a scheme of the source side of the heat pump system. The circulating pump and the electrical heater can be operated and monitored here. It can be chosen to either operate these components manually or to use the PID controller. When using the PID controller it has to be set manually 'on' and a set point as well as parameters have to be specified. By being able to adjust the parameters of the PID controller on-line in the 'Front Panel' it is possible to immediately react on problems with the controller settings. The measured values of the temperature sensors at the evaporator and the volume flow meter are displayed in the scheme as well.

For monitoring and controlling the heat sink of the heat pump system the tab 'Sink side' is used. As for the source side also here a scheme of the periphery is depicted and the measured values are positioned next to the components they are placed at on the test rig. In Figure A-10 the separate water cycle of the desuperheater can be seen. It is directly installed to the storage tank with a capacity of 200 litres. One temperature sensor detects a mean temperature of the tank and for cooling purposes of the tank it is also adjusted to the thermal system of the IWT.

Two PID controllers are necessary for the control of the heat sink. Whereas one PID controller operates the circulating pump of the water cycle, the other controls the cycle which detracts the heat energy from the condenser. In this brine cycle of the thermal system of the IWT, a speed controlled circulating pump works as actuator for the system's PID controller. It can be chosen to use either the temperature sensor at the inlet of the condenser (TE_w01) or the sensor at the outlet of the system heat exchanger as process variable. The controller reacts much faster if the latter sensor is used. Nevertheless, this leads to a slight offset between the set point and the inlet temperature at the condenser.

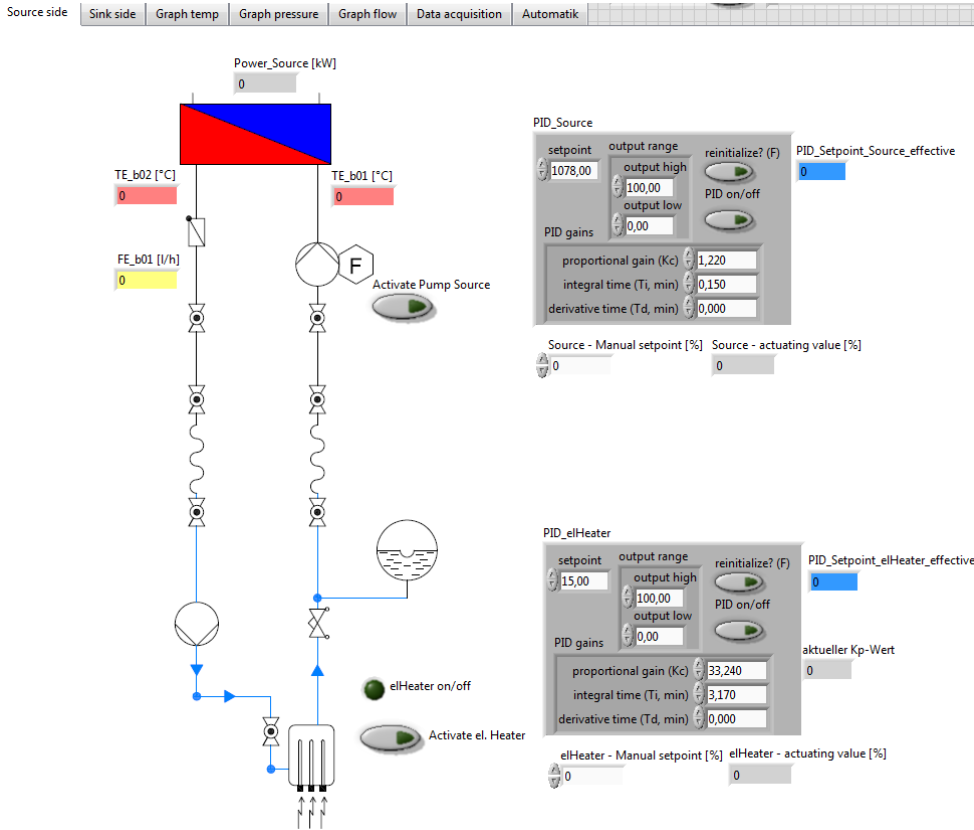


Figure A-9: Front Panel – Source side

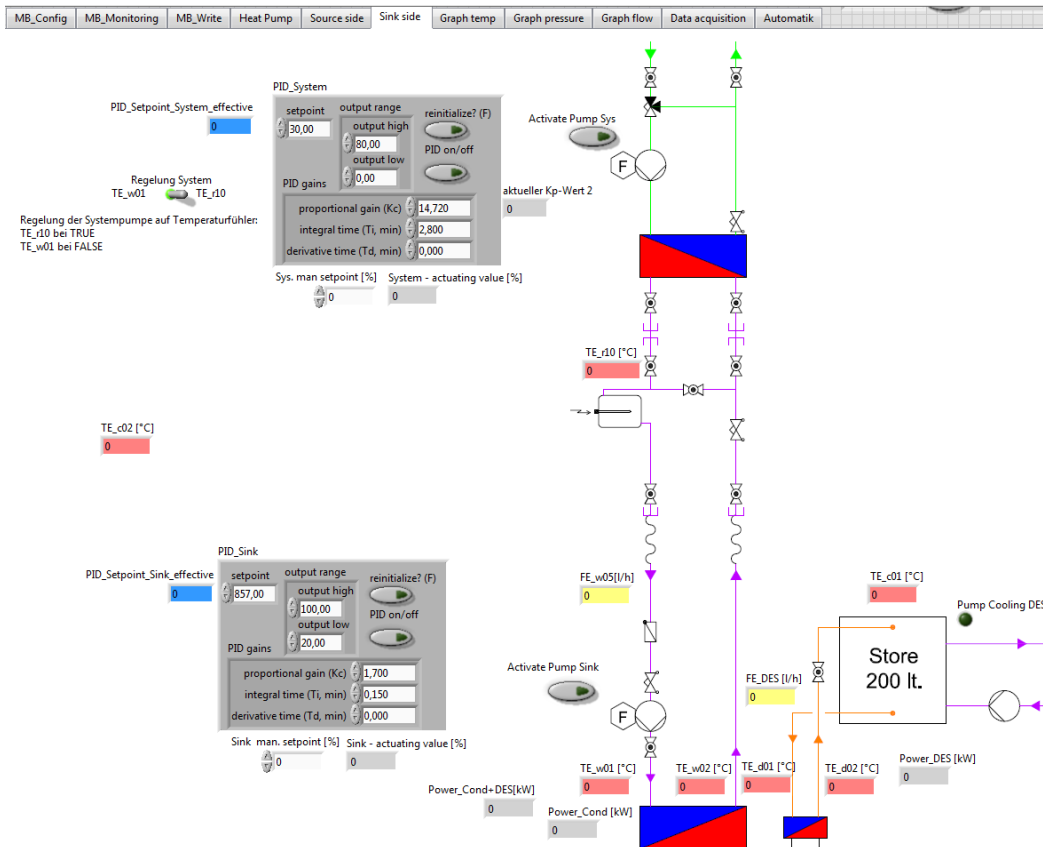


Figure A-10: Front Panel – Sink side

In the last tab 'Automation' at the 'Front Panel' all activation buttons for the automation programmes are placed (Figure A-11). The 'Automatic Superheat Control' is activated during all measurements whereas the other programmes are only activated for the 24-hour measurements.

The PID controller for the compressor speed is also placed in this tab. As the two different heating modes require a different calculation of the control variable, it can be selected between these two modes (DHW preparation and Space heating) in the controller. For monitoring reasons several additional values are displayed.

When 24-hour measurements are accomplished a simulation file is provided to simulate a special heating behaviour. This file is activated with the button 'Read Simulation values on/off'. All set points for all PID controllers are provided by this file.

With the 'Master Button' all automation programmes are activated at once. The heat pump system is then operated according to the provided values of the simulation file.

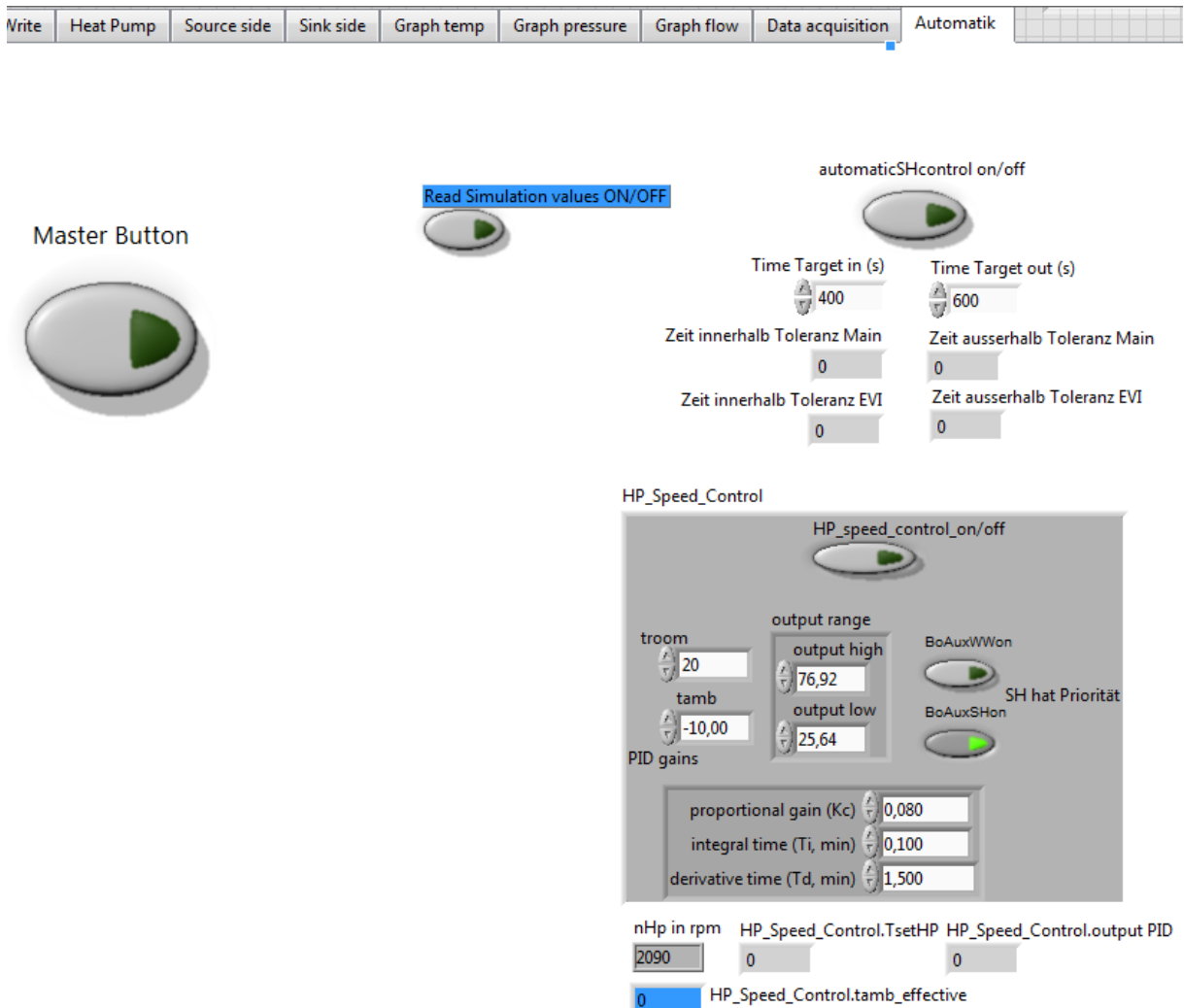


Figure A-11: Front Panel – Automation

A-2 Measurement matrix

The whole measurement matrix with the most important results and the corresponding uncertainties of measurement are listed in Table A-1. The measurements are sorted according to their measuring point number. They are arranged by the different operating conditions, starting with the lowest compressor speed of 1800 rpm, the lowest brine inlet temperature of -15 °C and the lowest condenser inlet temperature of 20 °C. Then the evaporator temperature rises and afterwards the condenser temperature is increased for one compressor speed. This system is continued for all compressor speeds. Not all of these operating conditions are within the compressor envelope and were not measured. In the last column a note is given when the operating point was outside of the envelope. Another note indicates when the mass flow meter showed implausible values during measurements. For these measurements the refrigerant mass flow was calculated which resulted in a bigger uncertainty of the calculated values.

All measurements from measuring point number 1 to 63 were used for the evaluation of the compressor and the heat pump cycle. Measurements number 64 to 72 were accomplished for the evaluation of the desuperheater mass flow.

Table A-1: Measurement matrix and results

Measuring Point No.	Compressor Speed n_{comp}	Evaporator Inlet Temperature T_{b01}	Condenser Inlet Temperature T_{w01}	Evaporation Temperature t_{evap}	Condensation Temperature t_{cond}	Electrical Power Input P_{el}	Pressure Ratio π	Relative Heat Losses $f_{comp,loss}$	Total Heating Capacity $Q_{cond,tot}$	Uncertainty of Measurement $Q_{cond,tot}$	COP	Uncertainty of Measurement COP	Overall Isentropic Efficiency $\eta_{is,overall}$	Uncertainty of Measurement $\eta_{is,overall}$	Overall Volumetric Efficiency $\eta_{vol,overall}$	Uncertainty of Measurement $\eta_{vol,overall}$	Note
#	[min ⁻¹]	[°C]	[°C]	[°C]	[°C]	[kW]	[-]	[%]	[kW]	[%]	[-]	[%]	[%]	[%]	[%]	[%]	
1	-	-	-	-	-	-	-	-	-	-	-	-	-	-	-	-	Envelope
2	1800	2	20	-2,55	23,28	0,44	2,15	13,9	2,48	4,9	5,67	5	54,1	6,3	78,3	3,1	
3	-	-	-	-	-	-	-	-	-	-	-	-	-	-	-	-	Envelope
4	-	-	-	-	-	-	-	-	-	-	-	-	-	-	-	-	Envelope
5	1800	2	30	-2,12	33,02	0,63	2,74	14,5	2,66	4,5	4,22	4,7	52,4	4	84,4	2,8	

APPENDIX

Measuring Point No.	Compressor Speed n_{comp}	Evaporator Inlet Temperature T_{b01}	Condenser Inlet Temperature T_{w01}	Evaporation Temperature t_{evap}	Condensation Temperature t_{cond}	Electrical Power Input P_{el}	Pressure Ratio π	Relative Heat Losses $f_{comp,loss}$	Total Heating Capacity $Q_{cond,tot}$	Uncertainty of Measurement $Q_{cond,tot}$	COP	Uncertainty of Measurement COP	Overall Isentropic Efficiency $\eta_{is,overall}$	Uncertainty of Measurement $\eta_{is,overall}$	Overall Volumetric Efficiency $\eta_{vol,overall}$	Uncertainty of Measurement $\eta_{vol,overall}$	Note
#	[min ⁻¹]	[°C]	[°C]	[°C]	[°C]	[kW]	[-]	[%]	[kW]	[%]	[-]	[%]	[%]	[%]	[%]	[%]	
6	1800	15	30	9,69	34,17	0,59	1,95	15,8	3,45	3,5	5,87	3,7	52,8	4,3	89,5	2	
7	-	-	-	-	-	-	-	-	-	-	-	-	-	-	-	-	Envelope
8	1800	2	45	-2,05	47,57	0,89	3,89	16,6	2,73	4,4	3,05	4,5	53	3,2	82,3	2,9	
9	1800	15	45	9,93	48,58	0,93	2,74	15,1	3,58	3,4	3,85	3,5	52,5	3	86,4	2,1	
10	2400	-10	20	-13,97	23,2	0,63	3,18	12,1	2,64	4,6	4,19	4,7	55,9	4,4	84,6	3,2	
11	2400	2	20	-3,35	24,53	0,62	2,29	10,2	3,52	3,5	5,65	3,7	56,7	4,6	89	2,3	
12	-	-	-	-	-	-	-	-	-	-	-	-	-	-	-	-	Envelope
13	2400	-10	30	-13,77	32,92	0,8	4,07	12,3	2,7	4,5	3,39	4,6	55,7	3,7	82,2	3,3	
14	2400	2	30	-3,13	34,06	0,81	2,91	10,7	3,55	3,4	4,38	3,6	58,2	3,5	86,2	2,3	
15	2400	15	30	8,6	35,69	0,77	2,09	12	4,47	2,8	5,83	3	59,1	3,7	89,6	1,7	
16	2400	-10	45	-13,84	47,24	1,1	5,78	15,5	2,76	4,3	2,51	4,5	53,1	3,2	79,3	3,4	
17	2400	2	45	-2,96	48,56	1,14	4,1	12,5	3,63	3,3	3,18	3,5	57,8	2,8	83,9	2,4	
18	2400	15	45	8,68	50,13	1,18	2,95	11,7	4,7	2,6	3,98	2,8	59	2,6	87,3	1,8	
19	3000	-15	20	-19	23,49	0,79	3,86	11,5	2,92	4,2	3,69	4,3	56,4	4,2	85,5	3,3	
20	3000	2	23	-4,53	29,16	0,88	2,69	8,1	4,39	2,4	4,96	2,6	59,8	3,7	89,9	2,1	
21	3000	15	20	5,87	27,53	0,78	1,85	13,1	5,48	2,3	6,99	2,6	55,4	4,9	93	1,5	Error FE_r05
22	3000	-15	30	-18,86	33,13	0,97	4,94	12,1	2,99	4	3,07	4,2	56,8	3,6	83,6	3,4	
23	3000	2	30	-4,37	35,26	1,03	3,12	9,5	4,41	2,8	4,3	3	61,3	3,2	88,7	2,1	

APPENDIX

Measuring Point No.	Compressor Speed n_{comp}	Evaporator Inlet Temperature T_{b01}	Condenser Inlet Temperature T_{w01}	Evaporation Temperature t_{evap}	Condensation Temperature t_{cond}	Electrical Power Input P_{el}	Pressure Ratio π	Relative Heat Losses $f_{comp,loss}$	Total Heating Capacity $Q_{cond,tot}$	Uncertainty of Measurement $Q_{cond,tot}$	COP	Uncertainty of Measurement COP	Overall Isentropic Efficiency $\eta_{is,overall}$	Uncertainty of Measurement $\eta_{is,overall}$	Overall Volumetric Efficiency $\eta_{vol,overall}$	Uncertainty of Measurement $\eta_{vol,overall}$	Note
#	[min ⁻¹]	[°C]	[°C]	[°C]	[°C]	[kW]	[-]	[%]	[kW]	[%]	[-]	[%]	[%]	[%]	[%]	[%]	
24	3000	15	30	6,85	37,39	1,05	2,3	8,8	5,76	2,2	5,51	2,4	61,5	3,3	92,3	1,5	
25	3000	-15	45	-18,62	47,48	1,34	6,93	13,7	3,11	3,9	2,32	4	52,8	3,2	79,6	3,5	
26	3000	2	50	-3,8	54,37	1,6	4,81	10,4	4,58	2,7	2,87	2,9	58,6	2,4	85,2	2,2	
27	3000	15	50	7,47	56,23	1,69	3,51	10,8	5,72	2,2	3,39	2,4	59,8	2,3	87,5	1,6	
28	3600	-15	20	-19,85	24,19	0,97	4,06	10,3	3,49	3,5	3,6	3,7	56,9	4	87,3	3,1	
29	3600	2	20	-6,02	26,65	1,01	2,64	8	5,09	2,5	5,03	2,7	59,4	3,8	91,9	2	
30	3600	15	20	5,02	29,39	1,04	1,99	7,9	6,7	2	6,43	2,2	57,1	4,2	95,4	1,4	Error FE_r05
31	3600	-15	30	-19,73	33,74	1,18	5,18	10,8	3,57	3,4	3,02	3,6	57,2	3,4	85,1	3,2	
32	3600	2	30	-5,75	36,32	1,27	3,35	8	5,19	2,4	4,1	2,6	62,3	3	90,3	2	
33	3600	15	30	5,26	38,85	1,32	2,51	13,1	6,32	2	4,79	2,3	61,2	3	90,7	1,5	
34	3600	-15	45	-19,32	48,19	1,62	7,23	11,5	3,76	3,2	2,32	3,4	53,6	3	81,3	3,2	
35	3600	2	50	-5,23	55,2	1,93	5,14	9,1	5,4	2,3	2,79	2,5	59,4	2,3	86,5	2	
36	3600	15	50	5,76	57,4	2,06	3,8	9,3	6,76	1,9	3,28	2,2	61,9	2,1	89,9	1,5	
37	4200	-15	20	-20,75	24,68	1,15	4,26	9,5	4,03	3,1	3,5	3,2	57	3,8	88,8	3,1	
38	4200	2	20	-7,61	27,81	1,23	2,88	7,9	5,75	2,2	4,68	2,4	60,1	3,6	93,1	2	Error FE_r05
39	4200	15	20	3,62	30,8	1,28	2,15	7,3	7,66	1,8	5,98	2	59,1	3,8	96,8	1,4	Error FE_r05
40	4200	-15	30	-20,4	34,43	1,4	5,4	9,7	4,14	2,9	2,95	3,1	57,3	3,3	86,3	3	
41	4200	2	30	-7,35	37,21	1,51	3,62	7,1	5,9	2,1	3,91	2,4	63	2,9	91,8	2	

APPENDIX

Measuring Point No.	Compressor Speed n_{comp}	Evaporator Inlet Temperature T_{b01}	Condenser Inlet Temperature T_{w01}	Evaporation Temperature t_{evap}	Condensation Temperature t_{cond}	Electrical Power Input P_{el}	Pressure Ratio π	Relative Heat Losses $f_{comp,loss}$	Total Heating Capacity $Q_{cond,tot}$	Uncertainty of Measurement $Q_{cond,tot}$	COP	Uncertainty of Measurement COP	Overall Isentropic Efficiency $\eta_{is,overall}$	Uncertainty of Measurement $\eta_{is,overall}$	Overall Volumetric Efficiency $\eta_{vol,overall}$	Uncertainty of Measurement $\eta_{vol,overall}$	Note
#	[min ⁻¹]	[°C]	[°C]	[°C]	[°C]	[kW]	[-]	[%]	[kW]	[%]	[-]	[%]	[%]	[%]	[%]	[%]	
42	4200	15	30	3,38	40,01	1,58	2,73	11,2	7,31	1,8	4,62	2,1	63,6	2,8	93,1	1,5	
43	4200	-15	45	-20,06	48,92	1,9	7,56	10,4	4,37	2,8	2,3	3	54,3	2,9	82,3	3,1	
44	4200	2	50	-6,6	55,97	2,28	5,48	8,4	6,14	2,1	2,69	2,3	59,5	2,2	86,9	2	
45	4200	15	50	4,19	58,2	2,44	4,06	8,7	7,72	1,7	3,17	2	62,5	2	90,4	1,5	
46	4800	-15	20	-21,79	25,2	1,33	4,49	8,8	4,47	2,8	3,36	3	56,6	3,8	88,4	3,1	
47	4800	2	20	-8,67	28,52	1,44	3,04	6,1	6,5	2	4,52	2,2	60,6	3,4	93,5	2	
48	4800	15	20	2,03	31,79	1,51	2,32	7,1	8,4	1,6	5,55	1,9	60,3	3,5	96,4	1,4	Error FE_r05
49	4800	-15	30	-21,39	35,04	1,62	5,7	9	4,63	2,7	2,85	2,8	56,8	3,2	85,7	3	
50	4800	2	30	-8,5	38,06	1,76	3,84	8,4	6,43	2	3,64	2,2	61,9	2,8	90,1	2	
51	4800	15	30	2,16	41,07	1,87	2,91	9,4	8,25	1,6	4,42	1,9	64	2,7	93,1	1,4	
52	4800	-15	45	-21,16	49,43	2,2	7,98	9,6	4,91	2,5	2,23	2,7	53,4	2,8	81,7	3,1	
53	4800	2	50	-7,94	56,76	2,65	5,83	9,5	6,71	1,9	2,53	2,2	58,2	2,2	85,2	2	
54	4800	15	50	3,4	59,1	2,84	4,24	7,9	8,7	1,6	3,07	1,9	62,7	2	90	1,4	
55	5400	-15	20	-22,77	25,67	1,52	4,72	8,9	4,9	2,5	3,21	2,7	55,6	3,7	87,4	3,1	
56	5400	2	20	-9,81	29,36	1,67	3,23	6	7,11	1,8	4,25	2,1	59,8	3,3	92,1	2	
57	5400	15	20	1	32,84	1,77	2,46	7,1	9,14	1,5	5,16	1,8	60,3	3,3	95	1,4	Error FE_r05
58	5400	-15	30	-22,28	35,53	1,85	5,97	8,8	5,1	2,4	2,76	2,6	56	3,2	85	3,1	
59	5400	2	30	-9,53	38,91	2,04	4,07	8,6	7,08	1,8	3,46	2,1	60,9	2,7	89,1	2	

APPENDIX

Measuring Point No.	Compressor Speed n_{comp}	Evaporator Inlet Temperature T_{b01}	Condenser Inlet Temperature T_{w01}	Evaporation Temperature t_{evap}	Condensation Temperature t_{cond}	Electrical Power Input P_{el}	Pressure Ratio π	Relative Heat Losses $f_{comp,loss}$	Total Heating Capacity $Q_{cond,tot}$	Uncertainty of Measurement $Q_{cond,tot}$	COP	Uncertainty of Measurement COP	Overall Isentropic Efficiency $\eta_{is,overall}$	Uncertainty of Measurement $\eta_{is,overall}$	Overall Volumetric Efficiency $\eta_{vol,overall}$	Uncertainty of Measurement $\eta_{vol,overall}$	Note
#	[min ⁻¹]	[°C]	[°C]	[°C]	[°C]	[kW]	[-]	[%]	[kW]	[%]	[-]	[%]	[%]	[%]	[%]	[%]	
60	5400	15	30	1,1	42,15	2,18	3,09	8,5	9,18	1,5	4,2	1,8	63,8	2,6	92,6	1,4	
61	5400	-15	45	-22,44	49,79	2,53	8,45	9,8	5,38	2,3	2,13	2,5	51,5	2,9	80,6	3,2	
62	5400	2	50	-8,94	57,41	3,01	6,13	8,1	7,48	1,7	2,48	2	58	2,2	84,9	2	
63	5400	15	50	2,29	59,84	3,24	4,46	7,1	9,56	1,5	2,95	1,8	62,4	2	89,3	1,4	
64	3600	15	30	4,96	39,16	1,33	2,55	11,3	6,7	-	5,05	-	62	-	91,1	-	
65	4200	2	30	-7,31	37,61	1,52	3,65	6,2	5,88	-	3,86	-	62,9	-	91,4	-	
66	3600	-15	30	-19,55	34,02	1,2	5,18	10,3	3,58	-	2,99	-	56,9	-	84,8	-	
67	3600	15	30	4,97	39,23	1,33	2,55	11,2	6,71	-	5,06	-	62	-	91,1	-	
68	4200	2	30	-7,41	37,59	1,53	3,66	14,1	5,83	-	3,82	-	59,9	-	87,7	-	
69	3600	-15	30	-19,56	34,13	1,2	5,2	11,4	3,57	-	2,97	-	56,9	-	85	-	
70	3600	15	30	4,97	39,26	1,33	2,55	11,1	6,71	-	5,05	-	62	-	91,1	-	
71	4200	2	30	-7,32	37,61	1,52	3,65	5,9	5,88	-	3,86	-	62,9	-	91,3	-	
72	3600	-15	30	-19,52	34,11	1,2	5,18	10	3,58	-	2,99	-	57	-	84,9	-	